RAPPORTO TECNICO - TECHNICAL REPORT

METIS INSTRUMENT PROPOSAL
for the Solar Orbiter Mission
Part 2: Experimental Interface Control Document - Part B

Ester Antonucci (P.I.), S. Fineschi, G. Naletto, M. Romoli, D. Spadaro, S. Solanski, P. Lami and the Co-I's Team

Rapporto nr. 94   14/01/2008

METIS
EID - PART B

REF: INAF/OATO NR. 94
DATE: 15-JAN-2008
ISSUE 1
page 1 of 108

ISTITUTO NAZIONALE DI ASTROFISICA
NATIONAL INSTITUTE FOR ASTROPHYSICS

INAF

METIS INSTRUMENT PROPOSAL
for the
Solar Orbiter Mission

Part II
Experiment Interface Control Document – Part B

Principal Investigator:

Ester Antonucci (1)

Co-Proposers:

S. Fineschi (1), G. Naletto (2), M. Romoli (3), D. Spadaro (4),
S. Solanki (5), P. Lamy (6), and the Co-I's Team

(1) INAF – Astronomical Observatory of Turin, Torino, Italy
(2) University of Padua, Padova, Italy
(3) University of Florence, Firenze, Italy
(4) INAF - Astrophysical Observatory of Catania, Italy
(5) Max-Plank-Institute fuer Sonnensystemforschung, Germany
(6) Laboratoire d'Astrophysique de Marseille, France,

Leading Funding Agency:

ASI – Agenzia Spaziale Italiana
(Ref. S. Di Pippo – (simonetta.dipippo@asi.it) - Viale Liegi 26 – 00198 Roma Italy
Phone: +390685671 Fax: +39 06 8567267)

In cooperation with:

CNES – Centre National d'Etudies Spatiale
DLR – Detuches Zentrum fuer Luft und Raumfahrt

Prepared by	**METIS Team**
approved by	**E. Antonucci - METIS PI**
reference	
issue	**1**
revision	**0**
date of issue	**15 January 2008**

METIS
EID - PART B

REF: INAF/OATO NR. 94
DATE: 15-JAN-2008
ISSUE 1
page 2 of 108

Distribution

Name	Organisation
Marcello Coradini	ESA/HQ (D/SCI) 8-10 rue Mario Nikis 75738 Paris Cedex 15 France
Richard Marsden	ESA/ESTEC (SCI-SM) + P.O. Box 299 1 (part VI) 2200 AG Noordwijk The Netherlands
Philippe Kletzkine	ESA/ESTEC (SCI-P) + P.O. Box 299 1 (part VI) 2200 AG Noordwijk The Netherlands
Simonetta Di Pippo	ASI – Osservazione dell'Universo Viale Liegi, 26 00198 Roma, Italia
Prof. Sergio De Julio	INAF Viale del Parco Mellini n.84 00136 Roma

Change Log

date	issue	revision	pages	reason for change
15/01/2008	01	0	all	First Issue

METIS
EID - PART B

REF: INAF/OATO NR. 94
DATE: 15-JAN-2008
ISSUE 1
page 3 of 108

Table Of Contents

METIS
EID - PART B

REF: INAF/OATO NR. 94
DATE: 15-JAN-2008
ISSUE 1
page 4 of 108

METIS
EID - PART B

REF: INAF/OATO NR. 94
DATE: 15-JAN-2008
ISSUE 1
page 5 of 108

METIS
EID - PART B

REF: INAF/OATO NR. 94
DATE: 15-JAN-2008
ISSUE 1
page 6 of 108

METIS
EID - PART B

REF: INAF/OATO NR. 94
DATE: 15-JAN-2008
ISSUE 1
page 7 of 108

LIST OF FIGURES

METIS
EID - PART B

REF: INAF/OATO NR. 94
DATE: 15-JAN-2008
ISSUE 1
page 8 of 108

METIS
EID - PART B

REF: INAF/OATO NR. 94
DATE: 15-JAN-2008
ISSUE 1
page 9 of 108

LIST OF TABLES

**METIS
EID - PART B**

REF: INAF/OATO NR. 94
DATE: 15-JAN-2008
ISSUE 1
page 10 of 108

1. General Introduction

1.1 Background

The Solar Orbiter will provide the next major step forward in the exploration of the Sun and the heliosphere after the successful ESA missions: Ulysses and SOHO, as well as the NASA missions TRACE, RHESSI, STEREO and Hinode. Solar Orbiter is a key element of the International Living with a Star program which is focused on the space research which has the objective of understanding the governing processes of the connected Sun-heliosphere system.

Solar Orbiter was proposed in 1999 by the European solar scientific community with the aim of exploring the circumsolar region, obtain unique almost helio-synchronous observations and obtain the first out-of-ecliptic imaging and spectroscopic observations of the solar poles and the equatorial corona from high altitudes.

In 2007 Solar Orbiter has been included, along with the NASA Sentinels mission, in the ESA-NASA Heliophysical Explorers, HELEX, program which exploits the synergy of the two missions to answer the fundamental questions about the Sun-heliosphere linkage.

The highly successful SOHO mission with the high sensitivity visible light coronagraph covering uninterruptedly at wide angle the outer corona/inner heliosphere has allowed us to fully understand the importance of the coronal mass ejections in influencing the heliospheric and Earth-magnetospheric system. With the first ultraviolet coronagraph spectrometer flown on SOHO the study of the outer corona by means of the ultraviolet spectroscopy has initiated. Ultraviolet spectroscopy has allowed us to identify and investigate the solar wind at coronal level, via Doppler dimming techniques.

At the same time, EUV and FUV spectroscopic observations of the disk have shown that a highly dynamical and complex system of magnetic structures forms the base of the corona. It is through these structures that the energy created in the interior of the Sun must be transported and dissipated to heat the corona and accelerate the solar wind.

The METIS investigation benefits from the heritage of the scientific knowledge and experimental experience that has been arising in the last decades from the technology developments and data analysis/interpretation related to the SOHO coronagraphs and spectrometers. In addition, more recently innovative concepts for visible and ultraviolet coronagraphy have been maturing thanks to two programs aimed to instrumental and technological developments in view of the Solar Orbiter coronagraphy and spectrometry.

1.2 Summary of the proposal

The *Multi Element Telescope for Imaging and Spectroscopy, METIS*, investigation is proposed in response to the Announcement of Opportunity (D/SCI – 23482) for submitting scientific investigations for the Solar Orbiter mission, issued by the European Space Agency (ESA) on October 18, 2007, in the frame of the joint ESA-NASA HELEX (Heliophysical Explorers) program.

The METIS design, conceived for the purpose of performing both EUV spectroscopy on the solar disk and off-limb and near-Sun coronagraphy and spectroscopy, is motivated by the aim of addressing the three key scientific questions identified as the focus of the HELEX program. These questions concern: the origin and heating/acceleration of the solar wind streams; the origin, acceleration and transport of the solar energetic particles; and the transient ejection of coronal mass and its evolution in the inner heliosphere (coronal mass ejections, CME's).

The investigation aims to provide crucial tests apt to verify the hypotheses and models, that have been developed primarily during the SOHO era, on the following main issues of solar coronal physics:

METIS
EID - PART B

REF: INAF/OATO NR. 94
DATE: 15-JAN-2008
ISSUE 1
page 11 of 108

INAF
ISTITUTO NAZIONALE DI ASTROFISICA
NATIONAL INSTITUTE FOR ASTROPHYSICS

- Is the slow solar wind originating according to more than one physical process and which is the level of contribution of the possible different sources of slow wind to the heliospheric wind observed 'in situ'?
- How does the magnetic field topology control the outflow velocity and composition of the slow and fast solar wind?
- Is the magnetic field controlling the emergence of the fast wind at the base of coronal holes?
- Do polar plumes and inter-plume regions have a role in channeling the fast wind?
- Is ion cyclotron dissipation of fast Alfvén waves the primary energy deposition process in the fast wind?
- Is the reconnection at the base of coronal holes responsible for the generation of waves and turbulence that energize the fast wind?
- Which is the nature of coronal heating in open and closed field regions?
- Which is the source of the seed particles of the Solar Energetic Particles (SEPs)?
- Which is the role of coronal shocks driven by coronal mass ejections in energizing SEPs?
- Which are the mass and magnetic fluxes carried out of the Sun during transient events?
- How does the evolution of the coronal magnetic field, inferred from the large-scale evolution of the outer corona, trigger coronal mass ejections?
- How does the corona re-adjust after coronal mass ejections on medium-term time scales, ranging between 3 and 10 days (not yet established in the outer corona)?
- How do the quiescent streamers evolve on time scales ranging between 3 and 10 days?

The crucial tests for addressing and solving these still open issues can be achieved by combining the instrument's versatility with the uniqueness of the Solar Orbiter mission profile, which allows: a close approach to the Sun thus leading to a significant improvement in spatial resolution; quasi co-rotation with the Sun, which allows to freeze for several days both the on-disk inner corona and the outer corona in the plane of the sky and, thus, enable us to disentangle the evolution of coronal structures and solar rotational effects on medium-term time scales, and an out-of-ecliptic view of the Sun.

The METIS instrument, consisting of the COR, EUS and SOCS elements, is designed to combine and extend the spectroscopic and imaging capabilities of the SOHO, Hinode and STEREO spectrometers and coronagraphs in order to exploit at best the unique characteristic of the Solar Orbiter mission profile.

- It can simultaneously image the visible and ultraviolet emission of the solar corona (COR element) and diagnose, with unprecedented temporal coverage and spatial resolution (down to about 2000 km), the structure and dynamics of the full corona in the range from 1.2 to 3.0 (from 1.6 to 4.1) solar radii from Sun center, at minimum (maximum) perihelion during the nominal mission, a region which is crucial in linking the solar atmosphere phenomena to their evolution in the inner heliosphere.
- It can observe key wavelength bands within the EUV/UV wavelength region 50-150 nm (EUS element), on the solar disk and off-limb out to 1.4 solar radii. This spectral region is dominated by emission lines from a wide range of neutral and ionized atoms, formed in the atmosphere of the Sun at temperatures ranging from 0.01 to 10 million K, so that an imaging spectrometer observing these lines is the only means by which chromospheric, transition region, coronal and flare plasmas can be simultaneously observed and characterized, giving the essential link between the Sun's surface and the 'in situ' measurements performed in the inner heliosphere by the Solar Orbiter and the Sentinels.
- In addition, it can combine both coronagraphy and spectroscopy (SOCS element) to observe the key wavelength bands within the EUV/UV wavelength region from 30 to 125 nm, in the geo-effective coronal region from 1.7 to 2.7 solar radii from Sun center, at the closest approach, a region which is crucial in meeting the HELEX science goals.

For the first time METIS will be capable of obtaining:
- simultaneous imaging of the full corona in the visible and ultraviolet HI Ly α (121.6 nm)

METIS
EID - PART B

REF: INAF/OATO NR. 94
DATE: 15-JAN-2008
ISSUE 1
page 12 of 108

- monochromatic imaging of the full corona in the extreme ultraviolet He II Ly α (30.4 nm)
- spectral observations of He II Ly α in corona
- simultaneous spectro-images of the corona in the OVI doublet, the HI Ly α (121.6 nm), HeII Ly α (30.4 nm), Fe XVIII (97.4 nm) that can be performed simultaneously to coronal imaging
- spectral profiles of the Si XII 52.1 nm line (2 MK) in the third order and of the Ne VIII 77.0, 78.0 nm in the second order with unprecedented spectral resolution of 47,000, allowing measurements of absolute LOS velocities (with respect to the lower chromosphere) and line widths down to 1 km/s over a resolved element of 160 km;
- measurements of the velocity patterns (outflows, for instance) in coronal holes with high accuracy and minimal projection effects in several key lines, from the chromosphere (e.g., He I 58.4 nm) to the upper transition region (Ne VIII 77.0 nm).

These measurements will allow a complete characterization of the three most important plasma components of the corona and the solar wind (electrons, protons, helium),in addition to the minor ions components.

The METIS suite has been designed following a highly innovative integrated approach, which takes advantage as much as possible of common subsystems for the three elements, such as the optical bench, the electronics, the DPU. A great advantage from the spacecraft point of view is that METIS makes use of a single aperture which is feeding the solar light to all the instrument elements, COR, EUS and SOCS. That is, a single aperture door is indeed needed instead of the two foreseen in the nominal payload for COR and EUS. The integrated design of METIS translates into a much reduced thermal load inside the payload, and a power saving, while the required mass is essentially equivalent to the one allocated for the independent COR and EUS instruments. A further advantage, at the instrument level, is that the three elements, COR, EUS and SOCS, can be implemented using the resources nominally allocated on the spacecraft for the two elements, COR and EUS. This is a point of paramount importance because the scientific return which can be obtained by the METIS instrument is in this way greatly enhanced with respect to that expected in the case of the nominal payload, at essentially no additional cost with respect to the allocated resources. In fact, both the envelope and mass resources required for METIS stay well within the allocated resources, while there is a saving in terms of power. Actually, a minor increase of mass is required with respect to the allocated COR+EUS one (the present best estimate of METIS total mass is 37.0 kg including margins, with an increase of 0.5 kg with respect to the 36.5 kg mass allocated for COR+EUS), but this is largely compensated by the reduction in the number of instrument doors to be allocated by the S/C (one aperture cover only is required for METIS, instead of the two presently considered for COR and EUS). It has always to be underlined that with this mass, METIS will reach extremely enhanced scientific and technical requirements, with a scientific return much larger than the one that could be obtained with two independent COR and EUS instruments.

The METIS suite consists of three different elements, each one dedicated to a specific scientific aim:
   a. COR, a visible-EUV coronagraph
   b. EUS, an EUV-FUV disk spectrometer
   c. SOCS, an EUV coronal spectrometer

The three elements share the same optical bench, electronics, and S/C heat shield aperture.
COR is based on a classical externally occulted design, in which light enters through an external occulter located at the outside panel of the S/C heat shield. The external occulter is supported by a suitable truss, which protrudes from the S/C instrument bay inside the heat shield; also an extended external occulter can be inserted in the optical path, to allow observation of the solar corona also when the S/C is off-pointing from the Sun center. Three different coronal light wavelengths can be selected by a suitable filter mechanism: either visible, collected by a visible detector after being passed through a suitable polarizer, and/or ultraviolet (HI 121.6 nm or HeII 30.4 nm lines) collected by a suitable UV detector.
EUS is the element of METIS dedicated to perform the spectral analysis of the solar disk. It includes the telescopes and all the related mechanisms. Light from the solar disk passes through the METIS aperture on the S/C heat shield and is collected by a suitably coated telescope, which can be rotated around an axis

METIS
EID - PART B

REF: INAF/OATO NR. 94
DATE: 15-JAN-2008
ISSUE 1
page 13 of 108

passing through its vertex to scan the solar disk along the East-West direction. A heat trap is located on the backside of this mirror to dissipate the heat from the solar disk not reflected by the telescope. The EUV light reflected by the telescope is focused on the spectrograph slit plane, and after that dispersed by a toroidal variable line-spacing grating onto three independent detectors mounted at suitable positions to collect three interesting portions of the solar spectrum. The grating and the detectors are shared with the SOCS element, dedicated to perform the spectral analysis of the outer corona. Depending on the observation strategy, a mirror can be inserted into the optical path by a suitable mechanism to image selected portions of the solar corona, instead of the disk, on the spectrometer entrance slit. For coronal spectroscopy, the single entrance slit is replaced by a fixed array of slits (the slits of interest are selected by a suitable slit mechanism), in order to perform the spectral analysis of the corona at different radial heights simultaneously.

The METIS investigation is proposed by an International Consortium under the responsibility of the Principal Investigator, Ester Antonucci, INAF-Osservatorio Astronomico di Torino. Experiment Manager of the METIS project is Giampiero Naletto, University of Padua and the METIS Investigation Scientists is Silvano Fineschi, INAF-Osservatorio Astronomico di Torino. The METIS elements are in turn under the leadership of the following Co-PIs: Marco Romoli, University of Florence (COR), Daniele Spadaro, INAF-Osservatorio Astrofisico di Catania (EUS) and Dan Moses, Naval Research Laboratory, US (SOCS). The METIS proposal is endorsed by the Italian Space Agency (ASI) as Leading Funding Agency.

The consortium is formed the following Italian institutions: Istituto Nazionale di Astrofisica (INAF), the Universities of Florence, Padua, Pavia, Catania, the Consiglio Nazionale delle Ricerche – Istituto di Fisica della Materia (CNR-INFM), the Politecnico of Torino, and the following foreign institutions: Naval Research Laboratory (NRL), US, Max-Planck-Institut für Sonnensystemforschung (MPS), Lindau, Germany, Laboratoire d'Astrophysique de Marseille (LAM), France, the Institute d'Astrophysique Spatiale (IAS), France, University of Athens, Greece, Royal Observatory of Belgium, Bruxelles, Belgium and Mullard Space Science Laboratory, UK. In terms of hardware contributions, NRL intends to provide the SOCS optical bench and sensors MCP, and is submitting to NASA a proposal in response to the NASA Focused Opportunity for Solar Orbiter, FOSO (deadline 31 January 2008), MPS intends to provide the two detectors of the COR element, LAM intends to provide the mirrors and mountings for COR.
INAF is the leading scientific institute and ASI is the leading founding national space agency of METIS investigation consortium.

1.3 Document concept and architecture

The EID-B defines the PI response to the technical requirements in part A specifying in detail the interface information applicable to METIS. Part B will form the sole formal and binding document for all technical and programmatic agreements between the ESA Solar Orbiter Project Office and the Principal Investigator.
The EID A and B will be placed under formal configuration and change control once signed and thus any change requires formal agreement between ESA and the PI.
The EID- B will become one of the applicable documents to the Solar Orbiter prime contractor.

Since the EID-B will accompany METIS until its realization, if selected, it has been decided to not limit it to the description of the interfaces with the S/C, and some sections have been added to describe in some detail the optical characteristics and the performance of the instrument. These sections have a more scientific relevance, but it has been decided to include also this part to maintain a traceability of the possible instrument evolution.

1.4 Issue Schedule

The EID-B of METIS is issued together with all the proposal documentation package; it will be re-issued in case of selection.

METIS
EID - PART B

REF: INAF/OATO NR. 94
DATE: 15-JAN-2008
ISSUE 1
page 14 of 108

INAF
ISTITUTO NAZIONALE DI ASTROFISICA
NATIONAL INSTITUTE FOR ASTROPHYSICS

2. Key Personnel and Responsibilities

In the tables hereafter, the METIS key personnel including Co-I's are listed.

Table 2.1. Key METIS personnel list.

Name	Role	Affiliation/Address	Contact information
Antonucci Ester	PI	INAF Osservatorio Astronomico di Torino Via dell'Osservatorio, 20 10025 Pino Torinese TO, Italy	+39 011 8101913 Office +39 011 8101930 Fax antonucci@oato.inaf.it
Fineschi Silvano	METIS Investigation Scientist	INAF Osservatorio Astronomico di Torino Via dell'Osservatorio, 20 10025 Pino Torinese TO, Italy	+39 011 8101919 Office +39 011 8101930 Fax fineschi@oato.inaf.it
Naletto Giampiero	Experiment Manager	University of Padova Department of Information Engineering Via Gradenigo, 6/B 35131 Padova PD, Italy	+39 049 8277646 Office +39 049 8277699 Fax naletto@dei.unipd.it
Romoli Marco	COR Co-PI	University of Florence Department of Astronomy and Space Science Largo Enrico Fermi, 2 50125 Firenze FI, Italy	+39 055 2307767 Office +39 055 224193 Fax romoli@arcetri.astro.it
Spadaro Daniele	EUS Co-PI	INAF Osservatorio Astronomico di Catania Via S. Sofia, 78 95123 Catania CT, Italy	+39 095 7332234 Office +39 095 7330592 Fax dspadaro@oact.inaf.it
Moses J. Daniel	SOCS Co-PI	US Naval Research Laboratory Code 7661 4555 Overlook Avenue, SE Washington, DC 20375 – 0001, USA	+1 202 404 8108 Office +1 202 767 5636 Fax dan.moses@nrl.navy.mil
Ciaravella Angela	COR Investigation Scientist	INAF Osservatorio Astronomico di Palermo Piazza del Parlamento, 1 90134 Palermo PA, Italy	+39 091 233454 Office +39 091 233-444 Fax ciarave@astropa.unipa.it
Zangrilli Luca	COR Instrument Scientist	INAF Osservatorio Astronomico di Torino Via dell'Osservatorio, 20 10025 Pino Torinese TO, Italy	+39 011 8101913 Office +39 011 8101930 Fax zangrilli@oato.inaf.it
Andretta Vincenzo	EUS Investigation Scientist	INAF Osservatorio Astronomico di Capodimonte Salita Moiariello, 16 8013 Napoli NA, Italy	+39 081 5575524 Office +39 081 5575433 Fax andretta@oacn.inaf.it
Poletto Luca	EUS Instrument Scientist	CNR-INFM-LUXOR c/o Department of Information Engineering Via Gradenigo 6/B, 35131 Padova PD, Italy	+39 049 8277680 Office +39 049 8277699 Fax poletto@dei.unipd.it
Doschek George	SOCS Investigation Scientist	US Naval Research Laboratory Code 7650 4555 Overlook Avenue, SE Washington, DC 20375 – 0001, USA	+1 202 7673527 Office +1 202 4047997 Fax george.doschek@nrl.navy.mil
Newmark Jeffrey	SOCS Instrument Scientist	US Naval Research Laboratory Code 7661 4555 Overlook Avenue, SE Washington, DC 20375 – 0001, USA	+1 202 767 0244 Office +1 202 767 5636 Fax newmark@nrl.navy.mil

The companies mainly involved in the development of METIS are:
Thales Alenia Space, Strada Antica di Collegno, 253 – 10146 Torino TO, Italy
Galileo Avionica, Via Einstein, 35 – 50013 Campi Bisenzio FI, Italy

Table 2.2. Involved industry main contact personnel.

Name	Role	Affiliation/Address	Phone / FAX / e-mail
Cesare Stefano	Contact person	Thales Alenia Space Strada Antica di Collegno, 253 10146 Torino TO, Italy	+39 011 7180740 +39 011 7180998 stefano.cesare@ thalesaleniaspace.com
Preti Giampaolo	Contact person	Galileo Avionica Via Einstein, 35 50013 Campi Bisenzio FI, Italy	+39 055 8950855 +39 055 8950613 giampaolo.preti@galileoavionica.it

The CoI list can be found at section 2.2 of the Management Plan (Part V document of the Proposal).

3. Instrument Description

In the following, a synthetic summary of METIS scientific objective and performance, and a brief description of the instrument system are contained.

3.1 *Scientific objectives*

Aim of the METIS (Multi-Element Telescope for Imaging and Spectroscopy) investigation, that we propose for the Solar Orbiter, is to address the problems still open in the field of coronal and solar wind physics, relevant to the three fundamental science questions identified as the focus of the joint ESA-NASA HELEX (Heliophysical Explorers) program, namely:

- What are the origins of the solar wind streams and the heliospheric magnetic field?
- What are the sources, acceleration mechanisms, and transport processes of solar energetic particles?
- How do coronal mass ejections evolve in the inner heliosphere?

Moreover, it will also:

- explore, at all latitudes, the energetics, dynamics and fine-scale structure of the Sun's magnetized atmosphere, as defined in the Solar Orbiter Science Requirements Document.

The basic scientific issues that are not yet fully clarified by the observations obtained with the in-flight spectrometers and coronagraphs of SOHO, Hinode and STEREO missions and the solar wind instrumentation on Ulysses, concern the physical processes that:

- generate the slow wind
- deposit energy in the regions of acceleration of the solar wind
- determine the elemental abundances in the extended corona and the solar wind
- supply the seed particles for solar energetic particles (SEP) acceleration;
- heat the outer solar atmosphere;
- lead to mass and magnetic fluxes carried out of the Sun in transient events.

In order to advance significantly in these fields, METIS will have the capability to:

- identify unambiguously the slow wind source via extensive high resolution observations, in space and time, of active region expansion, streamer formation and evolution;
- fully characterize the dynamics, kinetic temperatures and composition of the major plasma components, i.e., electron, hydrogen, helium and heavy ions, in the extended corona, site of the solar wind acceleration;
- detect populations of suprathermal ions that can become seed particles for SEP acceleration;
- study the velocity fields, temperature and composition of the solar atmospheric plasma at unprecedented high spatial, temporal resolution in order to eventually resolve the nature of the processes of energy deposition and dissipation;
- determine the 3D distribution and the directionality of the coronal mass ejections (CMEs).

By using a novel and unique approach which allows to combine ultraviolet spectrometry, on disk and off-limb, with UV spectro-imaging and visible and UV imaging coronagraphy capabilities, METIS will provide new and crucial observations, essential to address the above identified scientific objectives. METIS investigations are furthermore designed to benefit from the Solar Orbiter mission profile characterized by quasi-corotation intervals, close approach to the Sun and an out-of-ecliptic phase. METIS significantly extends the spectroscopic and imaging capabilities of the spectrometers and coronagraphs operating at present in space by integrating the functions of three telescopes in a single instrument.

The science expected from the METIS investigation can be summarized in the following list of items:

- mapping the origins of the slow and fast solar wind streams;
- understanding the plasma heating and acceleration of the solar wind;

METIS
EID - PART B

REF: INAF/OATO NR. 94
DATE: 15-JAN-2008
ISSUE 1
page 17 of 108

- which the origin of turbulence in the solar wind?
- which are the sources of the solar energetic particles (SEPs) and how are they accelerated?
- investigating the evolution of coronal mass ejections in the inner heliosphere;
- observation of plasma shocks at the CME front;
- determining the nature of the processes of energy deposition and dissipation;
- structure and evolution of streamers.

3.2 Scientific performance summary

The scientific objectives define the observational requirements of METIS that will be satisfied by the performance of the 3 instrument elements, COR, EUS, and SOCS. Table 3.1 is the traceability matrix showing the requirements flow from the scientific objectives to the observational specifications.

To have a better idea of the actual performance of the instrument, the Sun disk radiances are summarized in Annex 1, Table A1. 1. The corresponding count rates are shown in Annex 1, Table A1. 2. The off-limb radiances and count rates are shown in Annex 1, Table A1. 3.

METIS
EID - PART B

REF: INAF/OATO NR. 94
DATE: 15-JAN-2008
ISSUE 1
page 18 of 108

Table 3.1. METIS elements performance summary.

Element	Observational Drivers	Observational Requirements					Observing Mode	Data Product
		Channel	Spatial Res.	FOV	Spectr. Res.	Cadence & Exp. Time		
COR	Simultaneous UV, EUV & Visible images of full corona. Density maps Ne, N_H, $N_{He.\,m}$ He absolute abundance. Outflow velocity maps of H, He+.	Visible-light 500-600 nm	13" **Equiv. to 2" @1 AU at 0.22 AU**	1.8-3.5 Ro @0.22 AU	100 nm	@0.22 AU 1 min. (cad) (pB = 4 frames) 10 sec (exp.)	High cadence Synoptic (during Nominal Observing Mode)	pB Images Monochromatic He II images at 30.4 nm and HI images at 121.6 nm
		UV 122 nm EUV 30 nm		1.2-3.5 Ro @0.22 AU	$\Delta\lambda/\lambda = 10$ (1 nm)	UV (20 min cad, 1min, exp), EUV (1 hr, 2 min)		
EUS	Chromospheric, TR & coronal ions temperature, density, and l.o.s. outflow velocity (>3 km/s). Ions velocity distribution Elemental composition for FIP effect assessment Reconnection signatures Waves and turbulence signatures	96.8-109 nm OVI doublet FeXXIII, FeXVIII, SiXII, OVI	1" (on disk) **Equiv. to 0.14" @1 AU at 0.22 AU**	Inst. FOV 1"x 17' Rast. FOV 17'x 17'	Doppler w res. **3 km/s** (1/6 sub-pixel centroiding)	Exp. Time: 5 s Single step time: 20-50s Raster Cadence: 1-3 hr	Sit & stare or raster during Nominal Obs. Mode	Spectral images of the upper chromosphere, TR and inner corona on disk and at the limb up to 1.4 Ro (at 0.22 AU) at the brightest lines.
		116-127 nm FeXII, MgX, OV, NV, OIV	2" (off-limb) **Equiv. to 0.28" @1 AU at 0.22 AU**	Inst. FOV 2"x 40' Rast. FOV 60'x 40'	**2 km/s**			
		152-158 nm FeXXI, NeVIII, SV, OIV, NIV			**1 km/s**			
SOCS	Maps of ions kinetic T in the outer corona, outflow w (>30km/s) via Doppler dimming and los Doppler velocity. Images of reconnecting regions. OVI lines width broadening (CME shocks) Outer corona images at the West limb	OVI doublet 103,2, 103.7 nm, FeXVIII, SiXII	24" -60" **Equiv. to 3.5"-7.4" @1 AU at 0.22 AU**	Rad: 1.7-2.7 Ro	1/e los vel. distr. 60 km/s	Exp Time: 1 min. Cad. 10 min.	Sit & stare continuously during Time-share Obs. Modes and selected periods during Nominal Obs. Modes	Spectral images of off-limb corona at the brightest lines. (Instantaneous FOV at 1.7, 1.9, 2.3, 2.6 Ro, at 0.22 AU)
		HI Ly-α 121,6 nm		Tang to limb: 2.0 Ro @ 0.22 AU	50 km/s			
		HeII 30.4 nm			100 km/s			

METIS
EID - PART B

REF: INAF/OATO NR. 94
DATE: 15-JAN-2008
ISSUE 1
page 19 of 108

3.3 Instrument description

Herein, a description of the instrument system is contained, while more details on the instrument interface are contained in the following chapters.

3.3.1 Functional description

3.3.1.1 Measurement principle

The measurement principle is based on coordinated operations of the three elements that constitutes the METIS suite. This has to be selected in order to maximize the scientific return in each phase of the mission by suitably sharing the allowable resources in terms of power and data rate.

3.3.1.2 General Instrument Architecture

In an approach oriented to the best sharing of tasks between the imaging and the spectroscopic investigation of the Sun, and in particular of the solar corona, and to the best coordination between them, a highly integrated instrument is proposed. This instrument, named METIS (Multi Element Telescope for Imaging and Spectroscopy), performs imaging of the close solar corona in the visible and in the extreme ultraviolet (EUV) and spectroscopy of both sun disk and corona in the EUV, by means of an integrated instrument suite located on a common optical bench and sharing a single aperture on the satellite heat shield.

The proposed approach seems to be the most effective to obtain the highest scientific return, while minimizing the overall resource allocation. In fact, the proposed architecture takes advantage of the commonality between the different elements that constitute the suite. Moreover the suite is aimed to provide a simplified interface to the spacecraft, by internally handling the needs of the various elements.

The proposed instrument architecture is based on three different elements, with a common main electronics and power supply. The three elements form an Instrument Front End (IFE) and are identified as it follows:

- Visible and EUV coronagraph (COR)
- EUV disk spectrometer (EUS)
- Solar Orbiter Coronal Spectrometer (SOCS)

COR is an independent element, formed by optics, detector, thermal hardware (if needed), proximity electronics and electrical interface for power supply, telecommand / telemetry link. EUS and SOCS share the diffraction optics and the detectors, but have independent telescopes. All the three elements share a single aperture on the S/C heat shield, and are mounted on a common optical bench. In addition, main electronics and power supply at suite level are common for all the IFE elements.

> *The METIS suite has been designed in such a way to take advantage as much as possible of the common subsystems (optical bench, electronics, DPU, etc.). A great advantage from the S/C point of view is that there is a single aperture which is feeding the light to all the elements. This translates into a reduced thermal load inside the payload and a power saving with respect to the available resources allocated for COR and EUS. A great advantage at the instrument level is that three elements (COR, EUS and SOCS) can be implemented using the resources nominally allocated for only two (COR and EUS). This is a point of paramount importance because the scientific return which can be obtained by the METIS instrument is in this way greatly improved with respect to the nominal payload, at essentially a minor additional cost in terms of mass with respect to the allocated resources.*

A top-level architecture of the proposed METIS suite is sketched in Figure 3.1.

METIS
EID - PART B

REF: INAF/OATO NR. 94
DATE: 15-JAN-2008
ISSUE 1
page 20 of 108
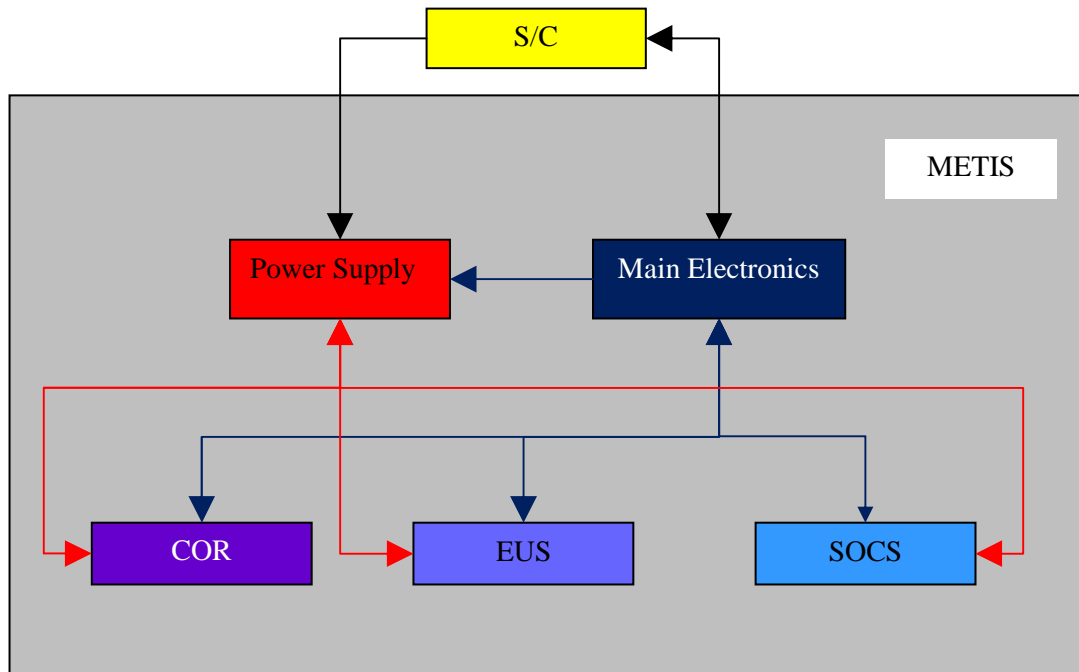
Figure 3.1. Overall METIS suite architecture.

3.3.1.3 Calibration

This section deals with the description of the calibration activities to be carried out on ground during assembly and verification phases and in flight during commissioning, cruise and observational phases to fully characterize the instrumental response.

The knowledge of the instrument performance, needed for an optimized data reduction, requires to perform measurements at several stages:

- **Sub-system tests:** measurements performed on subsystems (H/W units to be integrated in any of the elements) before the integration of the three elements forming METIS;
- **Element ground calibration**: measurements performed on each of the three METIS elements;
- **Instrument ground calibration**: measurements on the IFE, as a single instrument, performed after integration of the entire flight unit, prior to its delivery for integration on the S/C;
- **S/C calibration**: measurements performed on METIS when integrated on the S/C, prior to its launch;
- **In-flight calibration**: calibration performed both during cruise and operations.

Preliminary to all the test activities, an analysis shall be performed of the performance of each element on the basis of S/W simulation.

3.3.1.3.1 Sub-system tests

Subsystems of the three elements for which tests shall be performed and documented are shown in **Errore. L'origine riferimento non è stata trovata.**.

Table 3.2. List of subsystems of METIS elements.

COR	EUS	SOCS
External occulter mechanism	Sun disk telescope	Coronal telescope
Heat rejection mirror	Sun disk telescope scanning mechanism	Grating
Telescope (with multilayer optics)	Coronal telescope insertion mechanism	UV detectors
Internal occulter mechanism	Slit selection mechanism	
Filters and filter mechanism		
Visible polarizer		
UV detector		
Visible detector		

For each subsystem the following documents shall be part of the FM delivery Data Package:
- log book of test activities;
- data book on the experimental set-up (e.g., lamps spectral and radiometric response, filters and windows transmittance, monochromator spectral resolution, collimator(s) optical quality and FOV, etc.)
- data book of the characteristics of subsystem under measure (e.g., mirror coating reflectance, sensor filter transmittance, etc.)

Considering the past experience of the Institutes and Industries involved in the project, a significant part of the required equipment for the tests described in the following is already available.

For all the sensors, which are different for the visible (APS) and UV (IAPS, in both analog and photon counting modes), standard measurements will be performed as: linearity, quantum efficiency, offsets and saturation level, spectral and radiometric photo-response, photo-response non-uniformity (flat field), dark current level, evaluation of damaged pixels location (out of linearity, fixed output). Many of the above tests shall be provided by the manufacturer, but in some cases tests shall be performed by Institutes/Industries as appropriate.

The optical subsystems for each element shall be properly aligned and their alignment verified prior to the final element integration.

All the mechanisms present in the METIS instrument shall follow a full qualification process as required and explained in detail in the Engineering plan.

3.3.1.3.2   *Calibration at element and instrument level*

A subset of the calibration activities, mainly geometric and radiometric cross-calibration, shall be performed on the integrated IFE to verify the instrument behavior prior to the delivery.

The verification of co-alignment among the three elements is required to guarantee the correlation of observations taken by the different elements and to achieve the best scientific return from the combination of parallel and/or subsequent observations.

For the integrated suite of instruments the following activities are planned:
• co-alignment of the boresights of each element
• measurement of the relative spatial offsets
• spectral and cross spectral calibrations
• radiometric cross-calibration
• stray light evaluation

3.3.1.3.3   *In-flight calibration*

In flight calibrations will mainly consist of: a) internal calibration; b) radiometric calibration with stellar objects (within the nominal FOV at aphelion, without any S/C off-pointing, TBC); c) spectral calibration with reference chromospheric lines.

METIS
EID - PART B

REF: INAF/OATO NR. 94
DATE: 15-JAN-2008
ISSUE 1
page 22 of 108

3.3.1.4 Functional diagram

The hardware configuration approach is based on a high level of integration between the three METIS elements. This means that duplication of common functions will be avoided whenever possible, in order to achieve maximum resource saving for the whole suite.

From a mechanical point of view, this means that each element is not intended to be designed as a self standing instrument, so requirements on the structure (e.g., stiffness, vibration performance) can be optimized. In fact, all the mechanical testing activities (including vibration and alignment) will be carried on at a suite level more than at an element level. In this way, global saving on mass can be obtained.

The METIS elements will be integrated on a common bench, that constitutes the mechanical interface towards the spacecraft. This is aimed also to guarantee the needed stability in co-alignment between the three elements, that is requested for best coordinated operations and data combined use.

From an electrical point of view, the proposed IFE approach allows the sharing of two main functions among the elements, that are implemented at suite level to avoid duplication, namely:

− main electronics function,

− power supply.

The first is mainly devoted to data management and compression, instrument control and telecommand/telemetry handling from/to the S/C interface. The second is optionally incorporated in the METIS capabilities and is devoted to supply all the subsystems with the required power, providing a common set of required voltages.

A schematic of the METIS functional diagram is shown in Figure 3.2. The used acronyms are defined in section 10.
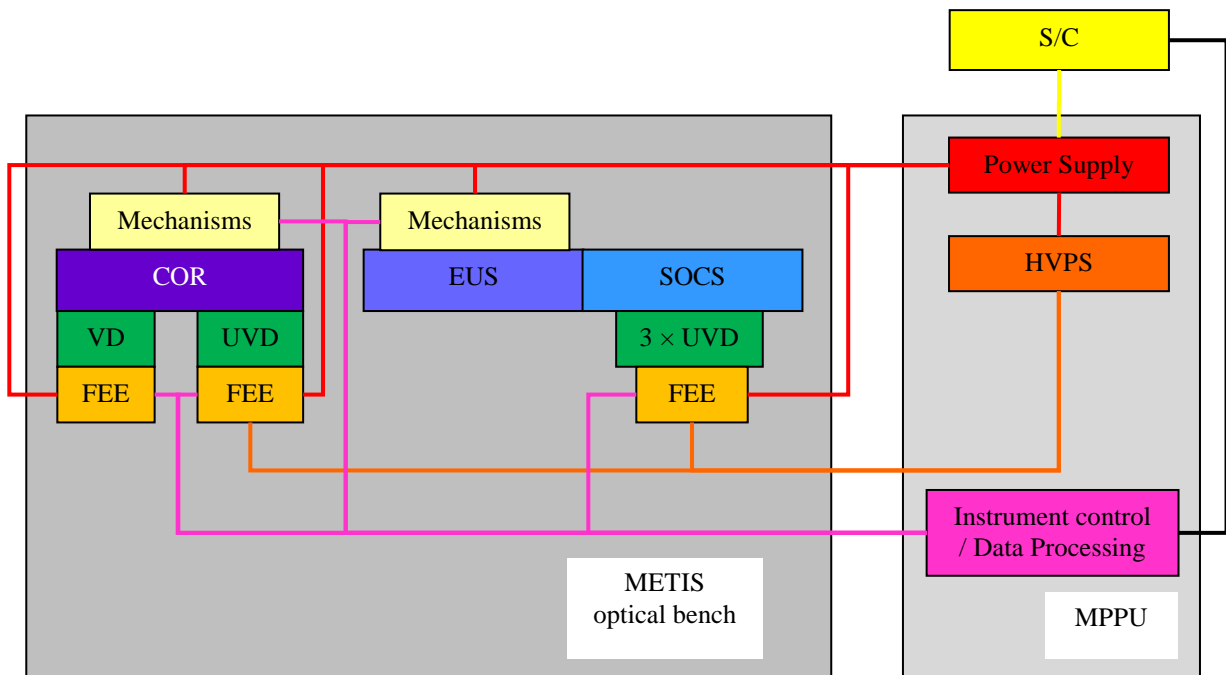
Figure 3.2. METIS functional block diagram.

3.3.2 Hardware description

In this section a brief summary of what are the main hardware characteristics of the METIS instrument is given. A more detailed description of METIS and of its elements will be given in the next sections.

**METIS
EID - PART B**

REF: INAF/OATO NR. 94
DATE: 15-JAN-2008
ISSUE 1
page 23 of 108

3.3.2.1 Overall instrument

The METIS instrument is an integrated suite which constitute, from a system point of view, a single interface towards the spacecraft for thermal, mechanical, electrical and optical aspects.

This suite integrates three different elements on a single optical bench also to guarantee the needed stability in coalignment between the optical heads, that is necessary for best coordinated operations and data analysis, and between the instrument and the other Solar Orbiter payloads.

A schematic of METIS is given in Figure 3.3.
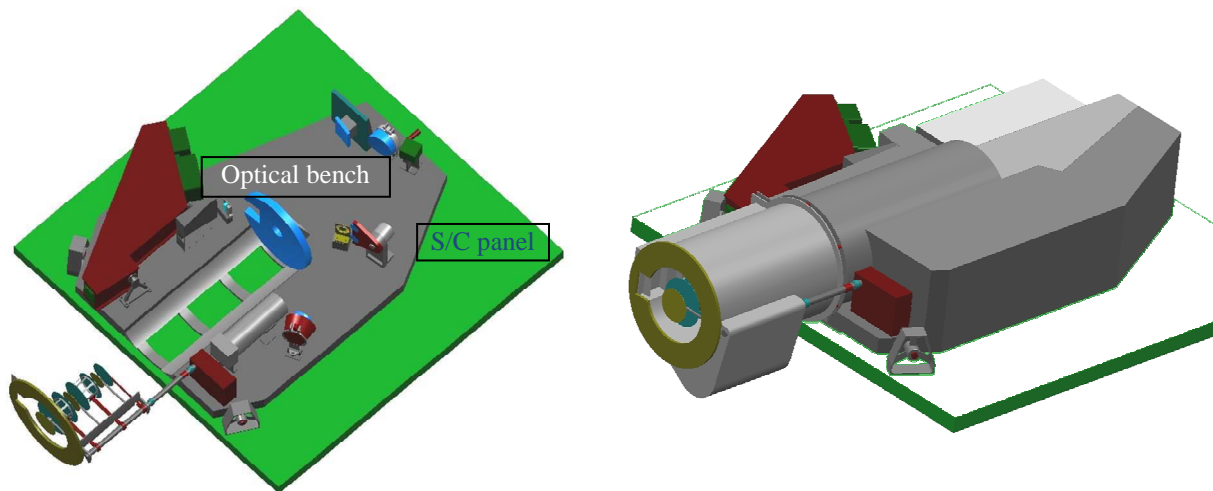
Figure 3.3. METIS layout: on the left the optical elements and the bench are shown; on the right, there is a view of the instrument with baffles and enclosure.

3.3.2.2 METIS elements

The METIS suite consists of three different elements, each one dedicated to a specific scientific aim:

a. COR, a visible-EUV coronagraph
b. EUS, an EUV disk spectrometer
c. SOCS, an EUV coronal spectrometer

The three elements share the same optical bench, electronics, and S/C heat shield aperture.

COR is based on a classical externally occulted design, in which light enters through an external occulter located at the outside panel of the S/C heat shield. The external occulter is supported by a suitable truss, which protrudes from the S/C instrument bay inside the heat shield. An annular shaped Sun-disk rejection mirror reflects back the disk light through the front aperture to minimize the thermal load inside the instrument, and leaves the coronal light reaching the telescope through a hole at its center located in the shadow of the external occulter. Three different coronal light wavelengths can be selected by a suitable filter mechanism: either visible, collected by a visible detector after being passed through a suitable polarizer, and/or ultraviolet (HI 121.6 nm or HeII 30.4 nm lines) collected by a suitable UV detector.

When the S/C is off-pointed from the Sun center (see the note at page 38 of RD-1) the "nominal" external occulter is not sufficient to shadow the COR aperture on the heat rejection mirror, if the S/C is at perihelion. So, in this case, an *extended* external occulter will be inserted with a suitable mechanism.

EUS is the portion of the spectroscopic element of METIS which includes the telescopes and all the related mechanisms. Light from the Sun disk passes through the METIS aperture on the S/C heat shield, through a slot in the COR heat rejection mirror, and is finally collected by a suitably coated telescope. The latter can be

METIS
EID - PART B

REF: INAF/OATO NR. 94
DATE: 15-JAN-2008
ISSUE 1
page 24 of 108

rotated around an axis passing through its vertex to scan the Sun disk along the East-West direction. A heat trap is located on the backside of this mirror to dissipate the heat from the Sun disk not reflected by the telescope. In fact, to reduce the heat load on the spectrograph entrance slit, the mirror is made in high transparent quartz and coated with a thin layer of SiC: in this way, the mirror mainly reflects the EUV light of interest, and at the same time transmits the great majority of visible and IR light arriving from the sun disk which is collected by the heat trap. The EUV light reflected by the telescope is focused on the spectrograph slit plane; the slit can be selected, depending on the observation strategy, by a suitable mechanism.

By means of another mechanism, a mirror can be inserted on the optical path to image selected portions of the solar corona, instead of the disk, on the spectrometer entrance slit. This allows to realize spectroscopic measurement also on the corona, and not only on the Sun disk.

In both cases, after the entrance slit, light enters the SOCS element, which is the actual spectrometer of METIS.

SOCS is essentially an independent box which includes the spectroscopic capabilities of METIS. It consists of a fixed array of slits (the slits of interest are selected by means of the just mentioned slit mechanism), a TVLS grating and a set of three independent detectors mounted on suitable position to collect three different interesting portions of the solar spectrum. SOCS allows to perform the spectral analysis of both the Sun disk and corona, but working in different ways in the two cases. In fact, the scanning mechanism of the EUS disk telescope allows to select the portion of the Sun disk to be analysed, but the corona telescope cannot perform such a scan. So, to allows simultaneous observation of different portions of the corona, a multi-slit system has been implemented. Essentially, in this case, there are four different slits at the SOCS entrance slit plane, which allows to analyse four different portions of the solar corona at different solar heights. Each slit produces its own spectrum, which is collected by the SOCS detectors.

3.3.3 Software description

Software architecture, as for hardware architecture, is based on the highest possible level of integration, in order to achieve a single interface to the spacecraft and avoid duplication of functions that are common to IFE elements. In particular, data compression is centralized for all the elements. A common communication protocol is identified for the link between the elements and the common

electronics. Spacewire represents a viable choice, thanks to its flexibility and speed. Spacewire interface can be implemented within FPGA. This approach has also the advantage to make the operation of a single element easier (through a suitable EGSE) during assembly and verification, before its integration at instrument level.

Spacewire is envisaged even for communication between the main electronics and spacecraft, both for data link and for telecommand / telemetry link.

Specific features to be developed for METIS on board S/W can be identified in the following topics:

- Autonomous MCP protection. To increase the MCP lifetime, an internal watchdog routine or task shall be defined to verify if the incoming radiation is below a specific threshold. Passing the threshold will put the instrument in safe mode.
- S/C offset from the Sun center: The S/C will have to deliver periodically the pointing offset telemetry from the Sun Center in order to protect the COR element.

3.3.4 Instrument data sheet

In this chapter, the general METIS data sheet is given, together with the data sheets of each of the IFE elements in separate paragraphs.

METIS
EID - PART B

REF: INAF/OATO NR. 94
DATE: 15-JAN-2008
ISSUE 1
page 25 of 108

3.3.4.1 METIS data sheet

Name / acronym	METIS / Multi Element Telescope for Imaging and Spectroscopy

Objectives	Visible and EUV coronography with the COR element
	Sun disk EUV spectroscopy with the EUS element
	Coronal EUV spectroscopy with SOCS

General description	Instrument suite consisting of three elements (COR, EUS, SOCS) mounted on a single optical bench, allocating common resources, and using a single aperture on the S/C heat shield.

Heritage	SCORE/HERSCHEL
	SUMER/SOHO
	UVCS/SOHO

Parameter		Units	Value / Description	Remarks
Sensor / detector				
COR visible detector		1	APS	Integration mode
	Format		2048 × 2048	
	Pixel size	μm	25	
	Dynamic range	bit	16	
	Operating temperature	°C	–40	
COR UV detector		1	IAPS	Photon counting mode
	Format		2048 × 2048	
	Pixel size	μm	25	On the focal plane. The actual pixel size of the APS for the IAPS is 12 μm (see section 4.6.1.1.4)
	Dynamic range	bit	N/A	This detector works in photon counting mode
	Operating temperature	°C	20	
SOCS/EUS detector		3	IAPS	Both analog and photon counting regimes
	Format		2048 × 2048	
	Pixel size	μm	12	
	Dynamic range	bit	14	When working in analog mode (N/A in photon counting mode)
	Operating temperature	°C	20	
Optics				
	Type			Different per each METIS element
	Unobstructed FOV	sr	2π	To be able to observe the very weak solar corona, no object can potentially scatter sun disk light inside the instrument aperture
	Energy passband		EUV to visible	
	Pointing		$+X_{Opt}$ S/C axis	
Configuration				
	Physical Units	No	1	
	Layout			

REF: INAF/OATO NR. 94
DATE: 15-JAN-2008
ISSUE 1
page 26 of 108

METIS
EID - PART B

ISTITUTO NAZIONALE DI ASTROFISICA
NATIONAL INSTITUTE FOR ASTROPHYSICS

Location S/C		±Z panel	See section 3.3.5
Physical			
Sensor Mass	kg	2.7	Mass of the five METIS detectors, including housing, mounts and doors
Thermal Hardware Mass	kg	1.0	METIS total thermal H/W mass (conductive straps, thermal washers, thermistors)
Harness Mass	kg	1.2	
Electronics Mass	kg	8.2	METIS Processing & Power Unit (MPPU)
Detector FEE	kg	1.1	For five METIS detectors
Total Mass	kg	29.6	METIS total mass, without contingency
Sensor dimensions		∅70 mm × 55 mm	COR VD
		∅90 mm × 75 mm	COR UVD
		∅55 mm × 40 mm	EUS/SOCS
Harness Length	cm	~100	From the detector FEE to the MPPU
Electronics Dimension	cm^3	22 × 25× 35	MPPU box envelope
Power			
Average	W	40.2	Before margins (25%)
Peak power	W	TBD	
Stand-by	W	TBD	
Data rate / volume			
Average data rate	bits/sec	27 k	
Peak data rate	bits/sec	TBD	
Minimum data rate	bits/sec	TBD	
Data volume /orbit	GByte	32	
Data storage	GByte	31	
Thermal			
Electronics Dissipation	W	37	MPPU dissipation, including 25% margin
Sensor Dissipation	W	13.2	Dissipation of all the detector FEE, including 25% margin
Heat load to radiator	W	130	Thermal power to be dissipated from the sun disk rejection mirror M0 and the heat absorber behind the EUS M1
Operating T range	K	293 ÷ 323	
Non-operating range	K	TBD	
Other requirements		TBD	
Cleanliness			
EMC requirements		TBD	
DC magnetic		TBD	
Particulate		TBD	
Molecular		TBD	
Pointing			
APE	arcmin	< 2	ILS
RPE		< 1 arcsec/10 s < 0.5 arcsec/10 s goal	ILS
Miscellaneous			
Mechanisms	No.	6	COR mechanisms: 1. Extended external occulter insertion 2. Filter exchange 3. Internal occulter alignment (during commissioning phase only)

METIS
EID - PART B

REF: INAF/OATO NR. 94
DATE: 15-JAN-2008
ISSUE 1
page 27 of 108

			EUS mechanisms: 4. Scanning mirror 5. Coronal telescope insertion 6. Slit selector
Detector doors	No.	4	Single shot (TBC) 1 for COR, 3 for EUS/SOCS
Orbit requirements		N/A	
AIT/AIV requirements		TBD	

METIS
EID - PART B

REF: INAF/OATO NR. 94
DATE: 15-JAN-2008
ISSUE 1
page 28 of 108

3.3.4.2 COR element data sheet

Name / acronym	COR Element

Objectives	Full coronal images in visible light, HI Lyman alpha 121.6 nm, and He II 30.4 nm
	Mapping the origins of the solar wind streams
	Understanding the plasma heating and acceleration of the solar wind
	Sources of solar energetic Particles
	Investigating the evolution of CMEs in the inner atmosphere

General description	COR is an externally occulted coronagraph. The telescope is an off-axis Gregorian with three observing channels, designed for:
	- broad-band polarization imaging of the visible K-corona (VL channel); - narrow-band imaging of the UV corona in the H I Lyman-α, 121.6 nm line (HI channel); - narrow-band imaging of the EUV corona in the He II Lyman-α, 30.4 nm line (HeII channel); in an annular FOV between 1.2 and 3.0 $R_\odot$, when SO perihelion is 0.22 AU; between 1.6 and 4.0 $R_\odot$ when at 0.3 AU. The telescope mirrors have multilayer coating optimized for narrow band ($\lambda/\Delta\lambda$=10) reflectivity at 30.4 nm. The multilayer capped-layer has also good reflectivity in UV and visible light. In the EUV channel, the long wavelengths are blocked by an aluminium filter inserted in the optical path. In the UV channel, the insertion of the narrow band ($\lambda/\Delta\lambda$=10) interference filter allows to isolate the 121.6 nm radiation. Simultaneously, the visible light radiation back reflected by the interference filter is fed to the polarimeter of the visible light channel. A toric mirror is used to reject through the front aperture the sun-disc radiation entering the instrument. During S/C offset pointing, this radiation is still rejected back through the same aperture thanks to the optical design and the toric shape of this rejection mirror. The stray light rejection is provided by the external occulter, the sun disk rejection mirror, the internal occulter and the Lyot trap.

Heritage	SCORE/HERSCHEL

Parameter	Units	Value / Description	Remarks
Boom			
Type		Externally occulted off-axis Gregorian	
External occulter	mm	Annular sector[1]: inner Ø: 80.3, outer Ø: 180 Triple disk Ø: A1: 76.14, A2: 71.8 Spindle lingth: 200	Annular sector aperture with three occulting disks and a decentred rectangular aperture that feeds both EUS and SOCS Units.
Extended external occulter	mm	5 disk spindle: inner Ø: 108.4, outer Ø: 180 5 disks Ø: A1: 106.28, A2: 103,7 A3: 100.6, A4: 97 Spindle length: 200	Insertable mechanism
Boom length	mm	900	The heat shield is supposed to be 400 mm in thickness

---

[1] The annular sector has a decentred rectangular aperture that feeds both EUS and SOCS elements.

METIS
EID - PART B

REF: INAF/OATO NR. 94
DATE: 15-JAN-2008
ISSUE 1
page 29 of 108

Sun disk rejection mirror (M0)	mm	Toric[2]: Ø: 264, Curvature radius: 900 Thickness: 12 Substrate: SiC Coating: SiC,	The toric shape is obtained by rolling an arc of circumference with center off-axis around the optical axis of the boom
Telescope			
Type		Externally occulted off-axis Gregorian	
Stop aperture diameter	mm	40	
Effective focal length	mm	400	
Unobstructed Field Of View		Annular between 1.2 and 3.0 $R_\odot$	When SOLO perihelion is 0.22 AU
		Annular between 1.6 and 4.0 $R_\odot$	When at 0.3AU
Primary mirror (M1)	mm	Off axis ellipsoidal: Ø: 80 , off-axis: 105, Curvature radius: 480, conic: -0.543 Thickness: 45	Optimized for HeII 30.4 nm
Distance M0 – M1	mm	400	
Internal occulter (IO)	mm	Outer diaphragm Ø: 40.4, inner disk Ø: 21, Distance among disks: 13	The outer diaphragm blocks the image of EO outer edge. The inner disk blocks the image of EO disk A2.
Distance M1 - IO	mm	288.9	
Secondary mirror (M2)	mm	Off axis ellipsoidal: Ø: 57.4, off-axis: 155.5, Curvature radius: 449.9, conic: -0.136 Thickness: 60	
M1 and M2 Coatings		Multilayer SiC-Mg	ptimized for HeII 30.4 nm
Distance M1 – M2	mm	600	ptimized for HeII 30.4 nm
Distance M2 – UV focal plane	mm	600	
Sensor / detector			
Type		APS and IAPS	Visible channel: APS UV and EUV channels: IAPS
Format	pixel	2048×2048	
Pixel size	µm	25	
Scale factor:		0.52 arcsec/µm; 12.9 arcsec/pixel	
Number of detectors		2	
Polarimeter			
Linear polarization analyzer		LCVR rotator + linear polarizer	baseline
Filters			
		HI 121.6nm band pass filter (HF)	HF: Al+MgF$_2$ HeF: Al
		VL band pass filter	
		HeII 30.4 low pass filter (HeF)	
Mechanisms			
		Extended external occulter	HWRP: only in case a LCVR plate cannot be used.
		Internal occulter alignment	
		Filter exchange	
		EUV detector door (single shot TBC)	
		(HWRP)	

METIS
EID - PART B

REF: INAF/OATO NR. 94
DATE: 15-JAN-2008
ISSUE 1
page 30 of 108

3.3.4.3   EUS element data sheet

Name / acronym	EUS / EUV disk Spectrometer

Objectives	To perform on-disk spectroscopy with a spatial resolution of 1 arcsec over a rastered FOV of 17×17 arcmin^2, with a < 20 s exposure time and a spectral cadence < 30 min
	To perform off-limb spectroscopy with a spatial resolution of 2 arcsec, binning on the detector to decrease the resolution down to 1 arcmin with a spectral cadence of 10 min and a radial coverage up to 1.4 solar radii

General description	EUS adopts a stigmatic design in a compact package with high throughput. It consists of a single-element parabolic telescope which creates the image of the Sun on a spectrometer entrance slit. A TVLS grating gives a stigmatic spectrum of each of the points along the slit height. The spectral imaging of an extended area is obtained by a rotation of the primary mirror. Three detectors are aligned on the spectral curve to acquire simultaneously the imaging spectra on six spectral intervals.

Heritage	SUMER/SOHO
	UVCS/SOHO

Parameter	Units	Value / Description	Remarks
Telescope			
Type		Off-axis parabola	
Size	mm^2	62 ($\perp$ to the slit) $\times$ 75	
Coating		Boron carbide	
Distance from the entrance aperture (heat shield)	mm	1250	The heat shield is supposed to be 400 mm in thickness
Mirror to slit distance	mm	730	
Raster angle	arcmin	± 30	Rotation about an axis passing through the mirror center and parallel to the slit
Slit			
Size	mm^2	0.004×8.5	Lithographically etched on crystal Si wafers
Grating			
Type		TVLS	
Central groove density	gr/mm	3600	
Incidence angle	deg	2.5	
Tangential radius	mm	212	
Sagittal radius	mm	217.2	
Ruled area	mm^2	26 ($\perp$ to the grooves) $\times$ 30	
Coated area	mm^2	13 ($\perp$ to the grooves) $\times$ 30	Half of the grating ruled area is coated for EUS observations
Coating		Boron carbide	
Slit to grating distance	mm	150	
Sensor / detector			
Type		IAPS	Both analog and photon counting regimes
Format	pixel	2048×2048	
Pixel size	μm	12	
Useful area	mm^2	24.6×24.6	
Number of detectors		3	
Spectral channel 1 (detector 1)			

METIS
EID - PART B

REF: INAF/OATO NR. 94
DATE: 15-JAN-2008
ISSUE 1
page 31 of 108

Spectral range	nm	96.8-109.0 (1st order) 48.4-54.5 (2nd order)	
Grating to detector distance	mm	438	Magnification 2.9
Instantaneous FOV		1.1 arcsec × 40 arcmin	
Spectral resolving element	pm/pixel	5.96 (1st order) 2.98 (2nd order)	
Spatial resolving element	arcsec/pixel	1.2	
Spectral channel 1 (detector 1)			
Spectral range	nm	96.8-109.0 (1st order) 48.4-54.5 (2nd order)	
Grating to detector distance	mm	438	Magnification 2.9
Instantaneous FOV		1.1 arcsec × 40 arcmin	
Spectral resolving element	pm/pixel	5.96 (1st order) 2.98 (2nd order)	
Spatial resolving element	arcsec/pixel	1.2	
Spectral channel 2 (detector 2)			
Spectral range	nm	116.2-126.6 (1st order) 58.1-63.3 (2nd order)	
Grating to detector distance	mm	461	Magnification 3.1
Instantaneous FOV		1.1 arcsec × 37 arcmin	
Spectral resolving element	pm/pixel	5.08 (1st order) 2.54 (2nd order)	
Spatial resolving element	arcsec/pixel	1.1	
Spectral channel 3 (detector 3)			
Spectral range	nm	151.6-158.4 (1st order) 75.8-79.2 (2nd order) 50.5-52.8 (3rd order)	
Grating to detector distance	mm	532	Magnification 3.5
Instantaneous FOV		1.1 arcsec × 33 arcmin	
Spectral resolving element	pm/pixel	3.32 (1st order) 1.66 (2nd order) 1.11 (3rd order)	
Spatial resolving element	arcsec/pixel	1.0	
Mechanisms			
		Scanning mirror	
		Coronal telescope insertion	
		Slit selector	

METIS
EID - PART B

REF: INAF/OATO NR. 94
DATE: 15-JAN-2008
ISSUE 1
page 32 of 108

3.3.4.4 SOCS element data sheet

Name / acronym	SOCS / Solar Orbiter Coronal Spectrometer

Objectives	To perform VUV/EUV spectroscopy & imaging measuring hydrogen and singly-ionized helium densities, outflow velocities and kinetic distributions over a 1.7 up to 2.6 $R_\odot$ @ 0.22 AU with a spectral resolution: $\Delta\lambda/\lambda = 1.6\text{-}3.6\cdot10^{-4}$
	To observe 4 simultaneous spectral images at 4 different radial distances (1.7, 1.9, 2.3, 2.6 $R_\odot$ @ 0.22 AU).

General description	SOCS acquires simultaneous spectral images of the extended corona in three different spectral bands and at four different radial distances. The instrument shares with the grating and the detectors with EUS. A low-resolution telescope in the shadow of the solar disk creates an image of the corona on the entrance plane of the spectrometer where a multiple slit system is located. The TVLS grating creates stigmatic spectral images of the different slits on the detectors.

Heritage	SUMER/SOHO
	UVCS/SOHO

Parameter	Units	Value / Description	Remarks
Telescope			
Type		Off-axis parabola	
Size	mm^2	20 ($\perp$ to the slit) $\times$ 40	
Coating		Multilayer	Coating optimized for 30.4 nm reflectivity and 103/121.6 nm reflectivity
Distance from the entrance aperture (heat shield)	mm	670	The heat shield is supposed to be 400 mm in thickness
Mirror to slit distance	mm	190	
Multi-slit			
Size of each slit	mm^2	0.02 $\times$ 8.5	Lithographically etched on crystal Si wafers
Number of slits		4	
Slit angular distances from Sun center	deg	2 (slit no. 1) – 2.3 (2) – 2.7 (3) – 3.1 (4)	
Slit separation	mm	1.0 (slit 1 to 2) – 1.3 (2 to 3) -1.3 (3 to 4)	
Grating			
Type		Toroidal with variable-line-spaced grooves	Same grating as EUS Unit
Coated area	mm^2	13 ($\perp$ to the grooves) $\times$ 30	Half of the grating ruled area is coated for SOCS observations
Coating		Multilayer	
Sensor / detector			
Type		MCP + phosphor screen + APS read-out	Same detectors as EUS Unit
Spectral channel 1 (detector 1)			
Most intense spectral lines	nm	103.2-103.7	
Instantaneous FOV		22 arcsec $\times$ 2.5 deg	
Number of visible slits		4	
Binning factor		3 $\times$ 13	

METIS
EID - PART B

REF: INAF/OATO NR. 94
DATE: 15-JAN-2008
ISSUE 1
page 33 of 108

Image format	pixel	682 (spectral) × 157 (spatial)	
Spectral resolving element	pm/pixel	18	
Spatial resolving element	arcsec/pixel	57	
Spectral channel 2 (detector 2)			
Most intense spectral line	nm	121.6	
Instantaneous FOV		22 arcsec × 2.3 deg	
Number of visible slits		4	
Binning factor		4 × 14	
Image format	pixel	512 (spectral) × 146 (spatial)	
Spectral resolving element	pm/pixel	20	
Spatial resolving element	arcsec/pixel	57	
Spectral channel 3 (detector 3)			
Most intense spectral line	nm	30.4	
Instantaneous FOV		22 arcsec × 2.0 deg	
Number of visible slits		2	
Binning factor		16 × 17	
Image format	pixel^2	128 (spectral) × 120 (spatial)	
Spectral resolving element	pm/pixel	11	
Spatial resolving element	arcmin/pixel	1.0	
Mechanisms			
		Detector doors (single shot TBC)	

3.3.5 Instrument Requirements to Satellite

To suitably occult the disk of the Sun to observe the corona, the instrument line of sight (ILS) of COR (which corresponds to the ILS of METIS) has to point to the Sun center with an accuracy of a few arcseconds. Even if this accuracy can be reached during the alignment of METIS on the S/C (i.e. co-alignment between the COR boresight direction and the $+X_{Opt}$ of the S/C), it is not sure that this will be maintained after launch, as arcminutes disalignment are possible (see Table 6 of RD-1). In order to avoid a complex mechanism to re-align METIS in flight, with a consequent increase of complexity and mass of the instrument, it is requested that the S/C assumes, in flight, as direction pointing at the Sun center the COR/METIS ILS (and not the $+X_{Opt}$ of the S/C). This requirement on the S/C should not affect any of the other payload instrument of Solar Orbiter.

The METIS instrument has not an axial symmetrical configuration, and has a preferred orientation with respect to the S/C. In particular, EUS has to have the capability of scanning the solar disk along the East-West direction; moreover, SOCS has to realize the spectrum of the West side corona. This implies that the METIS optical bench has to be parallel to the Sun E-W direction (that is parallel to the X-Y plane of the S/C). Moreover, with the present optical METIS configuration, to allow SOCS to observe the West corona METIS should be mounted on the –Z panel of the S/C (with ±Z panel, we mean the S/C panel perpendicular to the Z_{Opt} axis as defined in section 4.3.1.2 of RD-1, "open" on the ± axis versus). However, a location on the +Z panel of the S/C is also possible, designing METIS in a mirror-like configuration with respect to the present one.

For safety reasons of the COR element, it is necessary to insert the extended external occulter when the S/C is off-pointing from the Sun center. It will be necessary to foresee a safety flag (TBC) to be sure that, if the S/C is at perihelion, the COR extended occulter will be inserted when the S/C is off-pointing from the Sun center.

In addition, in the actual COR configuration, the extended external occulter has been sized to be able to shadow the COR entrance aperture for S/C off-setting up to 1.25° (see the note in section 4.3.1.2 of RD-1) but only after the first perihelion. To avoid the need of switching off COR in case of S/C off-center pointing during the first perihelion only, a maximum offset angle of 1.20° should be realized.

For the same safety reason for the COR element, it is required that the S/C immediately communicates to METIS any possible situation of anomalous off-pointing, in order to switch off the detectors to prevent possible damages of the system.

3.4 Operational modes

The functional operating modes of the METIS suite can be subdivided (TBC) in:

- OFF
- SAFE: Safe PROM initialized and running; operational HK generated; configuration up/down-loading possible
- STANDBY: S/W up and running; channels waiting for TC from MMPU
- TEST: mainly used on ground, but implementation in-flight could be possible for subsystem testing
- SCIENCE (observational): one or more channels acquiring science or calibration data

The SCIENCE modes defined hereafter are adopted to address the scientific objectives described in section 3.1. These modes, subdivided per each METIS element, are reported in Table 3.3.

Table 3.3. List of METIS SCIENCE modes.

METIS Element	Channel	Observational mode ID	Pointing	Observation Product
COR	Visible & UV Imaging Coronagraph	COR-SC-UV	Sun Center (SC)	Simultaneous images in HI Ly α 121.6 nm and polarized visible light
COR	Extreme UV Imaging Coronagraph	COR-SC-EUV	SC	He II Ly α 30.4 nm monochromatic images
COR	Visible and UV Imaging Coronagraph	COR-OP-UV	OP	Simultaneous images in HI Ly α 121.6 nm and polarized visible light
COR	Extreme UV Imaging Coronagraph	COR-OP-EUV	OP	He II Ly α 30.4 nm monochromatic images
EUS	Disk Extreme Ultraviolet Spectrometer	EUS-D	SC	EUV rasters on disk (emission lines in the range 96.8-158 nm)
EUS	Off Limb Extreme Ultraviolet Spectrometer	EUS-L	OP	EUV rasters on disk (emission lines in the range 96.8-158 nm)
SOCS	Near-limb Extreme Ultraviolet Spectro-Coronagraph	SOCS	[OFF when OP East of Sun Center]	EUV coronal spectro-images OVI doublet, HI Lyα, He II Lyα

METIS
EID - PART B

REF: INAF/OATO NR. 94
DATE: 15-JAN-2008
ISSUE 1
page 35 of 108

4. Interface definition

4.1 Definition of Instrument Identification and Labelling

Each METIS unit will bear a unit identification label prepared following the indications given in section 4.1 of RD-1.

4.2 General design requirements

4.2.1 Standard metric system

Drawings, specifications and engineering data will use the International System (SI) Metric Standard, with the exceptions allowed in the ECSS-E-30 Part 1A – Table E-3 and 5. The key and derived units shall be specified in:
- Dimensions in millimeters [mm]
- Angles in degrees
- Temperatures in degrees Celsius
- Power / Heat in Watts [W]
- Energy in Joules [J]
- Mass in kilogram [kg]
- Magnetic field in Tesla [T]
- Time in seconds [s]
- Electric current in Ampere [A]
- Amount of substances in moles
- Luminous intensity in candelas

4.2.2 Lifetime requirements

Design lifetime requirements are applied (if not specified differently elsewhere in the documentation for mechanical, thermal and electrical design) with respect to environmental influences and use conditions.

Where the design margin is required for demonstration of resistance to failure modes, a factor of two times the nominal life time shall be included as a minimum.

In the frame of the instrument design the following life time requirements will be made applicable to all parties involved in the instruments:
- The shelf-life time will be compatible with a launch delay of 2 years from the nominal launch date (Ground Environmental Influence)
- The overall instrument life time will be compatible with the nominal mission duration of 9 years in space.
- An extended operational life time of 2 years beyond the nominal mission life is desirable. Provided technically and financially feasible the payload design will be compatible with this goal (Space Environmental Influence and Use Conditions).
- For items which degrade with usage the life time will be two times the nominal operational life time. Exceptions are the mechanisms where specific requirements apply.

A summary of life time requirements is contained in Table 4.1.

Table 4.1. Summary of life time requirements.

TBD months	Nominal lifetime	Ground
+ 2 years	Launch delay	Ground
+9 years	Nominal mission	Space
+2 years	Extended mission	Space

METIS
EID - PART B

REF: INAF/OATO NR. 94
DATE: 15-JAN-2008
ISSUE 1
page 36 of 108

4.2.3 Maintainability

The equipment will be designed to require a minimum of special tools and test equipment to maintain calibration, perform adjustment and accomplish fault identification.

Items to be removed before flight (red tag) will be visible after integration with the spacecraft.

Items requiring integration for safety, logistical or life reasons, close to launch, will be accessible without removing any equipment from the spacecraft.

Items which require adjustment, servicing or maintenance before launch shall be accessible without removing any equipment from the spacecraft.

4.2.4 Fault tolerances

The METIS design will use redundancy as the main means of designing fault tolerance.

In the event of a failure METIS will not automatically reconfigure in order to continue operations.

METIS will go to a safe mode in the event of a failure and TM records of the fault will be transferred to the spacecraft DMS.

Recovery from safe mode will be done through ground telecommand.

4.3 Definition of coordinate system for instrument and instrument units

METIS will have a right-handed Cartesian coordinate system to provide a local reference system (Unit Reference Frame, URF) to describe its physical properties.

A possible option for the definition of the URF system follows:

- the origin is located in the centre of the reference hole on the interface plane
- the mounting plane is the plane of the unit that is to be attached to the spacecraft and it shall contain the X_{URF} and Y_{URF} axis
- the $+Z_{URF}$ axis is normal to the mounting plane in the direction from the mounting plane to the unit
- the Y_{URF} axis should pass through the centre of at least one other mounting hole in addition to the one located at the origin.

The definition of the URF for METIS is shown in Figure 4.1. An analogous frame is defined for the METIS electronics box (MPPU) which is to be separately installed on the satellite.
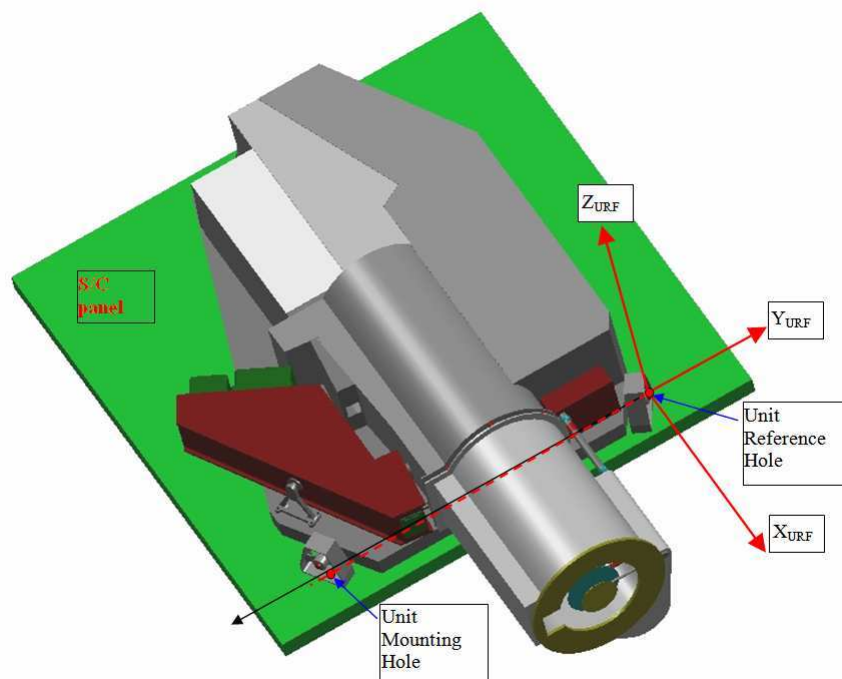
Figure 4.1. *Definition of the METIS URF*.

METIS
EID - PART B

REF: INAF/OATO NR. 94
DATE: 15-JAN-2008
ISSUE 1
page 37 of 108

4.4 Definition of Instrument Location and Alignment

4.4.1 Instrument Location

METIS requires a solar exposure, so it has to be located behind the heat shield.

As already mentioned in section 3.3.5, METIS needs a suitable location on the S/C. It can be mounted either on the –Z (with the present METIS optical configuration, see Figure 4.2) or +Z panel of the S/C (with ±Z panel, we mean the S/C panel perpendicular to the Z_{Opt} axis defined in section 4.3.1.2 of RD-1, "open" on the ± axis versus). The second option is applicable with a METIS configuration which is a mirror-like with respect to the present one.
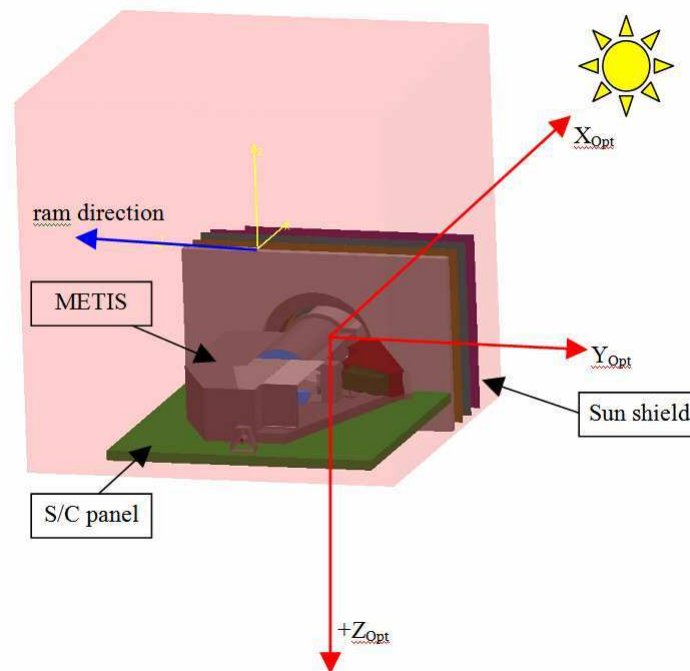
Figure 4.2. Example of METIS location on SO.

4.4.2 Instrument Alignment Requirements/Stability

The PI will specify with respect to the URF and in accordance to the pointing definitions:
- the ILS
- the FOV
- the UFOV
- the Vertex

The PI will provide the transformation matrix defining the ILS with respect to the METIS alignment references (alignment cube) for further inclusion in the alignment and pointing budgets at system level.

The PI will define the acceptable accuracy, knowledge and stability at 95% confidence level (2-σ) in terms of azimuth and elevation of the ILS with respect to the Spacecraft Mechanical Build Axes or other Payload units (co-alignment).

The PI will define the misalignment and in flight stability of the ILS with respect to the instrument alignment cube.

METIS
EID - PART B

REF: INAF/OATO NR. 94
DATE: 15-JAN-2008
ISSUE 1
page 38 of 108

These values, in correlation with the instrument internal (including mounting error) alignment accuracy, knowledge and stability will be used to compute the mechanical mounting accuracy knowledge requirement of the unit.

An optical reference system will be employed to determine and verify the required angular and positional alignment as well as the co-alignment of the three elements of METIS.

For any unit equipped with an optical reference cube, the normal to the faces of that cube will define the UORF. The instrument reference cubes will be mounted on a fixed part of the instrument structure. Their positions will be agreed with ESA / prime contractor in order to account for System level integration constraints.

METIS will have to be actively aligned with respect to the spacecraft optical axes. The means to adjust the unit (i.e. shims, screws, eccentrics...) will be considered as part of the mechanical interface.

In addition a description of the adjustment method (including the value of the minimum and maximum tilt angle achievable) and of the adjustment hardware used for that purpose will be submitted to the ESA Project Office / Prime for approval.

It will be demonstrated that the adjustment activities will not introduce stresses in the instrument and in the spacecraft structure (or that the stresses are quantified and stay below an acceptable level).

The PI will determine the position of the alignment cube with an accuracy of ±0.1 mm with respect to the position of the internal scientific relevant detectors. The PI will ensure that the faces of the alignment cube are representative for the ILS. The maximum allowed deviation will be less than 1 arcmin.

The acceptable, from a scientific point of view, METIS pointing error in terms of APE, RPE, PDE, AME are summarized in Table 4.2.

Table 4.2. Acceptable METIS pointing errors.

Pointing parameters	Line of sight	Around line of sigth
APE	< 2 arcmin	< 20 arcmin
PDE	< 1 arcmin/10 days	< 10 arcmin/10 days
RPE	< 1 arcsec/10 s < 0.5 arcsec/10 s (goal)	<2 arcsec/10 s
AME	No req	<3 arcmin in 10 s
Co-alignment of EUS with EUI and VIM	1 arcmin	2 arcmin

The S/C guarantees a short-term pointing stability better than 1 arcsec over 10 s (2-σ) (see Table 6 of section 4.4.2.3 of RD-1). Since this is the typical exposure time we foresee for the on-disk observations with 1 arcsec spatial resolution, to avoid worsening the expected spatial resolution performance, a better pointing stability, with a RPE of the order of at least 0.5 arcsec over 10 s would greatly be preferred. Longer exposure times (e.g. 60 s) will lead to dynamical blurring that are larger than that induced by the pointing instability (1 arcsec at 0.22 AU is equivalent to 150 km and typical motions in the transition region and corona are between several and several tens of km/s), therefore no image stabilization is required.

For coronal spectral acquisitions, the spacecraft pointing stability even for the long exposure times foreseen for SOCS is anyway better than needed according to the spatial resolution expected in the corona.

The EUS element needs to be co-aligned with EUI and VIM within 1 arcmin along the line of sight.

The PI will define the need for in-flight alignment calibration with respect to the AOCS reference sensors or with respect to other instruments.

EUS needs to be co-aligned with EUI and VIM within 1 arcmin along the line of sight. In fact EUI will provide crucial information on the spatial morphology and temporal evolution of the targets spectroscopically studied by METIS. On the other hand, VIM will provide high-resolution data on the photospheric magnetic fields and relevant extrapolations in corona.

METIS
EID - PART B

REF: INAF/OATO NR. 94
DATE: 15-JAN-2008
ISSUE 1
page 39 of 108

As already mentioned in section 3.3.5, we require that the maximum spacecraft offset pointing does not exceed ±1.20° with respect to the Sun center direction (only during the first perihelion) to avoid disk light entering the COR element optical path.

4.5 External Configuration Drawings

The external configuration of METIS instrument is shown in Figure 4.3 and Figure 4.4. The main dimensions of the external envelope are provided in Figure 4.5. The instrument power supply and data handling electronics is contained in a box (the METIS Processing & Power Unit) having an envelope of $220\times250\times350$ mm^3.
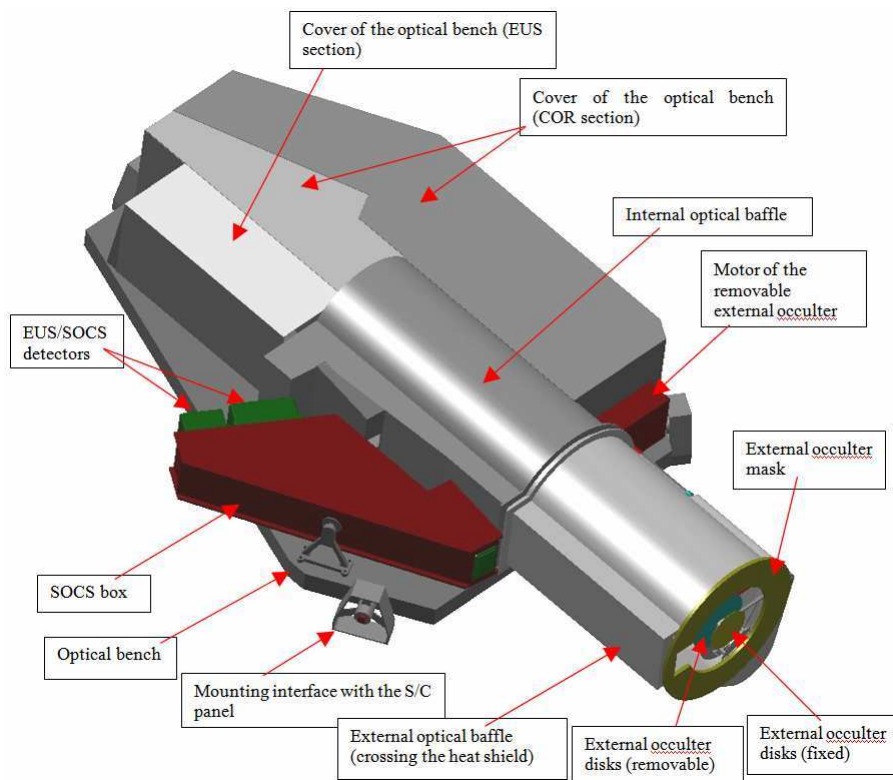
Figure 4.3. View of METIS external configuration.

METIS
EID - PART B

REF: INAF/OATO NR. 94
DATE: 15-JAN-2008
ISSUE 1
page 40 of 108
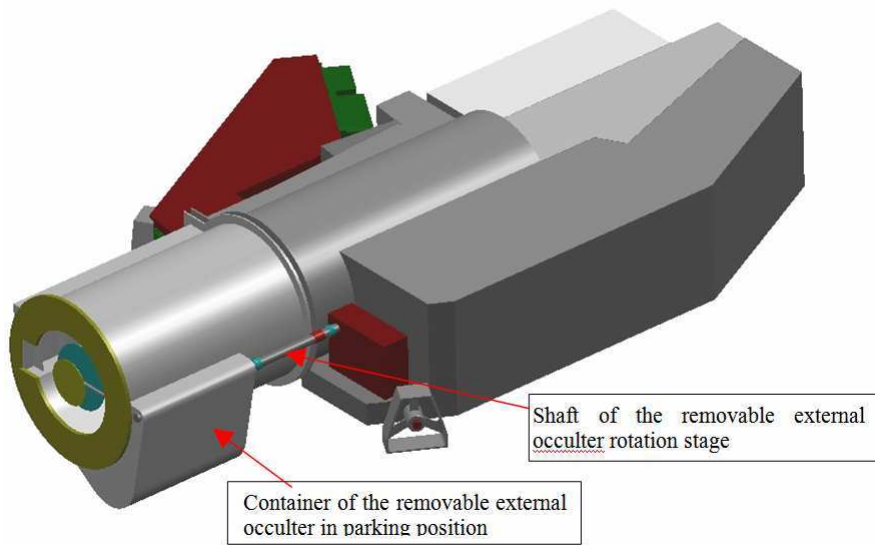
Figure 4.4. Different view of METIS external configuration.
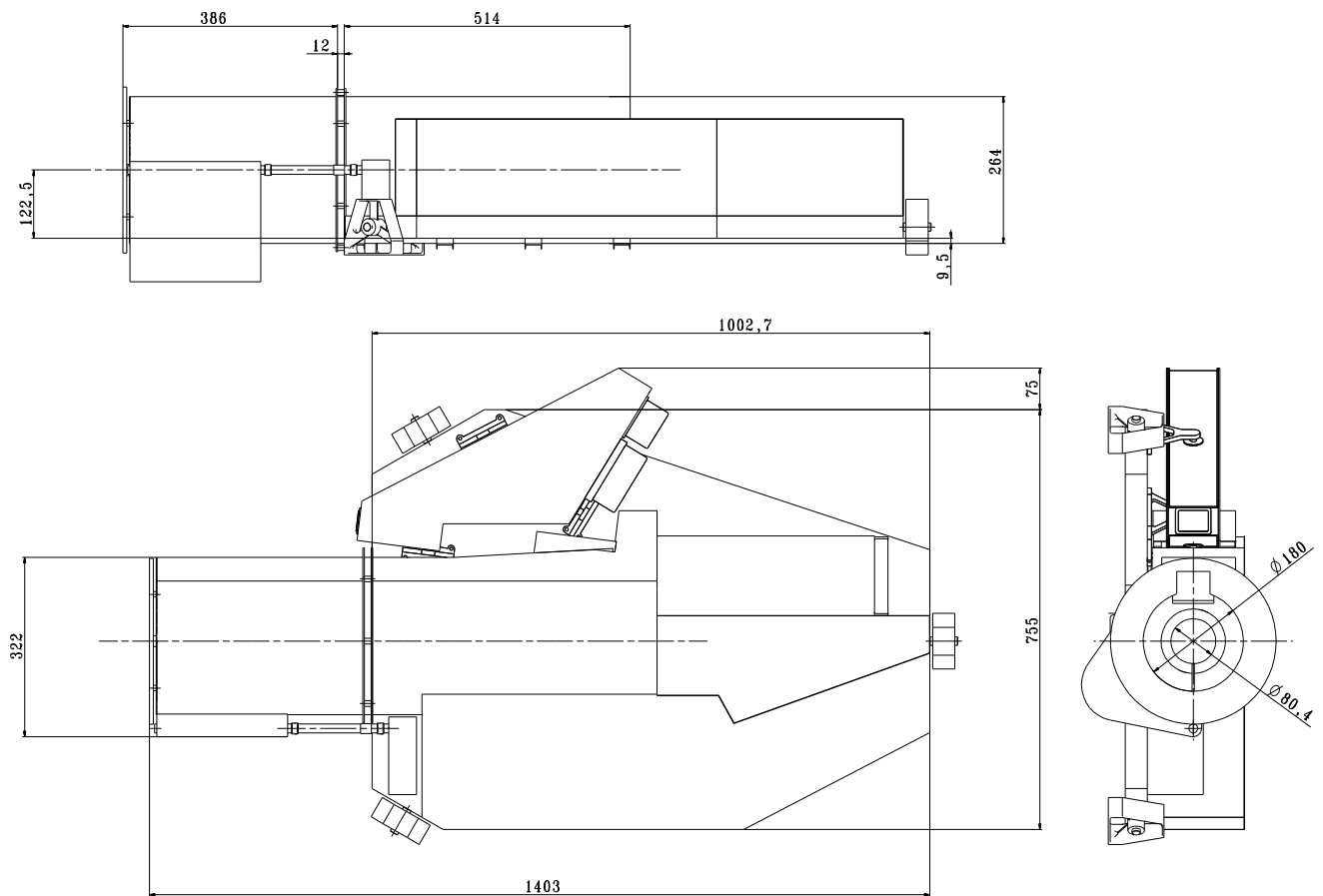
Figure 4.5. METIS external envelope main dimensions.

METIS
EID - PART B

REF: INAF/OATO NR. 94
DATE: 15-JAN-2008
ISSUE 1
page 41 of 108

4.6 Instrument configuration and mechanical interfaces

4.6.1 METIS design and configuration description

The three METIS elements, namely COR, EUS and SOCS, will be integrated on a common bench that constitute, from a system point of view, a single interface towards the spacecraft for thermal, mechanical, electrical and optical aspects. This is aimed also to guarantee the needed stability in coalignment between the optical heads, that is necessary for best coordinated operations and data analysis, and between the instrument and the other SO payloads.

The common optical bench will provide to the optical channels:
- adequate stiffness to satisfy alignment and co-alignment stability requirements;
- adequate thermal conductivity to allow heat dissipation toward the satellite.

From an electrical point of view, two functions are individuated as common to all the optical heads, and are implemented at a suite level to avoid duplication, namely: power supply, main electronics. The first is devoted to supply all the subsystems with the required power, providing a common set of voltages that has been individuated. The second is mainly devoted to data compression, instrument control (managing individual and coordinated operations of the various subsystems) and S/C interface. All the electronics will be integrated in the METIS Processing & Power Unit (MPPU), separated from the optical bench, and that will be suitably located on the S/C.

The integrated approach will provide simplification of the external interface, not only for integration aspects, but also for the thermal control of all system and for the heat rejection.

In the following sections a description of the optical design and performance of each of the METIS channel is given.

4.6.1.1 COR element description

COR is an externally occulted coronagraph designed for:
- broad-band polarization imaging of the visible K-corona;
- narrow-band imaging of the UV corona in the HI Lyman-α, 121.6 nm line;
- narrow-band imaging of the EUV corona in the HeII Lyman-α, 30.4 nm line;

in an annular FOV between 1.2 and 3.0 solar radii, when HELEX perihelion is 0.226 AU. Between 1.6 and 4.0 solar radii when at 0.3 AU. The concept is shown in Figure 4.6.

The coronagraph critical issue of solar disk light rejection is taken care of by means of a novel optical design for a reflecting coronagraph, widely used in traditional externally occulted coronagraphs. This optical design has been thoroughly studied in the design of the SCORE coronagraph developed for the sub-orbital mission HERSCHEL [1-4].

A combination of multilayer coating of the mirrors, optimized to enhance reflectivity in the EUV He line, and of band-pass filters contribute to the capability of imaging the solar corona in three different wavelength bands by means of a single telescope. These mirrors are coated with multilayer optimized for 30.4 nm, but still have good reflectivities at 121.6 nm and in the visible.

The visible light channel (VLC) and the UV and EUV channels (UVC and EUVC) are separated after the secondary mirror. In the UV mode, a multilayer filter reflects visible light and transmits narrow-band UV HI line. In this mode, both channels work simultaneously. In the EUV mode, the multilayer filter is replaced, by means of a two-position mechanism, by a low-pass aluminium filter that transmit the EUV HeII line. In this mode the VL channel is not operative.

The visible light channel includes an achromatic polarimeter for measuring the linear polarized brightness.

![INAF logo] ISTITUTO NAZIONALE DI ASTROFISICA
NATIONAL INSTITUTE FOR ASTROPHYSICS

METIS
EID - PART B

REF: INAF/OATO NR. 94
DATE: 15-JAN-2008
ISSUE 1
page 42 of 108
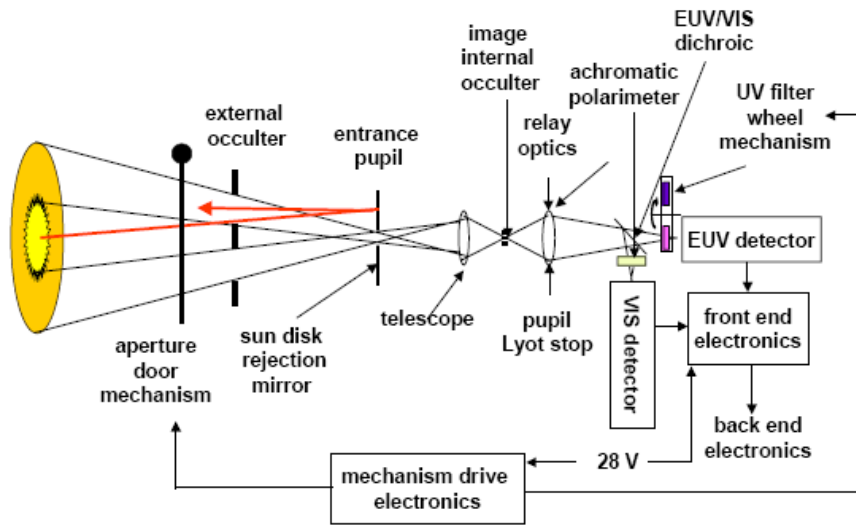
Figure 4.6. Conceptual block diagram of the coronagraph.

COR has the capability of being operative also during the spacecraft off-pointings by means of a mechanism that inserts an additional external occulter system, called extended external occulter (EEO), which is large enough to prevent disk light from entering the coronagraph aperture stop. In case of off-pointing, COR FOV will not be symmetrical with respect to Sun center.

4.6.1.1.1   COR Optical design and performance

Light enters COR through the external occulter (EO) aperture that provides the Sun disk occultation. EO is a multiple disk system that ensures both thermal protection for the optics and better stray-light rejection. An annular sector shaped Sun-disk rejection mirror (M0) reflects back the disk light through the front aperture. The hole in M0, in the shadow of EO is the aperture stop through which the coronal light enters the telescope. The telescope consists of aspherical primary (M1) and secondary (M2) mirrors in an off-axis Gregorian mount.

The image of EO produced by M1 is blocked by a stop called internal occulter (IO). Its function is to block the solar disk light diffracted by EO. In addition, M1 forms an image of the aperture stop on the plane of M2, that is collected by a light trap behind M2, which acts as the Lyot stop. This light trap performs the final stray light rejection.

The coronal radiation reflected by the secondary mirror impinges the filter wheel. The filter wheel (FM) accommodates two filters: a narrow band multilayer filter (HF) optimized to transmit the HI 121.6 nm line, and to reflect the visible light, an aluminum low pass filter (HeF) to select the HeII 30.4 nm line. With HF, the UV HI 121.6 nm corona and the VL K-corona are imaged simultaneously, respectively on the UV detector (UVD) and on the VL detector (VLD). With HeF, only the EUV HeII 30.4 nm is imaged on the UVD. In the VL channel the radiation is processed by a linear polarization analyzer (PL).

The optical specifications of the proposed coronagraph are given in Table 4.3; Figure 4.7 shows an optical schematics of COR and Figure 4.8 gives a view of COR optical path inside METIS.

METIS
EID - PART B

REF: INAF/OATO NR. 94
DATE: 15-JAN-2008
ISSUE 1
page 43 of 108
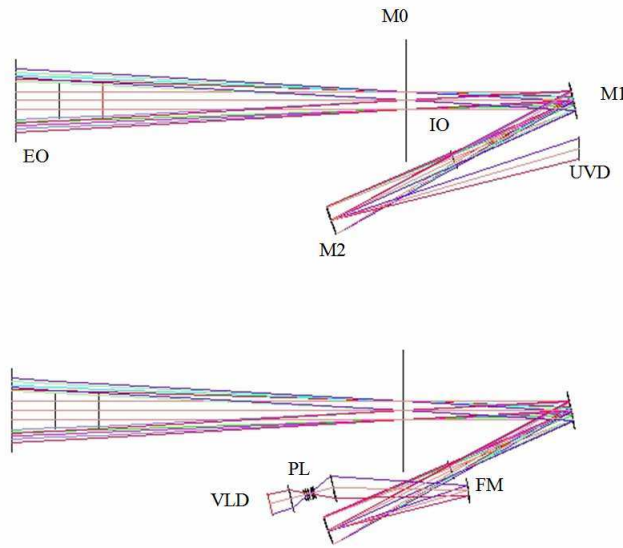
Figure 4.7. COR Optical path diagram. EUV and UV path (top); VL path (bottom).
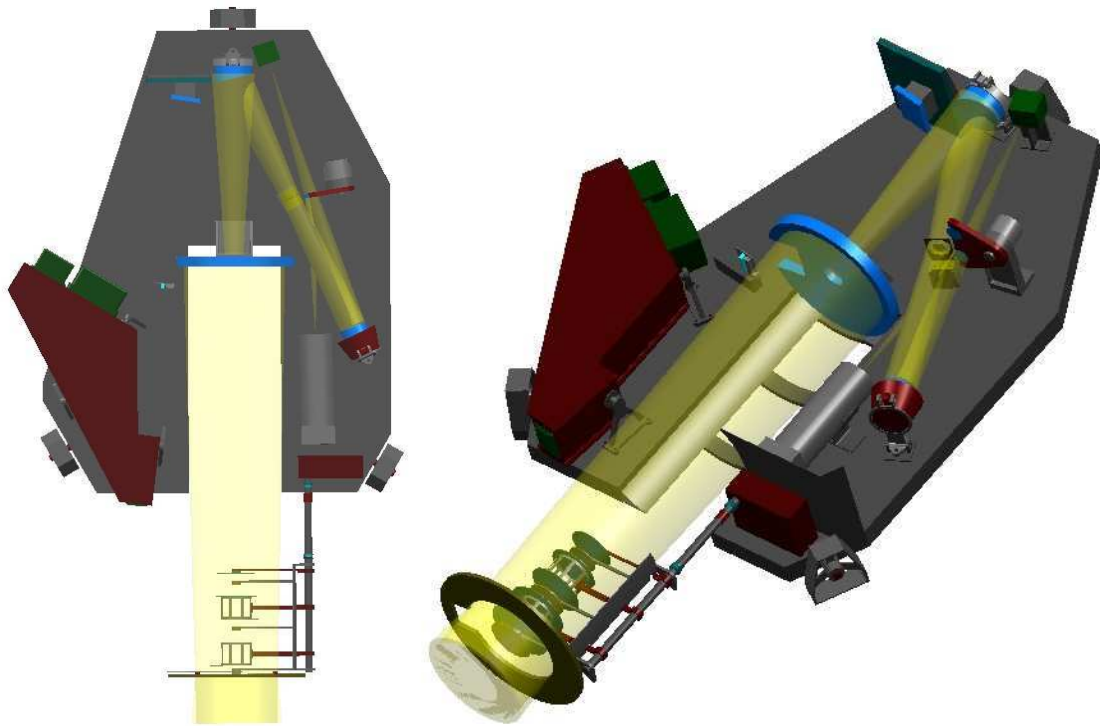
Figure 4.8. COR optical path inside METIS.

Table 4.3. COR optical specifications.

Field of View	Annular Sun-centered $1.2 - 3.0$ R$_\odot$ @ 0.226 AU $1.6 - 4$ R$_\odot$ @ 0.3 AU
Telescope type	Externally occulted off-axis Gregorian
Effective focal length	400 mm

METIS
EID - PART B

REF: INAF/OATO NR. 94
DATE: 15-JAN-2008
ISSUE 1
page 44 of 108

External occulter (EO)	Annular sector[3]: inner Ø: 80.3 mm, outer Ø: 180 mm
	Triple disk Ø (in mm): A1: 76.14, A2: 71.8
	Distance EO-A1 and A1-A2: 100mm
Extended external occulter (EEO)	Annular sector: inner Ø: 108.4 mm outer Ø: 180 mm
	disks Ø (in mm): A1: 106.28, A2: 103,7 A3: 100.6, A4: 97
	Distance EO-A1, A1-A2, A2-A3, A3-A4: 50mm
Distance EO-M0 (EEO-M0)	900 mm (890 mm)
Sun-light Rejection mirror (M0)	Toric annular sector[4]: Ø: 264 mm, Curvature radius: 900 mm
	Substrate: SiC Coating: SiC, Thickness: 12 mm
Stop aperture	Ø: 40 mm
Distance M0 – M1	400 mm
Primary mirror (M1)	Off axis ellipsoidal: Ø: 80 mm , off-axis: 105 mm,
	Curvature radius: 480 mm, conic: -0.543
	Substrate: quartz Coating: Multilayer, Thickness: 45 mm
Distance M1 – M2	600 mm
Secondary mirror (M2)	Off axis ellipsoidal: Ø: 57.4 mm (TBC) , off-axis: 155.5 mm,
	Curvature radius: 449.9 mm, conic: -0.136
	Substrate: quartz Coating: Multilayer, Thickness: 60 mm
Internal occulter (IO)	Distance M1 – IO: 288.87 mm
	Annular sector: inner Ø: 21 mm, outer Ø: 40.4 mm
Filter mechanism (FM)	Distance M2 –FM: TBD mm
	HF: Al+MgF$_2$ HeF: Al
Distance M2 – UVD	600 mm
Spatial resolution	see Figure 4.9
Stray light levels	VL: < 10^{-9}
	UV, EUV: < 10^{-7}
Wavelength band-pass	VL: 450-650 nm
	UV HI (121.6 ± 10) nm
	EUV HeII (30.4 ± 2) nm
UV Detector	IAPS
	Scale factor: 0.52 arcsec/µm; 12.9 arcsec/pixel
	Image size: 50 mm (2048×2048) with 25 µm pixel size
VL Detector	APS
	Scale factor (TBC): 0.52 arcsec/µm; 12.9 arcsec/pixel
	Image size: 50 mm (2048×2048) with 25 µm pixel size

Stray light inside a coronagraph is mainly due to disk light entering EO and to disk light diffracted by the EO aperture. Disk light entering EO is rejected by M0, a toric shaped annular sector mirror whose central aperture is the stop aperture of the coronagraph. Disk light diffracted by EO is blocked by IO and the Lyot trap.

M0 is placed between EO and M1 and has the double scope of rejecting the solar disk light entering EO and minimizing the EO diffracted light reaching M1. Expected stray light level are reported in Table 4.3.

COR external occulter (EO) is a three disks system to perform the diffracted light apodization, following the state-of-the-art techniques for externally occulted coronagraphs. EO will receive a large direct thermal flux (TBD) at minimum perihelion (0.226 AU). Since the occulter aperture has to be clear at all directions toward the Sun the occulter must be approximately on the plane of the Sun shield.

A door that is part of the Sun shield closes the instrument when it is not operating to protect it and to reduce the thermal load in the spacecraft. EO is mechanically connected to the coronagraph, that is beneficial for the alignment.

---

[3] The annular sector has a decentred rectangular aperture that feeds both EUS and SOCS elements.

[4] The annular sector has a decentred rectangular aperture that feeds EUS element.

METIS
EID - PART B

REF: INAF/OATO NR. 94
DATE: 15-JAN-2008
ISSUE 1
page 45 of 108

COR extended external occulter (EEO) consists of a five disks system that will be inserted during S/C off-pointing in order to thermally protect COR telescope from disk light and to allow COR to operate also in this mode.

The baffle system interfaces EO to the telescope and must expand at an angle > 2.5 degrees in the direction away from the Sun, to prevent solar disk light to hit its surface, also in case of S/C off-pointing.

Optical performances of COR are given in terms of spatial resolution on the focal plane for all three channels. The effect of diffraction due to the vignetting of the entrance pupil by the external occulter is also evaluated and taken into account.

The optical aberrations in the East/West plane and in the North/South plane are not very different, therefore their average is taken. A plot of the spatial resolution (in pixel) as a function of heliocentric height is shown in Figure 4.9.
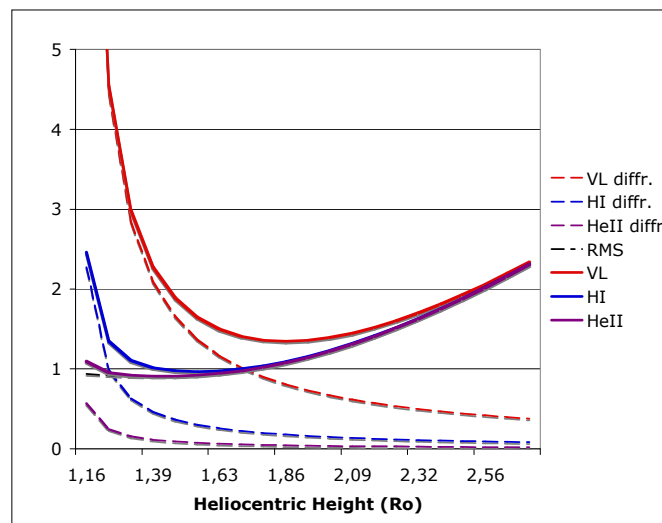
Figure 4.9. Spatial resolution as a function of heliocentric height for all three wavelength bands. The curves include the optical aberrations and an estimate of the diffraction.

References
1. Naletto, G., et al, Appl. Opt. **44**, 5046 (2005)
2. Landini, F., et al, Appl. Opt. **45**, 6657 (2006)
3. Romoli, M., et al., ESA **SP-641** (2007)
4. Fineschi, S., et al, Proc. SPIE **5901** (2005)

4.6.1.1.2   COR mirror optical coatings

Several ML structures can be considered to coat the coronagraph mirrors. Mo/Si has been already tested in several space experiments and provides long term stability, which is essential for successfulness of the space mission. In Figure 4.10 the theoretical performance of Mo/Si shows the presence of the needed multi-order reflectivity.

METIS
EID - PART B

REF: INAF/OATO NR. 94
DATE: 15-JAN-2008
ISSUE 1
page 46 of 108
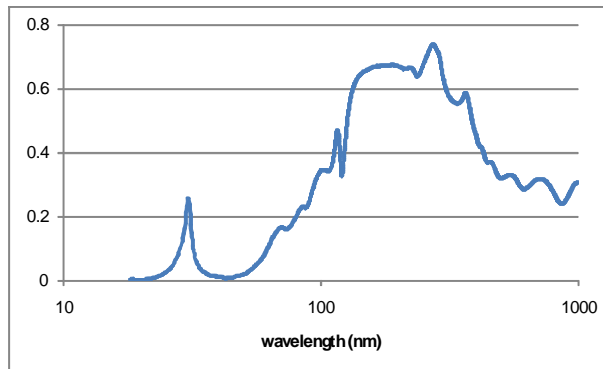
Figure 4.10. Si/Mo ML reflectivity versus wavelength.

But the baseline multilayer coating is the EUV optimized SiC/Mg with a cap layer reflecting visible and UV radiation. As it can be seen in Figure 4.11 this kind of multilayer shows a better reflectivity than the standard Mo/Si
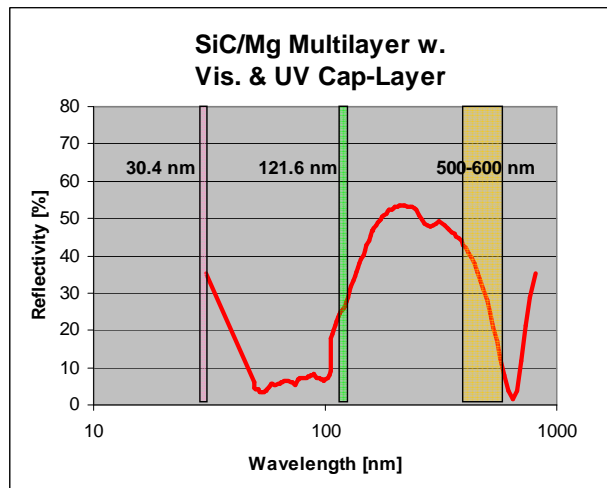
Figure 4.11. Reflectivity of SiC/Mg ML versus wavelength.

4.6.1.1.3   COR mechanisms

The mechanisms required by COR, in addition to the METIS aperture door mechanism which is S/C provided, are the following:

1. EEO mechanism (EEOM): this is a precision two-position mechanism to insert the EEO without mechanically interfering with the fixed EO
2. Internal occulter alignment mechanism (IOM): this mechanism will be necessary to adjust during the commissioning phase the position of the internal occulter to compensate for external occulter misalignment and S/C off-pointing. This mechanism is designed to adjust the IO position along the axes perpendicular to the local optical axis.
3. Filter exchange mechanism (FEM): this is a precision two positions mechanism, that accommodates the HF and the HeF, to switch from H-VL observation mode to He observation mode.
4. Polarizer rotation mechanism (PRM) (if LCVR is not adopter): this is a mechanism needed in the case a traditional polarimeter will be used. It will drive a rotating half wave retarder plate inside a range of about +/- 100° with 1° resolution.

METIS
EID - PART B

REF: INAF/OATO NR. 94
DATE: 15-JAN-2008
ISSUE 1
page 47 of 108

The positioning accuracy, operation range and resolution of COR mechanisms relative to the local reference system (LRS)[5] are given in Table 4.4.

Table 4.4. COR mechanism positioning accuracy, range and resolution.

Item		EEOM	IOM	FEM	PRM
Positioning accuracy (LRS)	Δx (mm)	0.2	0.05	1	1
	Δy (mm)	0.2	0.05	1	1
	Δz (mm)	1.0	0.2	TBD	1
	ΔM_x (°)	0.2	0.1	TBD	1 (TBD)
	ΔM_y (°)	0.2	0.1	TBD	1 (TBD)
	ΔM_z (°)	-	1.0	-	1
Tuning Range (LRS)	Δx (mm)	-	±5.0	-	-
	Δy (mm)	-	±5.0	-	-
	Δz (mm)	-	-	-	-
	ΔM_x (°)	-	-	-	-
	ΔM_y (°)	-	-	-	-
	ΔM_z (°)	120 (TBD)	-	TBD	±100
Tuning Resolution (LRS)	Δx (mm)	-	0.005	-	-
	Δy (mm)	-	0.005	-	-
	Δz (mm)	-	-	-	-
	ΔM_x (°)	-	-	-	-
	ΔM_y (°)	-	-	-	-
	ΔM_z (°)	-	-	-	-

4.6.1.1.3.1   Extended external occulter insertion mechanism (EEOM)

The extended occulter insertion mechanism is a two position precision rotating mechanism. Its mechanical characteristics are summarized in Table 4.7.

Table 4.5. Mechanical characteristics of the filter mechanism.

Extended external occulter insertion mechanism	Requirement
Mechanism positions	2
Rotation angle	60°
Mechanism mass	350 g

This mechanism is a simplified version of the EUS mirror scan mechanism and is essentially the same mechanism used to exchange the filters (see section 4.6.1.1.3.3).

The heritage for this mechanism is coming from the scan mechanisms which are working on the following flying instruments: VIMS spectrometer (Cassini), VIRTIS spectrometers (Rosetta, VEX, Dawn) and UVCS (SOHO).

4.6.1.1.3.2   Internal occulter mechanism (IOM)

This mechanism will be necessary to adjust the position of the internal occulter to compensate for possible external occulter misalignment during the mission life. The mechanism is designed to adjust the internal occulter position along the two axes perpendicular to the local optical axis. The mechanism is a repeatable

---

[5] LRS has the origin in the vertex of the optical component, as defined by the optical ray tracing; the z-axis defined by the local optical axis; the y-axis parallel to COR optical bench; and the x-axis to complete the right-handed set.

METIS
EID - PART B

REF: INAF/OATO NR. 94
DATE: 15-JAN-2008
ISSUE 1
page 48 of 108

two axis positioning mechanism type. In Table 4.6 the mechanical characteristics of the IOM are summarized.

Table 4.6. Mechanical characteristics of the IOM.

IOM mechanism	Requirement
IOM mechanism type	repeatable two axis positioning mechanism
Mechanism mass	350 g

For this mechanism we can consider two possible solutions:
- use of linear actuator for each axis
- use of two motors acting each through a cam in the two perpendicular directions. In this way the design of the cam can be optimized in order to obtain the required resolution.

4.6.1.1.3.3 Filter exchange mechanism (FEM)

COR observes three wavelength bands with the same telescope. This capability is obtained by means of mirrors ML coating whose reflectivity is optimized for the HeII 30.4 line, but with good performance at all wavelengths, and of band pass filters.
1. HI 121.6nm band pass filter (HF): a narrow band Al/MgF_2 filter selects a wavelength band of about 10 nm width, centered at 121.6 nm. This filter acts as a beam splitter on COR, reflecting the visible light and transmitting the HI line. The solar blindness of the intensified detector will remove the residual off-band visible light radiation that reaches the UV detector.
2. HeII 30.4 low pass filter (HeF): when the filter mechanism (FM) is switched to helium mode a double low pass thin aluminum filter, replaces the HF. The action of HeF combined with the multilayer reflectivity contribute to reject the longer wavelength off-band radiation. The use of two HeF minimizes the effects of filters microholes on the coronal image. Filter no. 2 is required for HeII imaging.
3. VL band pass filter (VLF): a visible light interference band pass filter is included in the polarimeter group to limit the visible light continuum for a correct operation of the achromatic polarimeter.

The filter mechanism is a precision rotating mechanism (two position for the HF and HeF filters). Its mechanical characteristics are summarized in Table 4.7.

Table 4.7. Mechanical characteristics of the filter mechanism.

Filter exchange mechanism	Requirement
Mechanism positions	2
Filter number	2
Rotation angle	90°
Mechanism mass	350 g

This mechanism is a simplified version of the EUS mirror scan mechanism.
The heritage for this mechanism is coming from the scan mechanisms which are working on the following flying instruments: VIMS spectrometer (Cassini), VIRTIS spectrometers (Rosetta, VEX, Dawn) and UVCS (SOHO).

4.6.1.1.3.4 Polarizer rotation mechanism (PRM) (if LCVR is not adopted)

The VL path is provided with a polarimeter assembly to observe the linearly polarized component of the K-corona. The baseline configuration of COR foresees an electro-optical polarimeter, based on nematic LCVR.

METIS
EID - PART B

REF: INAF/OATO NR. 94
DATE: 15-JAN-2008
ISSUE 1
page 49 of 108

The control hardware is compact, light-weight, with limited power consumption. This is a clear advantage over more classical methods of mechanical modulation by rotation of polarizing elements.

This device has not been space qualified yet; in case of qualification delay or unavailability, a half wave retarder plate (HWRP) followed by a fixed linear polarizer acting as analyzer, will be necessary. The HWRP mechanism will drive a HWRP inside the optical path. This optional solution will require the addition of a color filter in front of the polarimeter assembly. Its mechanical characteristics are summarized in Table 4.8.

Table 4.8. Mechanical characteristics of the HWRP mechanism.

HWRP mechanism	Requirement
HWRP mechanism type	rotating
HWRP mechanism rotation range	± 120°
HWRP mechanism angular resolution	1°
Mechanism mass	500 g

This mechanism could be a simplified version of the EUS mirror scan mechanism or a direct application of a hollow core motor with suitable dimension.

The heritage for the hollow motor is mechanism is coming from the scan mechanisms which are working on the following flying instruments: VIMS spectrometer (Cassini), VIRTIS spectrometers (Rosetta, VEX, Dawn) and UVCS (SOHO). The hollow motor solution has already been qualified for the STEREO mission.

4.6.1.1.4 COR detectors

The COR visible detector (VD) will be a custom developed Active Pixel Sensor (APS). The choice of an APS over a CCD is driven by the harsh radiation environment of SO. The characteristics of the sensor should be the following:

Table 4.9. Main characteristics of the COR visible detector.

Format	2k × 2k pixels
Pixel size	25 μm
Readout noise	≤ 5 e$^-$
Frame rate	0.1 Hz
Spectral range sensitivity	450 nm < λ < 900 nm
Dynamic range	16 bit
Fill factor (thinned back-illuminated)	100%
Snapshot shutter	

The most critical parameter with the currently available technology is the readout noise, which has to be smaller than 5 e$^-$. This point could be addressed with a specific 1-2 years R&D program. However, a readout noise of 10 e$^-$, which is in the current technological capability of European companies as for example E2V (UK), could be tolerable. Several suppliers could be available to develop a sensor with these characteristics.

Due to the relatively long acquisition frame period, the APS should be operated a low temperatures (of the order of –50 °C) and therefore should be equipped with a TEC device and a suitable radiator.

For this sensor, the ADC should be off-chip. Even if in this way the external electronics is more complex, having to include an analogical signal processing part, this allows more flexibility of ADC design, better radiation hardness options and less complexity of the sensor itself, allowing better performance in terms of noise. A block diagram of the detector and related electronics is shown in Figure 4.12.

METIS
EID - PART B

REF: INAF/OATO NR. 94
DATE: 15-JAN-2008
ISSUE 1
page 50 of 108
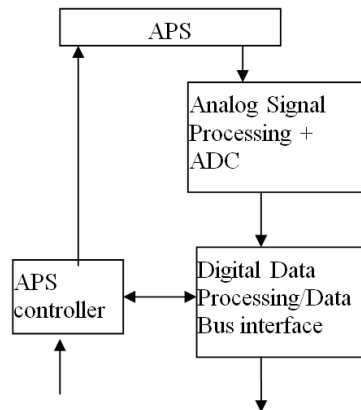
Figure 4.12. Block diagram of the COR visible detector and related electronics.

The COR-UV detector works in photon counting and will be of the same design of SOCS detectors, i.e. an IAPS (see section 4.6.1.3.4). The same APS sensor used for the SOCS detectors could be used: in fact the sensor format is the same ($2k \times 2k$), and the difference in the required pixel size (25 μm pixel size instead of 12 μm) can be overcome coupling a larger MCP intensifier (diameter > 50 mm) to the smaller sensor with a fiber optic taper of appropriate reduction ratio (2:1). Since the APS format is the same as the required detector format, there is no need to obtain sub-pixel resolution and the photon counting mode event centroiding requirement is minimal.

4.6.1.2 EUS element description

4.6.1.2.1 EUS optical design

The design goal for the spectrometer is to have a stigmatic system in a compact package with high throughput due to a minimum number of reflections. The concept is shown in Figure 4.13. The instrument consists of a single-element parabolic telescope which creates the image of the Sun on its focal plane. An entrance slit acts as the field stop to select the region of the Sun whose spectrum has to be acquired. A toroidal grating with variable-line-spaced grooves (TVLS grating) gives a stigmatic spectrum of each of the points along the slit height.
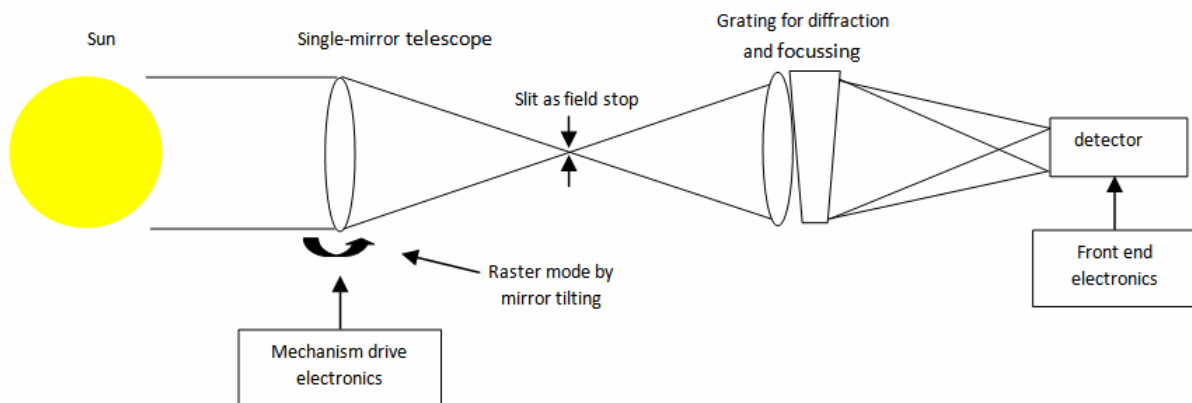
Figure 4.13. Conceptual block diagram of the spectrometer.

METIS
EID - PART B

REF: INAF/OATO NR. 94
DATE: 15-JAN-2008
ISSUE 1
page 51 of 108

Let us suppose to align the slit in the North-South direction. The region spectrally imaged on a single acquisition is a rectangular region with a narrow width in the East-West direction and a height in the North-South direction that is limited by the angular height of the slit itself. The spectral imaging of an extended area is obtained by rastering through the rotation of the primary mirror in the direction perpendicular to the slit (i.e. the East-West direction).

An optical schematic of the spectrometer is illustrated in Figure 4.14 and a view of the EUS optical path inside METIS in Figure 4.15. The entrance aperture, that is assumed to be the aperture on the heat shield, has a rectangular shape with size 50 mm (⊥ to the slit) × 60 mm (// to the slit). The telescope is placed 1250 mm far from the aperture. Since the heat shield is expected to be about 400 mm thick, the envelope of the optical design fits the <1 m class instrument. The pupil size is determined by a combination of the diffraction limit, geometrical aberrations, heat load and required light flux. An off-axis parabola primary mirror forms an image of the solar disk on its focal plane, where the entrance slit is placed. There is no secondary mirror, as e.g. with a Ritchey-Chretien design, and this helps maintaining a high effective area for a given aperture since the number of reflections is reduced to the minimum.
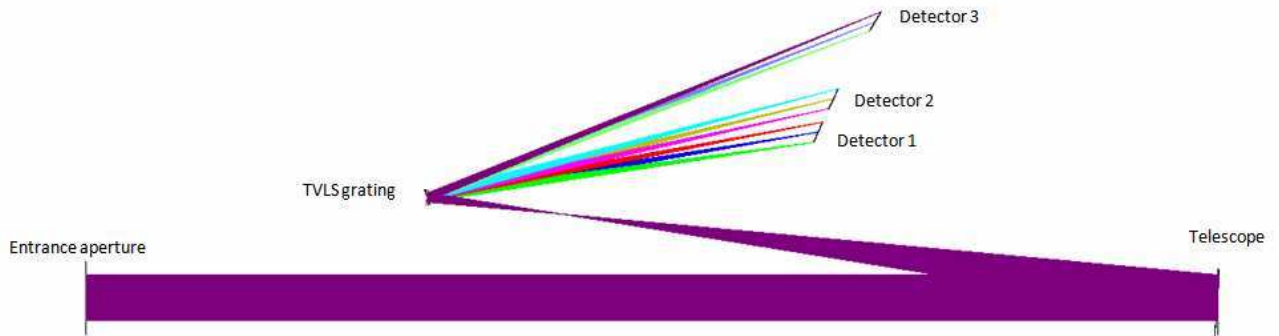
Figure 4.14. Scheme of the EUS optical configuration.

METIS
EID - PART B

REF: INAF/OATO NR. 94
DATE: 15-JAN-2008
ISSUE 1
page 52 of 108
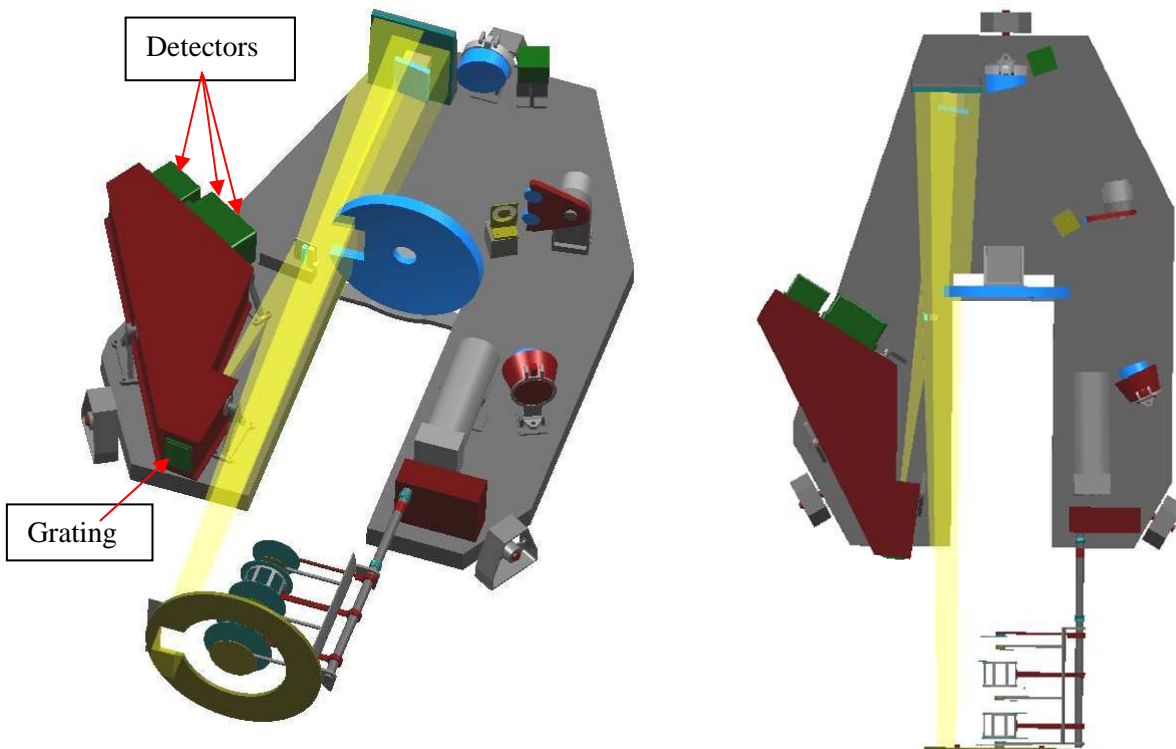
Figure 4.15. View of the EUS optical path inside the METIS suite.

The primary mirror is tipped to allow rastered images, that are exposures interlaced with mechanism movements to build up images simultaneously in selected wavelengths. The rastering is performed by a rotation of the mirror around an axis passing through its center and parallel to the slit. Although this is not the ideal rastering mechanism for a parabolic mirror, it gives good optical performance in a relatively broad angular range and is much simpler and safer than the ideal mechanism that would be a rotation around a pivot axis passing through the mirror focal point.

The slit presents a selected area of the solar image to the spectrometer whose core is the TVLS grating. The groove density along the grating surface is expressed as $\sigma(y) = \sigma_0 + \sigma_1 y + \sigma_2 y^2$, where the y coordinate spans along the surface in the direction perpendicular to the grooves with the origin on the grating vertex. Here σ_0 is the central groove density and σ_1 and σ_2 are the parameters of the ruling space variation. The TVLS grating design has been found to provide excellent off-axis imaging in configurations with magnification higher than unity, permitting high-quality performance in compact instrument packages [1,2]. Furthermore, it gives a flat focal surface in a broad spectral interval allowing the simultaneous acquisition of stigmatic images of spectral lines which are emitted by a broad range of plasma temperatures within the solar atmosphere. Three 2-D detectors are aligned on the spectral curve to acquire simultaneously the imaging spectra on six spectral intervals in the 1st and 2nd diffracted orders. We also expect observing third order lines on detector 3.

The optical parameters of the spectrometer are reported in Table 4.10. Six spectral intervals are simultaneously acquired on three detectors. The spatial resolving element ranges from 1.2 to 1.0 arcsec/pixel. The spectral resolving element corresponds to a velocity resolution of 18, 13 and 6 km/s respectively in channel 1, 2 and 3. These values can be definitely improved to a few km/s resolution by centroiding of the line profile.

INAF

ISTITUTO NAZIONALE DI ASTROFISICA
NATIONAL INSTITUTE FOR ASTROPHYSICS

**METIS
EID - PART B**

REF: INAF/OATO NR. 94
DATE: 15-JAN-2008
ISSUE 1
page 53 of 108

Table 4.10. EUS optical parameters.

ENTRANCE APERTURE	50 mm × 60 mm
TELESCOPE	Off-axis parabola
Incidence angle	3.6 deg
Mirror to slit distance	730 mm
Size	62 mm (⊥ to the slit) × 75 mm
Distance from the entrance aperture	1250 mm
Raster angle	±30 arcmin
ENTRANCE SLIT	
Size	4 μm × 8.5 mm
Angular aperture subtended by the slit	1.1 arcsec × 40 arcmin
GRATING	Toroidal with variable-line spacing
Central groove density	3600 mm^{-1}
Parameters of groove space variation	$\sigma_1 = 4.637$ mm^{-2}, $\sigma_2 = 0.02$ mm^{-3}
Radii	212 mm (tangential) and 217.2 mm (sagittal)
Ruled area	29 mm (⊥ to the grooves) × 40 mm
Illuminated area	13 mm (⊥ to the grooves) × 20 mm
Incidence angle	2.5 deg
Slit to grating distance	150 mm
DETECTORS	IAPS (both analog and photon counting)
Format	2048 × 2048
Pixel size	12 μm × 12 μm
Useful area	24.6 mm × 24.6 mm
Channel 1	
Spectral interval	96.8-109.0 nm (1st order)
	48.4-54.5 nm (2nd order)
Grating to detector distance	438 mm (center of the detector)
Magnification	2.9
Instantaneous FOV	1.1 arcsec × 40 arcmin
Spectral resolving element	5.96 pm /pixel (1st order)
	2.98 pm /pixel (2nd order)
Velocity resolving element	18 km/s @ 100 nm (50 nm)
Spatial resolving element	1.2 arcsec/pixel
Channel 2	
Spectral interval	116.2-126.6 nm (1st order)
	58.1-63.3 nm (2nd order)
Grating to detector distance	461 mm (center of the detector)
Magnification	3.1
Instantaneous FOV	1.1 arcsec × 37 arcmin
Spectral resolving element	5.08 pm /pixel (1st order)
	2.54 pm /pixel (2nd order)
Velocity resolving element	13 km/s @120 nm (60 nm)
Spatial resolving element	1.1 arcsec/pixel
Channel 3	
Spectral interval	151.6-158.4 nm (1st order)
	75.8-79.2 nm (2nd order)
	50.5-52.8 nm (3rd order)
Grating to detector distance	532 mm (center of the detector)
Magnification	3.5
Instantaneous FOV	1.1 arcsec × 33 arcmin
Spectral resolving element	3.32 pm /pixel (1st order)
	1.66 pm /pixel (2nd order)
	1.11 pm /pixel (3rd order)
Velocity resolving element	6 km/s @155 nm (77.5 nm)

Spatial resolving element	1.0 arcsec/pixel

4.6.1.2.2 EUS optical performance

The optical performances are evaluated in terms of: 1) spatial aberrations on the slit plane in the direction perpendicular to the slit, giving the actual width of the region in the direction perpendicular to the slit simultaneously imaged on the detectors; 2) spatial aberrations on the detector in the direction parallel to the slit, giving the limit of the spatial resolution; 3) spectral aberrations on the detector.

The angular extension of the region that is simultaneously imaged by the spectrometer in the direction perpendicular to the slit is limited by the angular width of the slit itself only if the aberrations on the slit plane are lower than the slit width. The FWHM aberrations are shown in Figure 4.16. They are lower or comparable to the slit width within 17 arcmin (instantaneous) × 17 arcmin (rastered) FOV. This means that the angular extension in the direction perpendicular to the slit of the region that is simultaneously imaged by the spectrometer is limited by the angular width of the slit, *i.e.* 1.1 arcsec, within 17 arcmin × 17 arcmin. Outside this FOV the extension of the region is limited by the aberrations and increases up to 3 arcsec at the extremes.
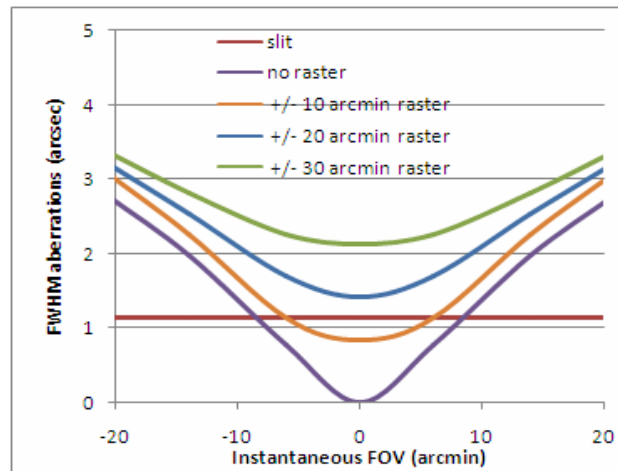
Figure 4.16. Spatial aberrations in the slit plane in the direction perpendicular to the slit.

The FWHM aberrations on the detector plane in the direction parallel to the slit are shown in Figure 4.17. They are almost lower than the pixel size within 30 arcmin (instantaneous) × 17 arcmin (rastered). Outside this FOV the aberrations increase to more than one pixel but they are anyway well below 3 pixels.

Finally, the spectral aberrations are within one pixel in the whole FOV for all the spectral channels because of the presence of the slit that defines the size of the source of the grating section. This confirms the advantage of the TVLS design for stigmatic spectral imaging of extended sources, as already demonstrated in the literature [2]. The ultimate spectral resolution is then limited by the detector pixel size in the whole FOV.

METIS
EID - PART B

REF: INAF/OATO NR. 94
DATE: 15-JAN-2008
ISSUE 1
page 55 of 108
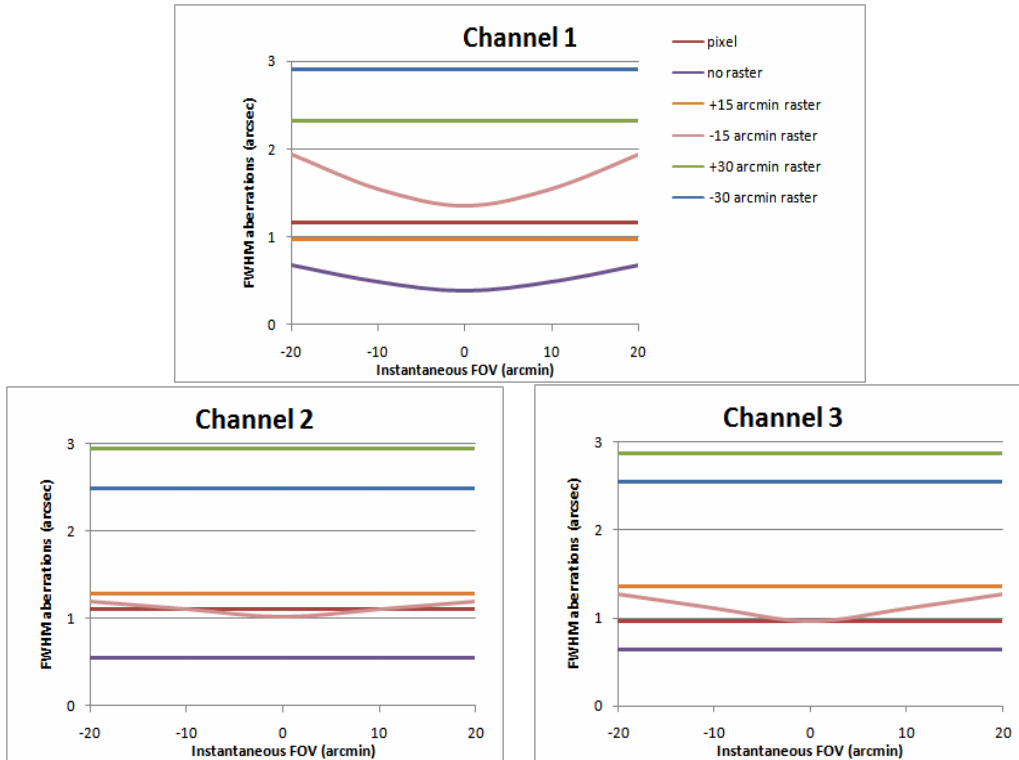
Figure 4.17. Spatial aberrations in the detector plane.

The instrument performance drives the EUS operational modes. If spectral images with the highest spectral and spatial resolutions are required, the FOV of operation has to be limited within 17 arcmin (instantaneous) × 17 arcmin (maximum rastered angle). This reduces also the detector area to be acquired, and the amount of data to be transmitted to ground.

The spectral imaging of FOVs as large as 40 arcmin (instantaneous) × 60 arcmin (rastered) requires the acquisition of the whole detector area at the expense of a slightly worse spatial resolution, degrading to 3 arcsec in the worst cases.

The performances of the two operational modes that are here defined as "mode 1" and "mode 2" are resumed in Table 4.11. When operating in "mode 2" the averaged spatial aberrations are about 2 arcsec.

Table 4.11. EUS performance when operating in the two described operational modes.

MODE 1	"Narrow FOV"
Instantaneous FOV	1.1 arcsec × 17 arcmin
Rastered FOV	17 arcmin × 17 arcmin
Channel 1	
Spatial resolving element	1.2 arcsec/pixel
Detector area to be acquired	2048 (spectral) × 880 (spatial)
Channel 2	
Spatial resolving element	1.1 arcsec/pixel
Detector area to be acquired	2048 (spectral) × 930 (spatial)
Channel 3	
Spatial resolving element	1.0 arcsec/pixel
Detector area to be acquired	2048 (spectral) × 1070 (spatial)
MODE 2	"Full FOV"
Detector area to be acquired	2048 × 2048
Channel 1	
Instantaneous FOV	2.2 arcsec (averaged) × 40 arcmin
Largest rastered FOV	60 arcmin × 40 arcmin

METIS
EID - PART B

REF: INAF/OATO NR. 94
DATE: 15-JAN-2008
ISSUE 1
page 56 of 108

Spatial aberrations on the FOV	1.9 arcsec (averaged)
Channel 2	
Instantaneous FOV	2.1 arcsec (averaged) $\times$ 37 arcmin
Largest rastered FOV	60 arcmin $\times$ 37 arcmin
Spatial aberrations on the FOV	1.9 arcsec (averaged)
Channel 3	
Instantaneous FOV	2.1 arcsec (averaged) $\times$ 32 arcmin
Largest rastered FOV	60 arcmin $\times$ 32 arcmin
Spatial aberrations on the FOV	1.9 arcsec (averaged)

Off-limb observations at heliospheric distances higher than 1 $R_\odot$ can be done when the spacecraft is pointed off-center. The maximum offset-pointing is here assumed to be 1 $R_\odot$. The range of the raster mechanism is ±30 arcmin, corresponding to scans from 1 $R_\odot$ to 1.4 $R_\odot$ @ 0.22 AU.

When looking at the corona, the detector is operated in "mode 2" to have the maximum extension of the instantaneous FOV. As already stated, the spectral performances are substantially unchanged even for large raster ranges with FWHM aberrations anyway lower than the pixel size. The spatial performances degrade with the raster interval and the averaged FWHM spatial aberration grow to about 2 arcsec. However, the corresponding spatial resolution is well suited for off-limb observations.

The main limitation to the maximum radial distance at which off-limb observations are meaningful is the scattering from the mirror of the telescope. When the stray light is almost equal or even higher than the light emitted from the inner corona, it starts to be impossible to perform any quantitative measurement. The scattering from the primary mirror has been calculated by the Harvey theory [3], assuming a surface with 0.2 nm rms micro-roughness that is within the present capabilities of the manufacturers. The expected stray light is shown in Figure 4.18. The signal from the corona is definitely higher than the light scattered from the disk in the 1 to 1.3 $R_\odot$ interval. At the extremes of the rastering interval, stray light and coronal emission are comparable.
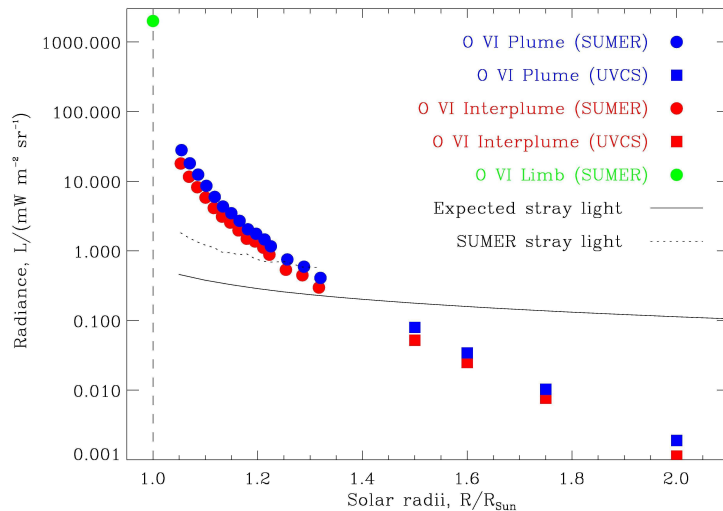
Figure 4.18. Stray light @103 nm (OVI doublet) from a mirror with 0.2 nm rms micro-roughness. The stray light from the mirror of SOHO/SUMER, which has 0.6 nm rms micro-roughness, is shown for comparison. SUMER and UVCS radiances refer to a coronal hole in 1996 and are corrected for the stray light (extracted from data in [4]).

The efficiency of the spectrometer takes into account the grating diffraction and the reflectivity of the coatings.

The diffraction efficiency has been calculated by software that uses the EM propagation theory. The grating profile has been assumed to have a saw-tooth shape with blaze angle of 15°. The blaze angle has been

METIS
EID - PART B

REF: INAF/OATO NR. 94
DATE: 15-JAN-2008
ISSUE 1
page 57 of 108

selected to give high efficiency at the fifth diffracted order at 30.4 nm for the spectroscopic observations of the extended corona (see the description of the spectro-coronagraph). Although the predicted diffraction efficiency is about 90% at the peak, the actual efficiency has been assumed to be 50%, mainly limited by the not ideal groove profile. At present, the 50% value is well within the capabilities of grating providers. If higher efficiencies will be achieved due to the sharpness of the saw-tooth profile, the effective area will consequently increase.

Two are the coatings that can be adopted for high normal-incidence reflectivity in the EUV region: silicon carbide (SiC) or boron carbide (B_4C) [5-8]. SiC has the highest reflectivity in the 60-150 nm region; nevertheless B_4C has definitely higher reflectivity at wavelengths shorter than 55 nm, where the SiC response drops down to almost zero reflectivity. We use B_4C to maintain a high effective area also for spectral lines around 50 nm. In the calculations, the reflectivity of the primary mirror is assumed to be 15% less than the nominal B_4C reflectivity because of the small thickness of the layer that is deposited on the telescope for a proper managing of the thermal load (see the paragraph on thermal load). The resulting efficiency is shown in Figure 4.19.

The photocathode selected for the photon counting IAPS detectors is potassium bromide (KBr) because of its high quantum efficiency in the whole EUV region and its long-term stability even in the case of exposures to air [9, 10]. However, the visibility of 2nd and 3rd order spectral lines is definitely compromised unless the strongest 1st order contribution is reduced at the detector stage, as already shown by SOHO-SUMER observations [11]. To enhance the contrast between 2nd and 1st order lines, a bare MCP (that is without any photocathode) can be used, because the detection efficiency of bare glass strongly increases at short wavelengths. The KBr quantum efficiency compared with bare MCP detectors is also shown in Figure 4.19: it is evident that KBr strongly enhances first order lines above 100 nm. To optimize the detection of all the spectral lines at the different diffraction orders, the detector MCP will have a differentially coated sensitive area, with photocathode coated and uncoated portions: second order lines will be observed on the uncoated portions of the MCP, while the first order ones will be observed on the KBr coated portions to reduce blending between orders.

Moreover, since the radiance on the HI Ly-α line at 121.6 nm is 2-4 orders of magnitudes higher than that of the other lines on the same spectral channel, in the case of a uniformly coated MCP the simultaneous detection in the 116.2-126.6 nm band requires an impracticable dynamic range. To minimize this problem, the portion of the MCP on which the HI Ly-α line falls will be uncoated, so reducing the contrast by a factor ≈20. In addition, the HI Ly-α flux is further reduced by a mesh with 10% transmission as successfully adopted in SUMER [11]. The mesh will be placed in front of the detector in order to cope with this intense line. The position of the mesh will be chosen to minimize the level of image modulation at 121.6 nm.

The schematic view of the differently coated areas on the detectors 2 and 3 is shown in Figure 4.20. The detector 1 is uniformly coated with KBr.
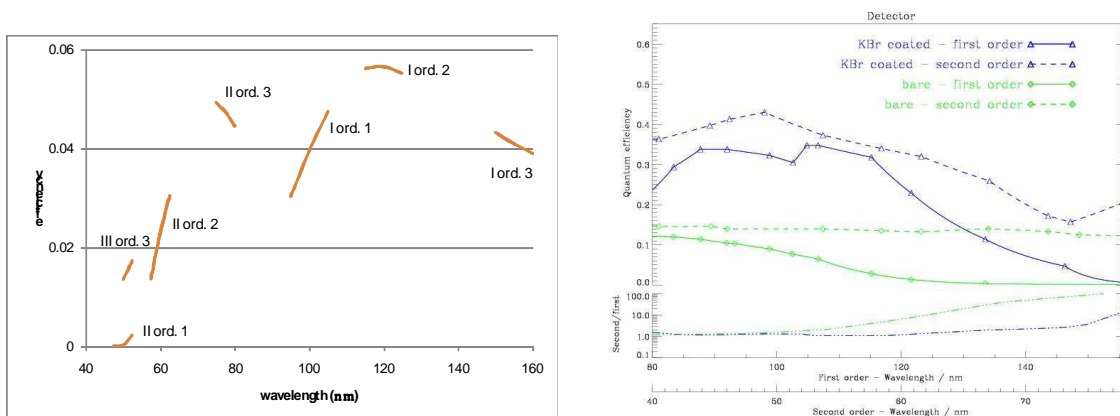
Figure 4.19. Efficiency curves. Right: efficiency of the spectrometer which includes the grating diffraction and the coating reflectivity. Left: efficiency of KBr coating and of the bare MCP detector: the top part shows the QE of both KBr coated and un-coated MCPs, the lower part shows the ratio between the 2nd-order and 1st-order QE.

METIS
EID - PART B

REF: INAF/OATO NR. 94
DATE: 15-JAN-2008
ISSUE 1
page 58 of 108
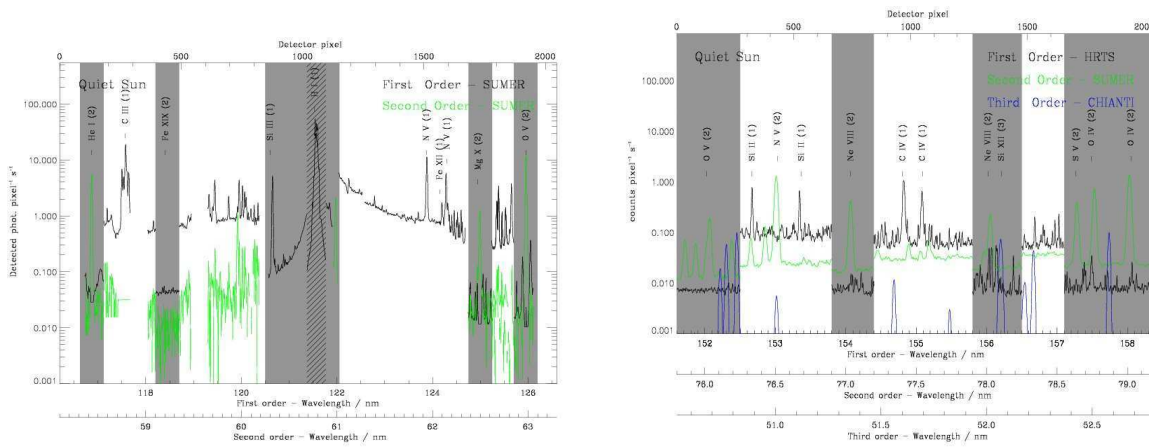
Figure 4.20. Coated (white) and bare (grey) areas on the MCP detectors no. 2 (right) and 3 (left). The dark-grey area centred at 121.6 nm evidences the HI Ly-α flux reduction.

To summarize the global efficiency performance of EUS, the spectrometer effective area is shown in Figure 4.21.
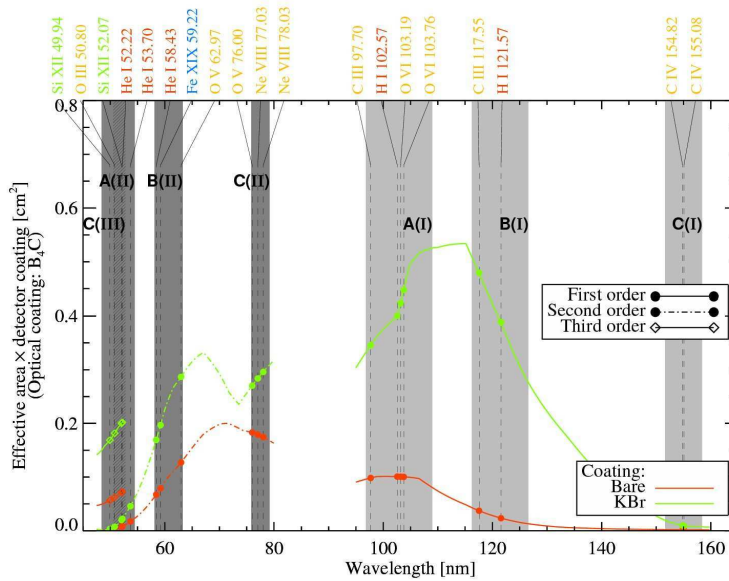
Figure 4.21. Effective areas of the spectrometer for the different MCP coating options of the IAPS: bare and KBr photocathode are considered.

4.6.1.2.3 EUS thermal load considerations

The thermal environment of SO sets very tight limits on the instrument aperture size due to the high solar irradiation at the perihelion passage, which is as high as 20 solar constants giving more than 80 W entering through the 30 cm^2 EUS aperture. To reduce the heat load on the telescope mirror, a dichroic design with low absorption of the solar visible and near infrared and good reflection of the VUV radiation is adopted.

The dichroic behavior is obtained by a proper combination of the optical coating and the primary mirror substrate. The off-axis parabola is made in quartz with a thin layer of B$_4$C coating. In fact, highly-reflective materials for normal incidence in the VUV such as SiC and B$_4$C are highly transparent in the visible and near IR if deposited in thin layers. In addition, also the quartz substrate is almost transparent to the thermal radiation, making it possible to build a mirror where the thermal load is transmitted to a great extent to the back side. This load is then dissipated through a space radiator. In addition, the quartz is ordinary machined to high quality surfaces with extremely low surface errors and micro-roughness.

METIS
EID - PART B

REF: INAF/OATO NR. 94
DATE: 15-JAN-2008
ISSUE 1
page 59 of 108

Data for SiC coating have already been published in the literature [12]. In case of a 9-nm-thick coating, 11% of the thermal power is reflected toward the slit, 83% is transmitted to the back and 6% is absorbed, making the mirror thermal management much simpler. The decrease of the VUV reflectivity due to the thin layer compared to a thick SiC substrate is about 15%.

The results expected in case of B_4C coating that is adopted in the present configuration, are substantially similar to those already measured for SiC.

References
1. R.J. Thomas, "Toroidal varied line-space (TVLS) gratings", Proc. SPIE **4853**, 411 (2002)
2. L. Poletto and R.J. Thomas, "Stigmatic spectrometers for extended sources: design with toroidal varied-line-space (TVLS) gratings", Appl. Opt. **43**, 2029 (2004)
3. J.E. Harvey and C.L. Vernold, "Transfer function characterization of scattering surfaces revisited", Proc. SPIE **3141**, 113 (1997)
4. L. Teriaca, G. Poletto, M. Romoli, and D.A. Biesecker, "The nascent solar wind: origin and acceleration", ApJ **566**, 588 (2003)
5. J.I. Larruquert and R.A.M. Keski-Kuha, "Optical properties of hot-pressed B4C in the extreme ultraviolet" , Appl. Opt. **39**, 1537 (2000)
6. J.B. Kortright and D.L. Windt, "Amorphous silicon carbide coatings for extreme ultraviolet optics", Appl. Opt. **27,** 2841 (1988)
7. G.M. Blumenstock and R.A.M. Keski-Kuha, "Ion-beam deposited boron carbide coatings for extreme ultraviolet", Appl. Opt. **33,** 5962 (1994)
8. R. A. M. Keski-Kuha, G. M. Blumenstock, C. M. Fleetwood, and D. R. Schmitt, "Effects of space exposure on ion-beam deposited silicon-carbide and boron-carbide coatings," Appl.Opt. **37,** 8038 (1998)
9. O.H.W. Siegmund, E. Everman, J.V. Vallerga, J. Sokolowski, and M. Lampton, "Ultraviolet quantum detection efficiency of potassium bromide as an opaque photocathode applied to microchannel plates", Appl. Opt. **26**, 3607 (1987)
10. J.I. Larruquert, J.A. Mendez, J.A. Aznarez, A.S. Tremsin, and O.H.W. Siegmund, "Optical properties and quantum efficiency of thin-film □lkali halides in the far ultraviolet", Appl. Opt. **41**, 2532 (2002)
11. K. Wilhelm et al, "SUMER – Solar Ultraviolet Measurements of Emitted Radiation", Sol. Phys. **162**, 189 (1995)
12. U. Schühle, H. Uhlig, W. Curdt, T. Feigl, A. Theissen, and L. Teriaca, "Thin silicon carbide coating of the primary mirror of vuv imaging instruments of Solar Orbiter", ESA SP-641 (2007)

4.6.1.2.4   EUS mechanisms

4.6.1.2.4.1   EUS telescope scan mechanism

The primary mirror must rotate around a vertical axis passing through its centre and parallel to the height of the entrance slit. Its characteristics are summarized in Table 4.12.

Table 4.12. Mechanical characteristics of the EUS telescope scan mechanism.

EUS-mirror mechanism	Requirement
Mirror dimensions	62 mm (H) $\times$ 75 mm (V)
Mirror mass	130 g
Mirror mounting	on the edge
Mechanism rotation	$\pm$ 30 arcmin
Mechanism precision	1 arcsec
Mechanism mass	1500 g
Option for precision: small scan $\pm$ 8.5 arcmin	1 arcsec
Option for precision: wide scan $\pm$ 30 arcmin	2 arcsec

The scan mechanism actuator is a single phase DC brushless torque motor that provides ripple free torque over the required limited angular excursion without electronic commutation. A current flowing in the stator

METIS
EID - PART B

REF: INAF/OATO NR. 94
DATE: 15-JAN-2008
ISSUE 1
page 60 of 108

winding produces a torque on the permanent magnet (Samarium-Cobalt) rotor polar expansions which can be considered constant over the above limited angular excursion. The angular detector is a multispeed x36 brushless resolver chosen to satisfy resolution and accuracy requirements of the scan axis.

The heritage for this mechanism is coming from the scan mechanisms which are working on the following flying instruments: VIMS spectrometer (Cassini), VIRTIS spectrometers (Rosetta, VEX, Dawn) and UVCS (SOHO). Starting from the UVCS heritage, a launch locking mechanism can be considered; in particular this mechanism will be a reversible mechanism with the locked position optimised in such a way that in case of failure, the mechanism will remain fixed in a precise operating condition.

The mechanism will be provided with the EUS mirror.

4.6.1.2.4.2   Coronal telescope insertion mechanism

This mechanism is used to insert the coronal telescope in the optical path through a linear displacement. Its main mechanical characteristics are described in Table 4.13.

Table 4.13. Mechanical characteristics of the coronal telescope insertion mechanism.

Coronal telescope insertion mechanism	Requirement
Coronal mirror dimensions	20 mm (H) ; 40 mm (V)
Coronal mirror mass	20 g
Coronal mirror mounting	on the edge
Mechanism positions	2
Mechanism linear displacement	63 mm
Mechanism linear displacement – precision	0.2 mm
Mechanism mass	400 g

For the mechanism we can consider a splindle-nut screw configuration connected with a stepper motor. A similar application has been realized for the BB of the PANCAM boom for ASI program.

As an option, instead of a linear translation it could be possible to make use of a scan of the mirror around a fixed point (scan radius 63 mm); the heritage would be the same as for a scan mechanism.

4.6.1.2.4.3   Slit covering mechanism

This mechanism is used to insert a small aluminum block to mask one or four slits alternatively through a linear displacement. For optical reasons the block must undergo a black alodine treatment. Its main mechanical characteristics are described in Table 4.14.

Table 4.14. Mechanical characteristics of the slit covering mechanism.

Slit covering mechanism	Requirement
Al block dimensions	6 mm (H) $\times$ 24 mm (V)
Al block mass	3 g
Mechanism positions	2
Mechanism linear displacement	63 mm
Mechanism linear displacement – precision	0.2 mm
Mechanism mass	400 g

The preferred solution is a rotating mechanism with a wheel designed with proper slits in order to satisfy each requirement in one position; this configuration allows to increase, if required, the number of possible slit architecture, also including a possibility for on ground calibration / alignment purpose.

The heritage for this mechanism is coming from the scan mechanisms which are working on the UVCS (SOHO). As an alternative, in case that the overall dimensions would prevent it, a solution similar to the one adopted for the coronal telescope insertion mechanism can be pursued.

METIS
EID - PART B

REF: INAF/OATO NR. 94
DATE: 15-JAN-2008
ISSUE 1
page 61 of 108

4.6.1.3   SOCS element description

4.6.1.3.1   SOCS optical design

The spectro-coronagraph acquires simultaneous spectral images of the extended corona in three different spectral bands and at four different radial distances. The instrument shares with the spectrometer the grating section and the detectors. The concept is shown in Figure 4.22 and a view of the SOCS optical path inside METIS in Figure 4.23. An image of the solar corona is created on the entrance plane of the spectrometer by a low-resolution telescope that is in the shadow of the solar disk. A field stop with multiple slits is at the prime focus of the telescope's mirror. This multi-slit field stop is the entrance aperture for the spectrograph. The TVLS grating creates stigmatic spectral images of the different slits on the detectors. The number of strips in the FOV is selected with enough separation to minimize the spectral overlap of the lines dispersed by the grating [1, 2].
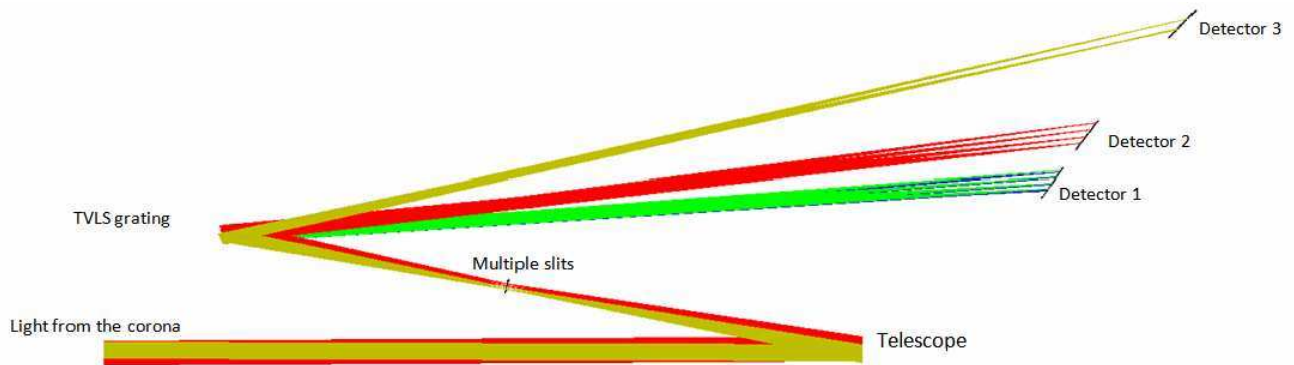
Figure 4.22. Schematic of the spectro-coronagraph with four slits to observe simultaneously at four radial distances from the Sun center. The most intense lines that are distinctly focused are the OVI doublet @103.2-103.7 nm on detector 1, the HI line @121.6 nm on detector 2 and the HeII line @30.4 nm (5th diffracted order) on detector 3.

METIS
EID - PART B

REF: INAF/OATO NR. 94
DATE: 15-JAN-2008
ISSUE 1
page 62 of 108
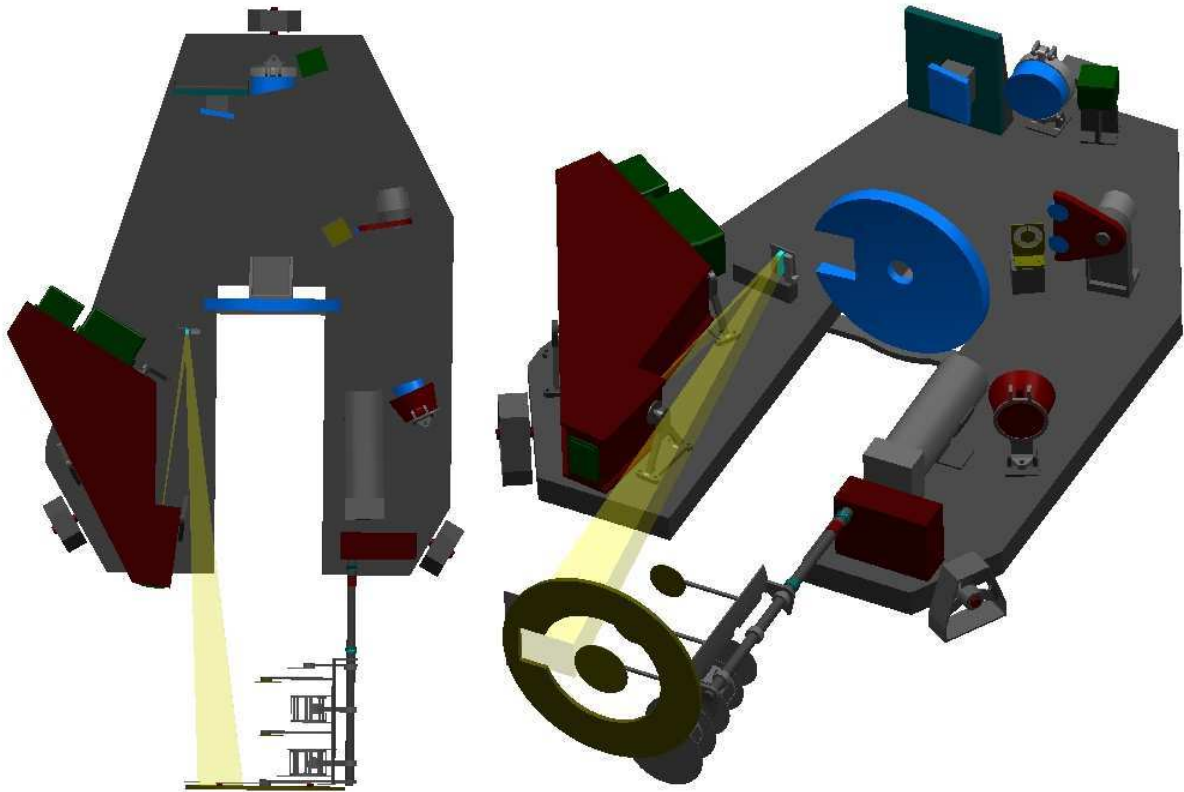
Figure 4.23. View of SOCS optical path inside the METIS suite.

The telescope that observes the corona is an off-axis parabola that is inserted in the optical path between the telescope of the spectrometer and the entrance slit plane in the shadow of the disk, as schematically shown in Figure 4.24. The mirror creates an image of the corona in the same focal plane of the telescope of the spectrometer. The single slit of the spectrometer is substituted by a multiple slit system with four slits that act as the field stop and let propagate toward the TVLS grating only the light coming from four distinct areas of the corona at different radial distances. The light coming from the multiple slits hits the grating in a lateral area distinct from the portion of the grating used for the on-disk observations and is then focused on the detectors.
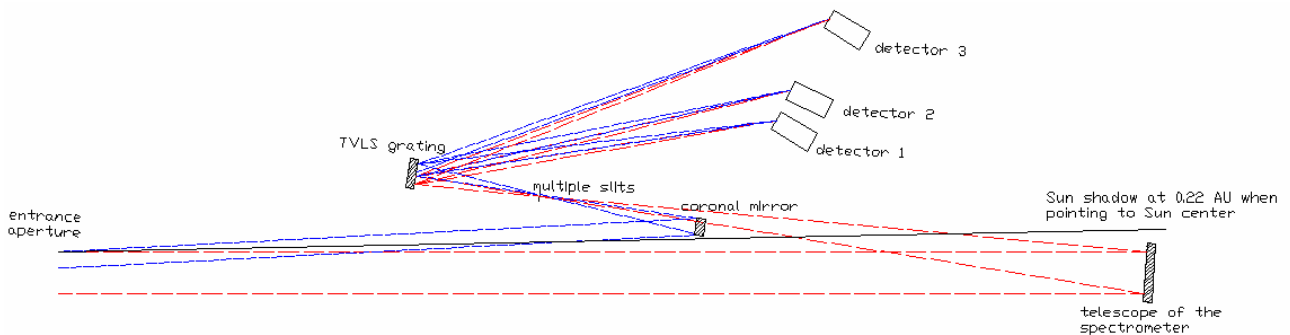
Figure 4.24. Schematic view of the instrument showing the position of the off-axis parabola to observe the corona, indicated in the drawing as "coronal mirror". The mirror is in the shadow of the Sun light when the spacecraft is pointed to the Sun center. The optical paths of the rays coming from the disk and reflected by the telescope of the spectrometer are shown in red. The optical paths of the rays coming from the corona and reflected by the coronal mirror are shown in blue. The red and blue rays hit the TVLS grating in different areas.

Since the areas illuminated on the grating for on-disk and coronal observations are different, also different coatings can be adopted to select a different spectral range for the spectro-coronagraph, in particular both the coronal mirror and the grating are multilayer coated to allow observations at the HeII line @ 304 Å. A front view of the grating surface with the two differently coated areas is shown in Figure 4.25.
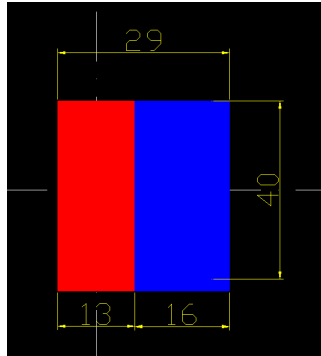
Figure 4.25. Front view of the TVLS grating surface. The area illuminated for on-disk observations is shown in red: it has size of 13 mm ($\perp$ to the grooves) × 40 mm and is coated with B$_4$C. The area illuminated for coronal observations is shown in blue: it has size of 16 mm ($\perp$ to the grooves) × 40 mm and is multilayer-coated. The grating vertex (that is the vertex of the toroidal surface) is the interception between the two dash-dot lines in the center of the red area. The grooves are ruled in the vertical direction. The whole ruled area is 29 mm ($\perp$ to the grooves) × 40 mm.

All the optical surfaces used for coronal observations, i.e. the coronal mirror and the lateral side of the grating, are multilayer-coated to reflect not only the 103.2-103.7 nm and 121.6 nm light but also the 30.4 nm light [3, 4]. As an example, the reflectivity curve of a Mo-Si coating optimized for the 30.4 nm line is shown in Figure 4.26. The coating has reflectivity higher than 0.3 for wavelengths above 100 nm. The standard Mo-Si multilayers are well known and space qualified and are adopted as a baseline for spectro-coronagraphic observations. We have looked also into adopting the SiC-Mg multilayer with SiC cap-layer. The performances of these multilayers are very promising [5]. The reflectivity above 100 nm can be increased to the expenses of the 30.4 nm response by increasing the cap-layer thickness. At present, this coating needs some technological developments for the space qualification. We will vigorously pursue all the efforts to optimize the choice of the best multilayer coating which optimizes the response in the whole spectral region of interest.

The characteristics of the telescope and the multi-slit system are listed in Table 4.15.
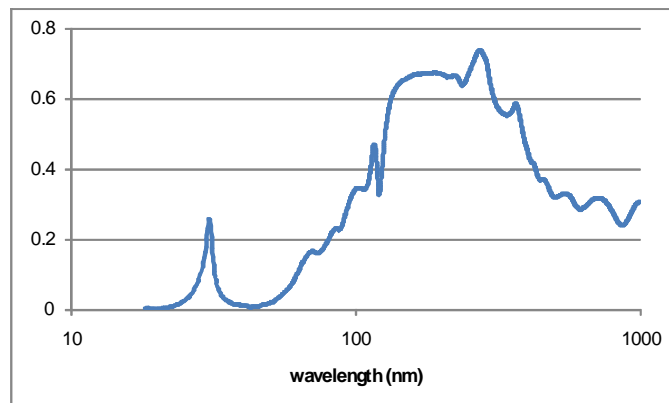
Figure 4.26. Reflectivity curve of a Mo-Si multilayer mirror. Parameters: 16.5 nm period, gamma 0.85, 25 periods, SiO$_2$ cap-layer.

METIS
EID - PART B

REF: INAF/OATO NR. 94
DATE: 15-JAN-2008
ISSUE 1
page 64 of 108

Table 4.15. SOCS optical parameters.

TELESCOPE	Off-axis parabola
Mirror to slit distance	190 mm
Size	20 mm ($\perp$ to the slit) $\times$ 40 mm
ENTRANCE SLIT	
Size of each slit	20 μm $\times$ 8.5 mm
Angular aperture subtended by the slit	22 arcsec $\times$ 2.5°
Number of slits	4
Slit angular distances from Sun center	2° – 2.3° – 2.7° – 3.1°
Radial distance @0.22 AU	1.68 $R_\odot$ – 1.93 $R_\odot$ – 2.27 $R_\odot$ – 2.60 $R_\odot$
DETECTORS	
Format	2048 $\times$ 2048
Pixel size	12 μm $\times$ 12 μm
Useful area	24.6 mm $\times$ 24.6 mm
Channel 1	
Most intense spectral lines	103.2-103.7 nm (OVI doublet)
Instantaneous FOV	22 arcsec $\times$ 2.5° (2.1 $R_\odot$ @ 0.22 AU)
Spectral resolving element	5.96 pm/pixel (1st order)
Spatial resolving element	4.4 arcsec/pixel
Number of visible slits	4
Spectral separation of the slits	2.2 nm (averaged)
Channel 2	
Most intense spectral lines	121.6 nm (HI Ly-α)
Instantaneous FOV	22 arcsec $\times$ 2.3° (1.9 $R_\odot$ @ 0.22 AU)
Spectral resolving element	5.08 pm/pixel (1st order)
Spatial resolving element	4.1 arcsec/pixel
Number of visible slits	4
Spectral separation of the slits	2.2 nm (averaged)
Channel 3	
Most intense spectral line	30.4 nm (HeII, 5th order)
Instantaneous FOV	22 arcsec $\times$ 2.0 deg (1.7 $R_\odot$ @ 0.22 AU)
Spectral resolving element	0.66 pm/pixel (5th order)
Spatial resolving element	3.5 arcsec/pixel
Number of visible slits	2
Spectral separation of the slits	0.45 nm

4.6.1.3.2 SOCS optical performance

The optical performances are evaluated in terms of: 1) spatial aberrations on the slit plane in the direction perpendicular to the slit; 2) spatial aberrations on the detector in the direction parallel to the slit; 3) spectral aberrations on the detector.

The FWHM aberrations on the slit plane in the direction perpendicular to the slit are shown in Figure 4.27. The slits are numbered from 1 to 4, no. 1 being the slit closest to the Sun center. The aberrations are lower than the slit width for slits 1-3 within 1° instantaneous FOV. For slit 4, the aberrations are ever higher than the slit width. The angular extension in the direction perpendicular to the slit of the region of the corona that is simultaneously imaged by the spectro-coronagraph ranges in the 22-43 arcsec interval that is well suited for coronal observations.

METIS
EID - PART B

REF: INAF/OATO NR. 94
DATE: 15-JAN-2008
ISSUE 1
page 65 of 108
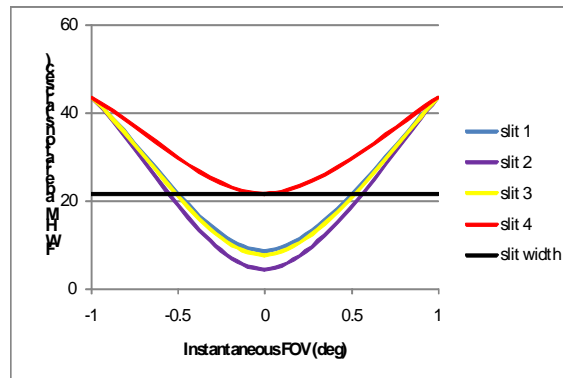
Figure 4.27. SOCS spatial aberrations in the plane of the multiple slits in the direction perpendicular to the slits.

The FWHM aberrations on the detector plane in the spatial direction are shown in Figure 4.28. They are almost constant within the instantaneous FOV and decreasing with the slit number: the aberrations for slit no. 1 are about 60 arcsec, those for slit no. 4 about 20 arcsec. The aberrations set the limit of the spatial resolving element in the images, *i.e.* the minimum number of pixels that have to be binned in the spatial (vertical) direction to have an image whose resolution is limited by the pixel size.
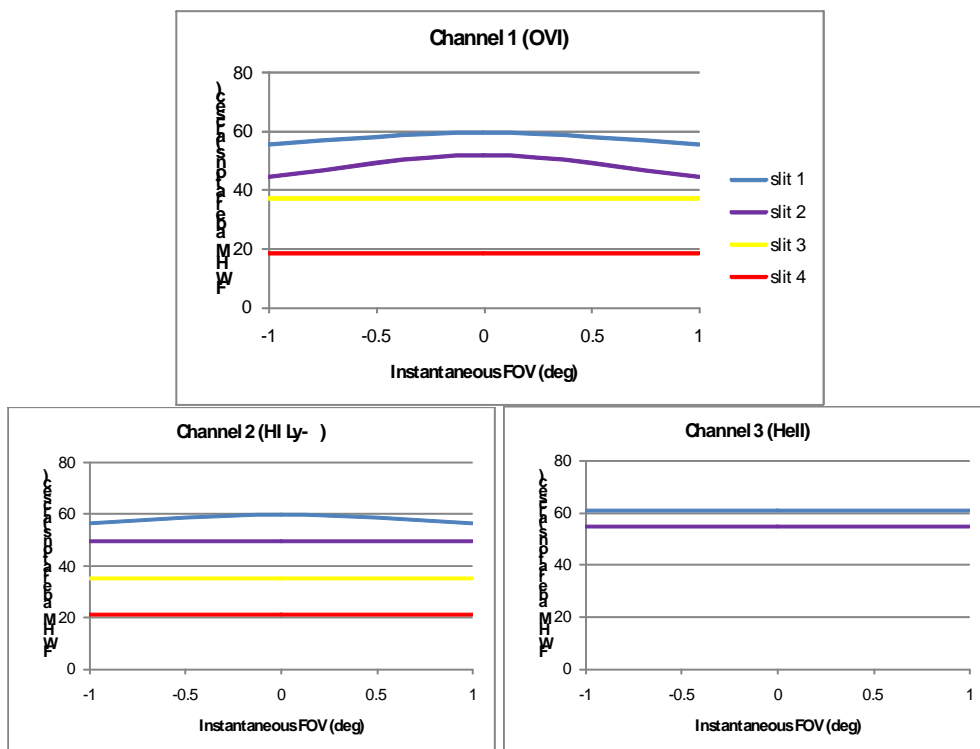
Figure 4.28. Spatial aberrations of the spectro-coronagraph in the detector plane.

The FWHM spectral aberrations on the detector plane are shown in Figure 4.29. They are constant within the FOV due to the stigmaticity of the TVLS design for extended sources. Again, the aberrations set the limit of the spectral resolving element in the images, *i.e.* the minimum number of pixels that have to be binned in the spectral (horizontal) direction.

The instrument performance in terms of aberrations drives the SOCS operational mode, *i.e.* the format of the coronal spectral images. If spectral images with spatial and spectral resolutions limited by the pixel size (and not by the aberrations) are required, the detector physical pixels have to be binned. This reduces considerably the amount of data to be transmitted to the ground.

METIS
EID - PART B

REF: INAF/OATO NR. 94
DATE: 15-JAN-2008
ISSUE 1
page 66 of 108

The parameters of the operational mode are reported in Table 4.16. The spatial binning factor is about 60 arcsec for all the slits. The spectral binning factor is respectively 18, 20 and 5.3 pm/pixel for channels 1, 2 and 3. The image format is reduced by one-two orders of magnitude. The telemetry required for the transmission of the data to the ground is then very limited.

The efficiency of the spectro-coronagraph takes into account the grating diffraction and the reflectivity of the coating. The grating profile has been assumed to have a saw-tooth shape with blaze angle of 15° that has been selected to give high efficiency at the V diffracted order at 30.4 nm. The peak efficiency has been assumed to be 50% that is well within the present capabilities of the grating manufacturers. The multilayer reflectivity has been assumed to be 0.25 @ 30.4 nm and 0.30 @ 103.2 and 121.6 nm, accordingly with present measurements on Mo-Si coatings. The resulting efficiency is reported in Table 4.17.
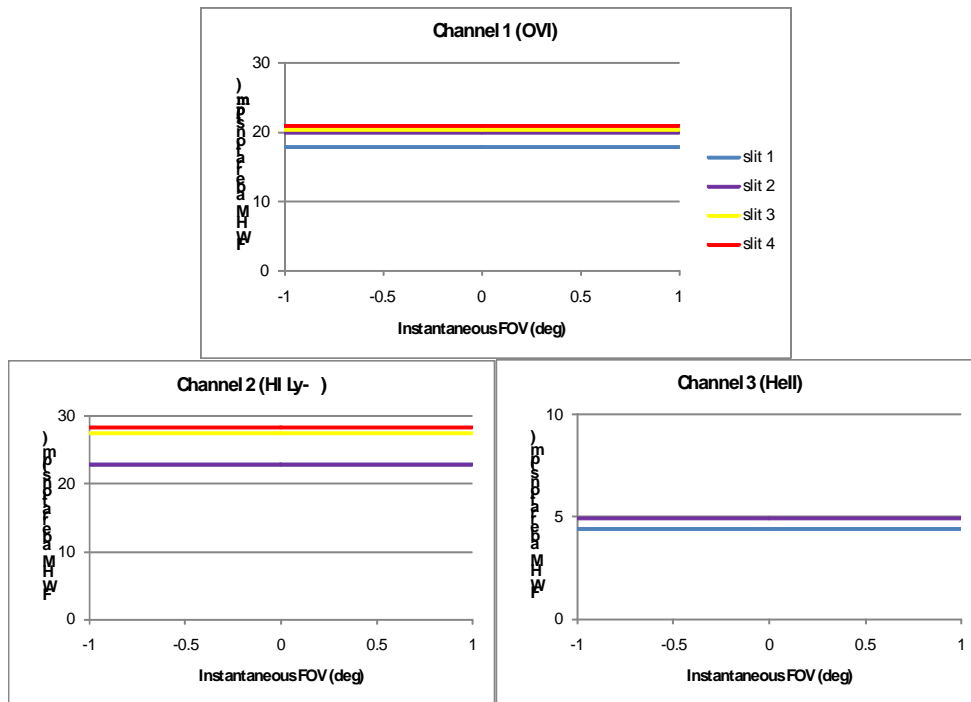
Figure 4.29. Spectral aberrations of the spectro-coronagraph in the detector plane.

Table 4.16. SOCS Operational mode.

SPECTRO-CORONAGRAPH OPERATIONAL MODE	
Channel 1	
Binning factor	3 (spectral) × 13 (spatial)
Image format	682 × 157
Spectral resolving element	18 pm/pixel
Spatial resolving element	57 arcsec/pixel
Channel 2	
Binning factor	4 (spectral) × 14 (spatial)
Image format	512 × 146
Spectral resolving element	20 pm/pixel
Spatial resolving element	57 arcsec/pixel
Channel 3	
Binning factor	8 (spectral) × 17 (spatial)
Image format	256 × 120
Spectral resolving element	5.3 pm/pixel
Spatial resolving element	59 arcsec/pixel

METIS
EID - PART B

REF: INAF/OATO NR. 94
DATE: 15-JAN-2008
ISSUE 1
page 67 of 108

Table 4.17. Efficiency of the spectro-coronagraph, including the reflection on the coronal mirror and the diffraction from the grating. Both the optical surfaces are assumed to be multilayer coated.

Channel 1 (103.2-103.7 nm)	0.025
Channel 2 (121.6 nm)	0.034
Channel 3 (30.4 nm)	0.045
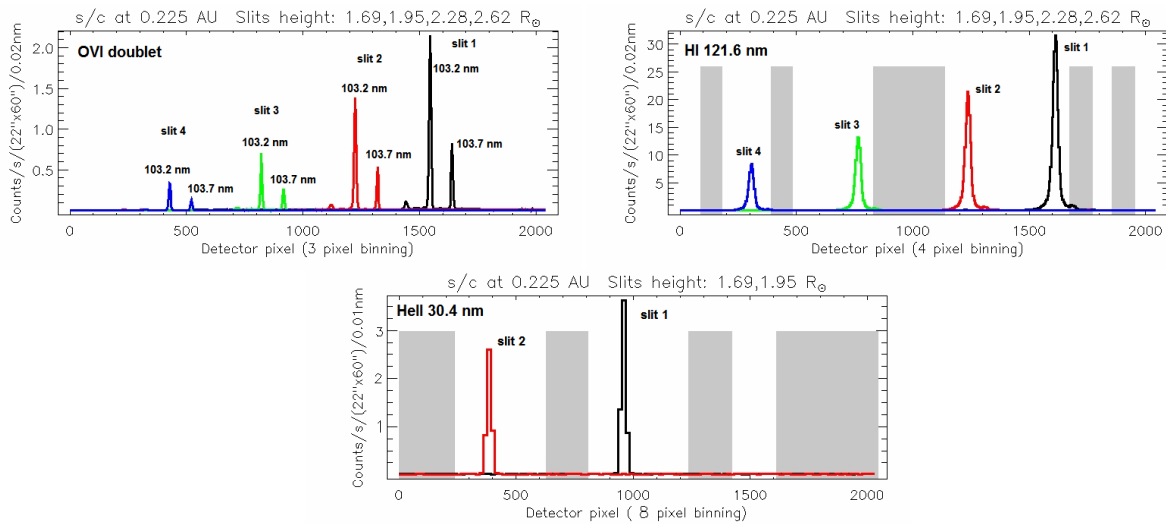
Figure 4.30. Spectral images of the multiple slits on the detectors. Top left: channel 1, OVI 103.2-103.7 nm doublet @ 1st diffracted order, four slits visible. Top right: channel 2, HI Ly-α 121.6 nm @1st diffracted order, four slits visible. Bottom: channel 3, HeII 30.4 nm @5th diffracted order, two slits visible. The grey portions show the uncoated areas on the detectors sensitive surface.

The angular separations of the four slits have been selected to give the images of the spectral lines on KBr coated areas on the detectors, in order to have the highest detection efficiency. The positions of the spectral images of the multiple slits are shown in .

The calculations of the effective area have to take into account of: 1) the coating reflectivity; 2) the grating diffraction efficiency; 3) the detection efficiency; 4) the illuminated area for each of the different slits; 5) the vignetting function within the instantaneous FOV.

The illuminated area of the coronal mirror changes in the horizontal direction (*i.e.* the direction perpendicular to the slits) with the angular distance from the Sun center, so also the effective area is different for each of the images of the four slits. The illuminated area varies from 7 mm × 40 mm for slit 1 (2° angular distance from Sun center) to 20 mm × 40 mm for slit 4 (3.1° angular distance from Sun center). The variation of the corresponding effective area is almost a factor 3.

Furthermore, the spectral image of each of the slits is vignetted within the instantaneous FOV because the illuminated area of the coronal mirror decreases in the vertical direction (*i.e.* the direction parallel to the slits) with the off-axis angle. The illuminated area varies from 40 mm (*i.e.* full vertical mirror) within ±0.7° FOV to 33.5 mm for ±1.25°, corresponding to a maximum vignetting of about 16%.

The resulting effective area is shown in Figure 4.31.

4.6.1.3.3 *Diffraction from the entrance aperture*

The edge of the entrance aperture is a source of diffracted light that can contaminate the spectral images of the corona. A simple optical simulation has been performed to simulate the worst case of diffraction from the external edge. A linear source is placed on the edge of the entrance aperture with emission isotropic in the

METIS
EID - PART B

REF: INAF/OATO NR. 94
DATE: 15-JAN-2008
ISSUE 1
page 68 of 108

half-solid angle. The coronal mirror creates an image of such source on the plane of the multiple slits. This is definitely a worst case not corresponding to the real case of diffraction, since the diffraction is not isotropic in the emission. The image on the slit plane is shown in Figure 4.32. The light emitted from the aperture enters the slit 1 to 3.
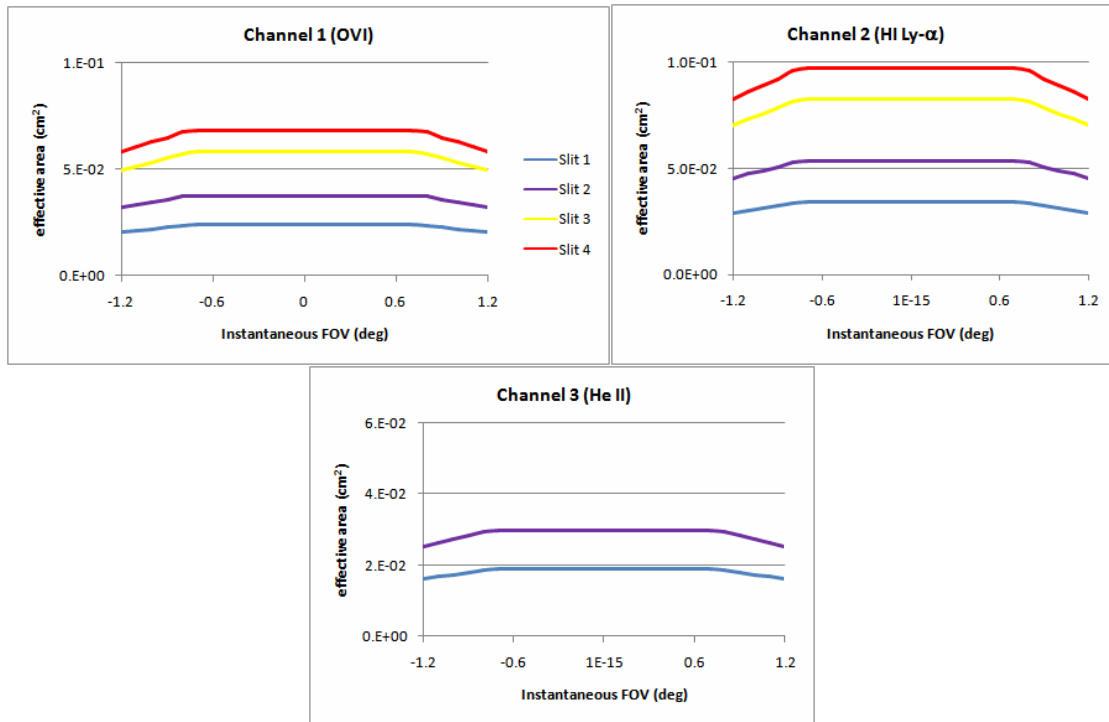
Figure 4.31. Effective area of the spectro-coronagraph.
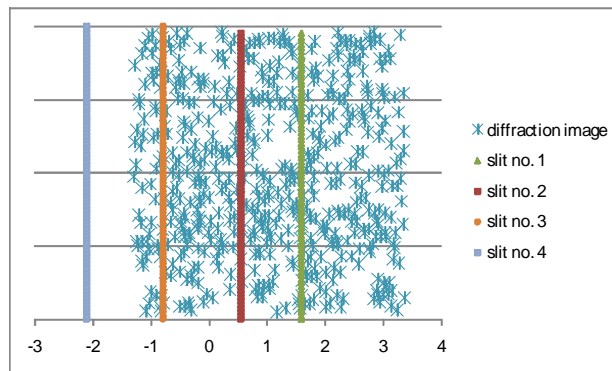
Figure 4.32. Image on the slit plane of a linear light source placed on the edge of the external aperture to simulate the effect of diffraction in the worst case.

There are two ways to reduce the contribution from diffraction. First of all, baffles will be added to the entrance tube in a geometry similar to what has already been done with SOHO-UVCS [6]. Secondly, an internal occulter could be placed inside the spectrometer. If a thin strip of non-UV reflecting material (e.g., a 1-mm thin rod made by teflon) is positioned 64 mm inside the spectrometer entrance arm, the image of the diffraction of the external edge is blocked completely with negligible vignetting of the disk light when the spectrometer is used in disk-spectroscopic mode. We are convinced that the adoption of both these methods could practically eliminate the contribution from the diffraction. Anyway, a detailed study will be performed during phase A.

METIS
EID - PART B

REF: INAF/OATO NR. 94
DATE: 15-JAN-2008
ISSUE 1
page 69 of 108

References
1. S. Fineschi, C. M. Korendyke, J. D. Moses, and R.J. Thomas, "Solar ultraviolet spectro-coronagraph with toroidal varied line-space (TVLS) grating", Proc. SPIE **5487**, 1165 (2004)
2. S. Fineschi, J.D. Moses, and R.J. Thomas, "Spectro-imaging of the extreme-UV solar corona" Proc. SPIE **5901**, 289 (2005)
3. D.L. Windt, S. Donguy, J. Seely, and B. Kjornrattanawanich, "Experimental comparison of extreme-ultraviolet multilayers for solar physics", Appl. Opt. **43**, 1835 (2004)
4. M.-G. Pelizzo, D. Gardiol, P. Nicolosi, A. Patelli, and V. Rigato, "Design, deposition, and characterization of multilayer coatings for the Ultraviolet and Visible-Light Coronagraphic Imager", Appl. Opt. **43**, 2661 (2004)
5. H. Takenaka, S. Ichimaru, T. Ohchi, and E.M. Gullikson, "Soft-X-ray reflectivity and heat resistance of SiC/Mg multilayer ", Jnl. Electr. Spectr. Rel. Phen. **144**, 1047 (2005)
6. J.L. Kohl et al, "Ultraviolet Coronagraph Spectrometer for the Solar and Heliospheric Observatory", Sol. Phys. **162**, 313 (1995)

4.6.1.3.4 SOCS detectors

EUS and SOCS use the same detectors, but in two completely different intensity regimes: in fact, since the two elements look either at the disk or at the extended corona, with orders of magnitude of different light intensities, the detectors have to be able to work with an extremely large dynamic range.

The baseline for the detector architecture is an Intensified Active Pixel Sensor (IAPS), since it allows operation in two different modes, photon counting and integration exposure, suitable, respectively, for low and high level of flux.

An IAPS consists of a microchannel plate (MCP) intensifier with phosphor screen output, optically coupled via fiber optic taper to an APS sensor [1,2]. A photocathode deposited on the entrance MCP face converts the incoming photons in primary photoelectrons, which are then multiplied by the MCP plate and then converted into optical photons by the phosphor screen. At the end of the process, the APS detects these optical photons. The schematic of the IAPS detector is shown in Figure 4.33.
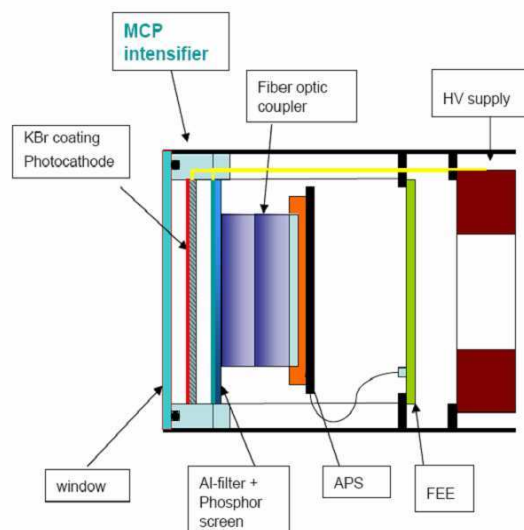
Figure 4.33. Schematic of the IAPS detector.

MCP intensifiers can be operated both in analog and in photon counting mode by changing their operating voltage:

- when the voltage across the channels of the MCP is below some threshold, the MCP works at low gain and the number of electrons at the output is proportional to the number of electrons at the input;

METIS
EID - PART B

REF: INAF/OATO NR. 94
DATE: 15-JAN-2008
ISSUE 1
page 70 of 108

- as the voltage increases, saturation effects dominate and the electronic clouds at the output tend to have similar charge; the pulse height distribution is guasi-gaussian and a good discrimination of the single photon signal from the exponentially decaying background distribution

The APS readout system is well suited for both operating modes:
- in analog mode the input image is read out by the APS directly sensing the output of the phosphor screen, integrating signals from a number of primary photons enough to guarantee a good SNR;
- in photon counting, the APS is operated at a frame rate high enough not to have overlapping of the spots generated by each primary photon; then each frame is searched to recognize these spots, computing the x, y coordinates of their centers.

A 2k×2k pixel sensor will be used. No sub-pixel resolution with event centroiding in photon counting mode is thus required, and even in photon counting mode the spot size can be as small as possible (positively affecting also the dynamic range) and the intensifier can be optimized for minimum event size (photon counting)/maximum limiting resolution (analog).

The three SOCS detectors will use basically the same design, with differently coated area to optimize the sensitivity for each channel at the 1st diffracted order or at the higher orders. Discussion about the differentially coated sensitive MCP areas for the three channels is reported in section 4.6.1.2.2.

Due to the spectral ranges of EUS and SOCS (where there is no transparent material to realize a window to work with a sealed detector), all the detectors will be in open configuration: the intensifier will be hosted in a vacuum housing with a door (single shot aperture, TBC) to be opened once in orbit and when in operation during the laboratory characterization and calibration phases. Moreover, the housing should be connected to an ion pump to maintain the operating level of vacuum, with the related high voltage supply. The ion pump will be used only during earth operations and will be removed before launch.

The maintenance of the MCP in a clean vacuum environment will avoid any degradation of the photocathode response due to exposure to water vapour or bad organic contamination [3].

The scrubbing and conditioning procedures to be adopted are well known and described in the literature [4,5]

The final choice of the APS sensor to be used as readout device will be done in subsequent phases of the project. E.g., a space qualified version of the already available Cypress LUPA-4000 could meet basic requirements. The relevant characteristics are the following:
- 2k × 2k pixels
- 12 μm pixel size
- 2 × 33 MHz outputs
- up to 30 frames/s full frame, full resolution
- fill factor 60%
- snap-shot shutter

The 12 μm pixel size allows a 1:1 optical coupling between MCP intensifier and APS, maximizing the efficiency (resulting in the request of a lower gain for the intensifier, which means longer life).

The sensor has 2 ADC, 10 bits, directly implemented on chip in order to provide digital outputs, thus reducing the complexity of the front-end electronics. Flexible windowing capability is useful due to the fact that EUS spectra take only a strip of the detectors, and reducing the area to be acquired significantly increases the frame rate and, as a result, the maximum flux at which the photon counting mode (that allows better SNR) can be used. The frame rates of the APS sensor in the two operational modes of the spectrometer are summarized in Table 4.18.

METIS
EID - PART B

REF: INAF/OATO NR. 94
DATE: 15-JAN-2008
ISSUE 1
page 71 of 108

Table 4.18. Frame rates of the APS sensor (assuming the LUPA-4000 device) for the EUS operation modes (described in Table 4.11). The maximum count rate for the photon counting mode (last column) is the count rate giving 10% loss of linearity.

Operational mode	Channel	Frame rate	Max countrate in photon counting
Narrow FOV	1	36 Hz	7 count/s/pixel
	2	34 Hz	7 count/s/pixel
	3	30 Hz	6 count/s/pixel
Full FOV	All channels	15 Hz	3 count/s/pixel

The Front End Electronics (FEE) will include the APS controller, which will provide the digital signal sequences to operate the sensor, and a digital data processing block, implementing different functions in the two, photon counting and analog, operating modes:

- in photon counting, it will acquire the two digital output looking for pixels over-threshold (containing photon events) and then accumulate counts in an array
- in analog mode, it will sum set of frames

The block functional diagram of the detectors is given in Figure 4.34.
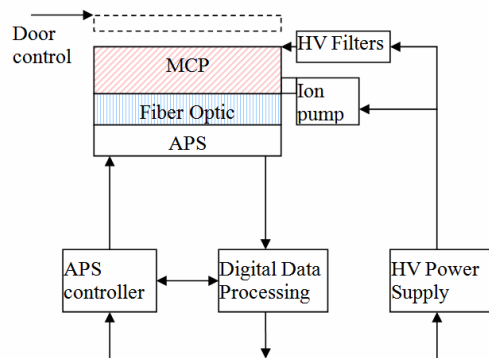
Figure 4.34. Block functional diagram of the EUS detector.

The intensifier will be procured from Sensor Science – a commercial spin-off of the UC Berkley MCP activity of Prof. O. Siegmund. The METIS detectors are a straightforward adaptation of the New Horizons Pluto-Alice unit illustrated in Figure 4.35. The New Horizons mechanism to open the vacuum door on orbit will be used without modification, thus retaining the space qualification of this mechanism. A quartz window in the door permits illumination of the detector with UV light (cutoff ~170 nm) without breaking vacuum. This is used for the initial MCP scrub as well as unit level checks of the UV throughput throughout the instrument development program (of particular importance to maintain sensor calibration when the GSE readout system is replaced by the flight electronics).

Individual photoelectrons are produced at the surface of the MCP and multiplied through its pores. Electrons from the back of the MCP are accelerated to a phosphor screen coupled to an APS chip using a 1:1 nominal ratio fiber optic. In photon counting regime, each photon event detected by the MCP generates a "splash" of light at the phosphor, which gives a signal in a 3×3 pixel area of the APS. The peak of the detected light splash in the APS gives the position of the input photon. The APS is a CMOS sensor with 2048 × 2048 pixels of size 12 µm × 12 µm. Each row of 2048 pixels is simultaneously digitized to 10 bits using on-chip circuitry. It is readout through 10 parallel ports each of 10-bit width.

The IAPS detector is controlled by a field programmable gate array (FPGA) located in close proximity. Separate low voltage and high voltage power converters (not shown) supply the necessary voltages to operate the detector. A block diagram is shown in Fig. Events are added with a zero or one to a Boolean readout frame stored within the detector electronics. The IAPS detector electronics has the capability to sum individual Boolean readout frames up to a user selected number of frames corresponding to times between 5

METIS
EID - PART B

REF: INAF/OATO NR. 94
DATE: 15-JAN-2008
ISSUE 1
page 72 of 108

seconds and 10 minutes within a single histogram frame to form one science "exposure". The histogram frame is 16 bits deep double-buffered so that one may be transmitted while another is accumulating.

Figure 4.35. Laboratory model of the IAPS.

The detector electronics are designed to accept a signal from the instrument shadow sensors in order to shut down the detector high voltage in the event of a loss of spacecraft fine pointing (a similar circuit was implemented for the same reasons on the detector for the SWIFT Optical Monitor).

In order to have a flyable model of this detector, testing and the space qualification are necessary. Particular attention must be devoted to fully characterize the capability of maintaining the high spatial resolution in both photon counting and analogue modes on the same detector. All the other elements (APS, FEE, remote electronics, …) have significant heritage from other ASI spaceflight programs and do not need any specific development. If the early characterization of the engineering model IAPS performance indicates a fundamental engineering problem with significant schedule impact, a backup solution can be easily found changing the SOCS optical design, and increasing the grating-to-focal plane distance. In fact, in this case, a larger pixel size is necessary, and consequently a larger detector, but at the same time this greatly reduces the spatial resolution criticality. In practice, an IAPS with a larger APS pixel size would allow to maintain the foreseen scientific performance of the instrument, at the minor cost of some increase of the needed mass resource.

References
1. M. Uslenghi et al, Proc. SPIE **4498** (2001)
2. G. Bonanno et al, Proc. SPIE **4498** (2001)
3. A.S. Tremsin, O.H.W. Siegmund, Proc. SPIE **5920** (2005)
4. J. Vallerga et al, Proc. SPIE **4498** (2001)
5. Martin, J. Vallerga, J. McPhate, and O. Siegmund, Proc. SPIE **4854** (2003)

4.6.2 Mechanical Interface Control Document

The instruments will be designed taking into account the allocated mass with adequate contingencies. At equipment level, the following design maturity mass contingencies will be applied:
- > 5 % for "Off-The-Shelf" items (ECSS Category: A / B)
- > 10 % for "Off-The-Shelf" items requiring minor modifications (ECSS Category: C)
- > 20 % for newly designed / developed items, or items requiring major modifications or re-design (ECSS Category: D).

The unit Accommodation Mass will include the total instrument hardware that is intended for flight. The mass budget will include at least:

- structure, mechanisms and optics;
- electronics up to the interfaces with the spacecraft power and data systems;

METIS
EID - PART B

REF: INAF/OATO NR. 94
DATE: 15-JAN-2008
ISSUE 1
page 73 of 108

- thermal control hardware, including any necessary thermal straps or heaters/thermistor,
- instrument blankets, cold fingers defined by the instrument (i.e. not part of the spacecraft TCS)
- electrical connectors, but not the mating harness connector
- attachment hardware but excluding standard fixation bolts to the spacecraft structure and washer
- potting compounds used in the units
- alignment references, e.g. mirrors, that are not removed before flight
- internal balance mass (for periodically operating mechanisms, if necessary)
- electrostatic screens and/or magnetic shielding (if necessary)
- in-flight covers, purge ports, purging pigtails

The current estimated mass and mass breakdown of the METIS instrument is provided in section 4.6.3.

Centre of Mass
The Centre of Mass (CoM) of the METIS instrument will be computed and specified with respect to the Unit Reference Frame (URF, defined in section 4.3). The currently estimated coordinates of the METIS CoM are (excluding the electronic box):

$$\text{CoM}_X = -0.314 \text{ m}, \ \text{CoM}_Y = -0.390 \text{ m}, \ \text{CoM}_Z = 0.116 \text{ m}.$$

The variations of the CoM coordinates due to the displacement of the motorized elements (in particular the EEO) will be specified.

Moments of Inertia
The Moments of Inertia (MoI) and Cross Products of Inertia will be computed, referred to a reference system parallel to the URF axes and with its origin at the CoM for all in-flight configurations (with and without cover and movable parts).

The currently estimated MoI's are (excluding the electronic box):

$$\text{Ixx} = 1.0 \text{ kg·m}^2 , \ \text{Iyy} = 3.8 \text{ kg·m}^2 , \ \text{Izz} = 4.5 \text{ kg·m}^2$$

The MoI will be measured with the accuracy defined in Design Verification Requirements (see section 6 of RD-1).

METIS MoI variations due to mechanisms will be defined in the EID-B and will be less than 0.1 Kgm^2 (TBC) (applicable to in flight configuration excluding one shot mechanisms). The current METIS configuration fulfills this requirement.

Unit Dimensions
The dimension, *d*, of METIS will be specified to a tolerance smaller than:
 + 0.5/-0.0 mm for *d* < 500 mm
 + 1.0/-0.0 mm for 500 mm < *d*

METIS
EID - PART B

REF: INAF/OATO NR. 94
DATE: 15-JAN-2008
ISSUE 1
page 74 of 108
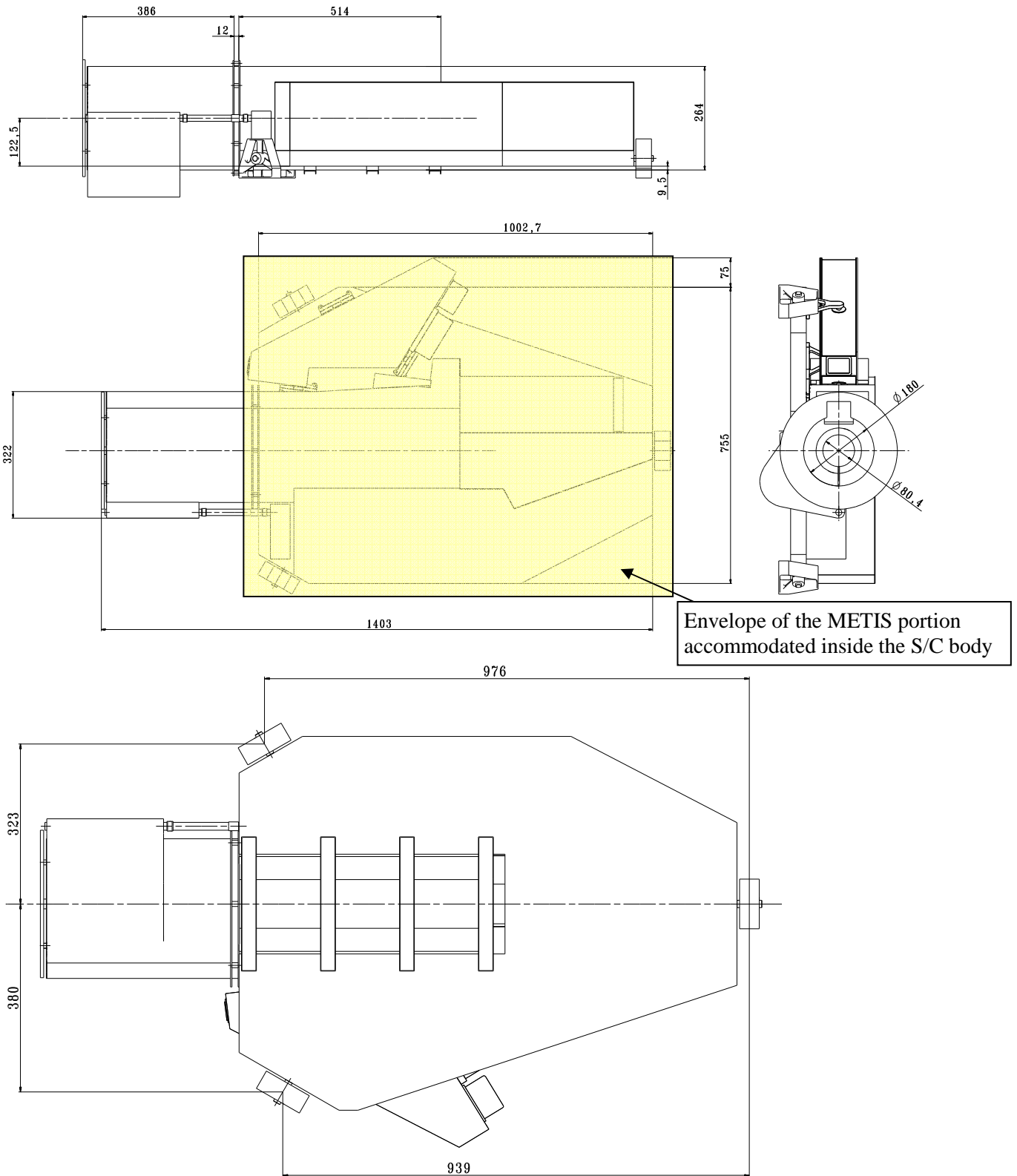
Figure 4.36. Main dimensions of the METIS instrument.

Envelope of the METIS portion accommodated inside the S/C body

METIS
EID - PART B

REF: INAF/OATO NR. 94
DATE: 15-JAN-2008
ISSUE 1
page 75 of 108

4.6.3 Definition of Instrument Size and Mass

4.6.3.1 Instrument Size

The main dimensions of the METIS instrument are shown in Figure 4.36.

The METIS portion (optical bench) to be accommodated inside SO S/C body (i.e. excluding external optical baffle and the external occulter accommodated across the heat shield) is a 1 m class instrument, as required in section 4.6.2 of RD-1 for the remote sensing instruments.

The MPPU, containing all the instrument electronics for the power supply and the data handling (see section 4.8), is a box with size 220 mm ×250 mm × 350 mm. It must be accommodated in a suitable location inside the S/C, not necessarily very close to the optical bench.

4.6.3.2 Instrument Mass Breakdown

The current estimate of the METIS instrument mass is provided in Table 4.19, together with its breakdowns among the various elements. The total mass, including a 25% contingency margin is 37.0 kg, which is 0.5 kg larger than to the sum of the masses allocated for EUS and COR in section 3.3.3 of RD-1. However, it has to be reminded that the merging of these two instruments implies a comparable mass saving at satellite level: in fact, in the METIS configuration COR and EUS share a single aperture on the heat shield, and therefore a single external door is sufficient for both instead of the two (one for COR and one for EUS) presently foreseen on the S/C. This means that METIS is fully compliant with the allocated resource of mass for the equivalent payload on SO.

Table 4.19. METIS instrument current mass breakdown.

METIS element	Mass [kg]
Optical bench and SOCS box structure	5.0
Optics and mounts	2.0
Detectors (including housing, mounts and doors)	2.7
Optics mechanisms	2.5
Optical baffles (internal, external) and mounts	2.6
Optical bench cover and mechanical interfaces with the spacecraft	1.8
External occulter (fixed, movable) and occulter mount, mechanism	1.5
Thermal control hardware	1.0
METIS Processing & Power Unit	8.2
Detector Front-End Electronics	1.1
Harness	1.2
Total without margin	29.6
Margin (25%)	7.4
Total with margin	37.0

4.6.4 Baffles

METIS is endowed with a main optical baffle that surrounds the path of the sun disk and corona light from the entrance in the instrument through the external occulter mask till the Sun-light rejection mirror M0.

This baffle is split in two segments:

- an "external optical baffle" that crosses the heat shield and provides the mechanical support to the external occulter;
- an "internal optical baffle" that is attached to the optical bench and is joined to the external baffle at the separation plane between the S/C front panel and the heat shield.

For accommodating the external optical baffle, a hole though the heat shield is needed with a diameter of approximately 400 mm. Around the external baffle, a frame, belonging to the spacecraft, is envisaged to support the heat shield layers (so that there is not physical contact between the heat shield and the optical

METIS
EID - PART B

REF: INAF/OATO NR. 94
DATE: 15-JAN-2008
ISSUE 1
page 76 of 108

baffle), but making the external baffle free to irradiate heat laterally through the gaps between the heat shield layers. The length of the external optical baffle can be adapted to the thickness of the heat shield.

In addition to this main optical baffle, other baffles are installed on the optical bench to separate the sun disk light beam (feeding the EUS/SOCS) from the sun corona light beam (feeding the COR) and to isolate the room where COR detectors are accommodated.

Different views of the METIS baffle system are shown in Figure 4.37 to Figure 4.40.

METIS
EID - PART B

REF: INAF/OATO NR. 94
DATE: 15-JAN-2008
ISSUE 1
page 77 of 108
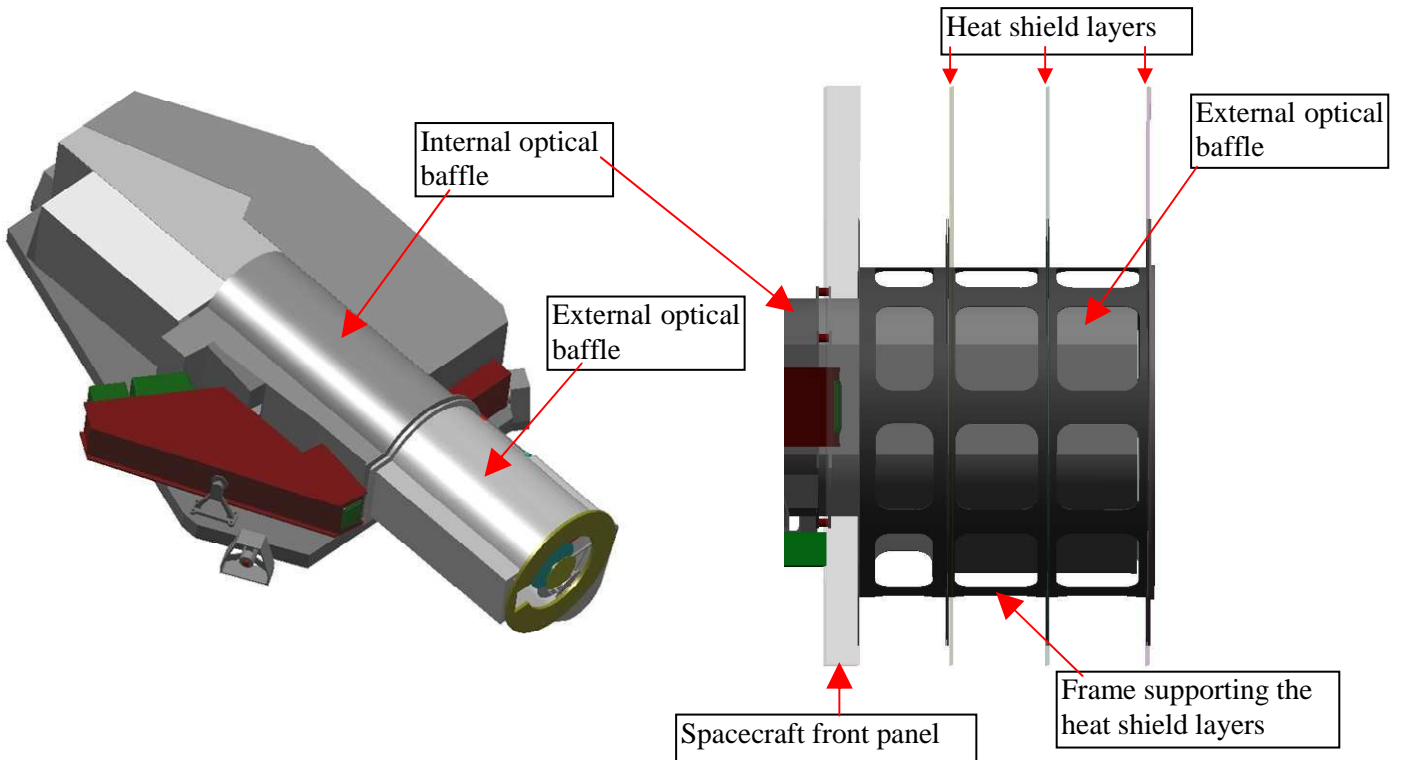
Figure 4.37. METIS external and internal optical baffles.
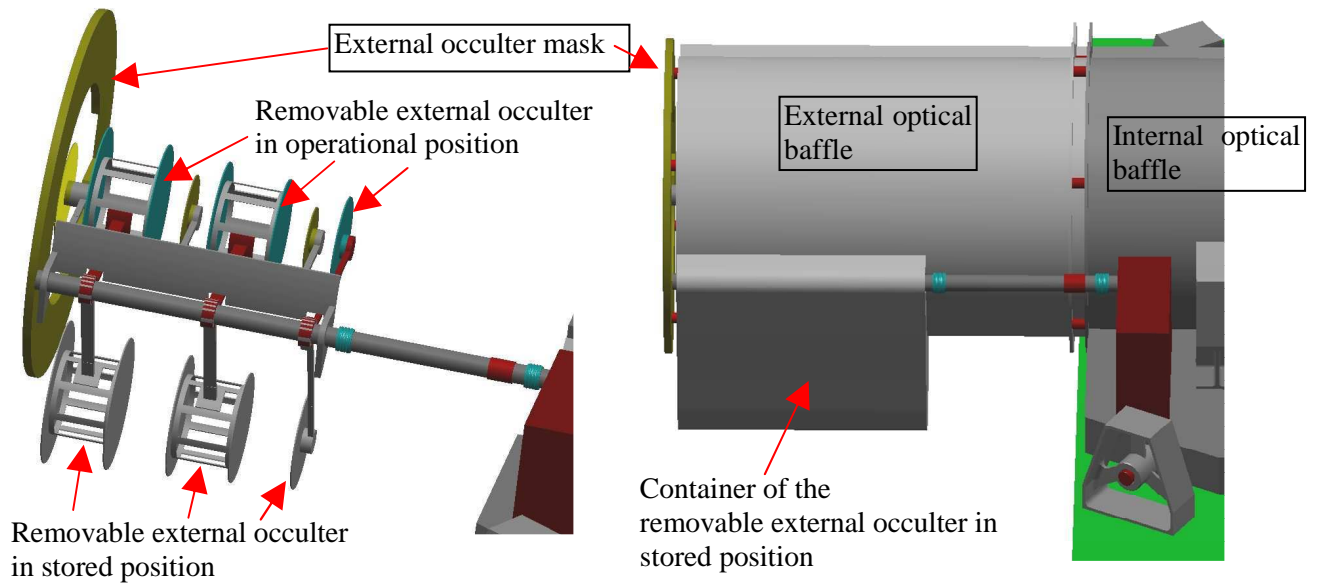
Figure 4.38. Interface between the external occulter and the external optical baffles.

METIS
EID - PART B

REF: INAF/OATO NR. 94
DATE: 15-JAN-2008
ISSUE 1
page 78 of 108

Diameter of the hole in the heat shield needed for the passage of the external optical baffle

400 mm

Frame supporting the heat shield layers
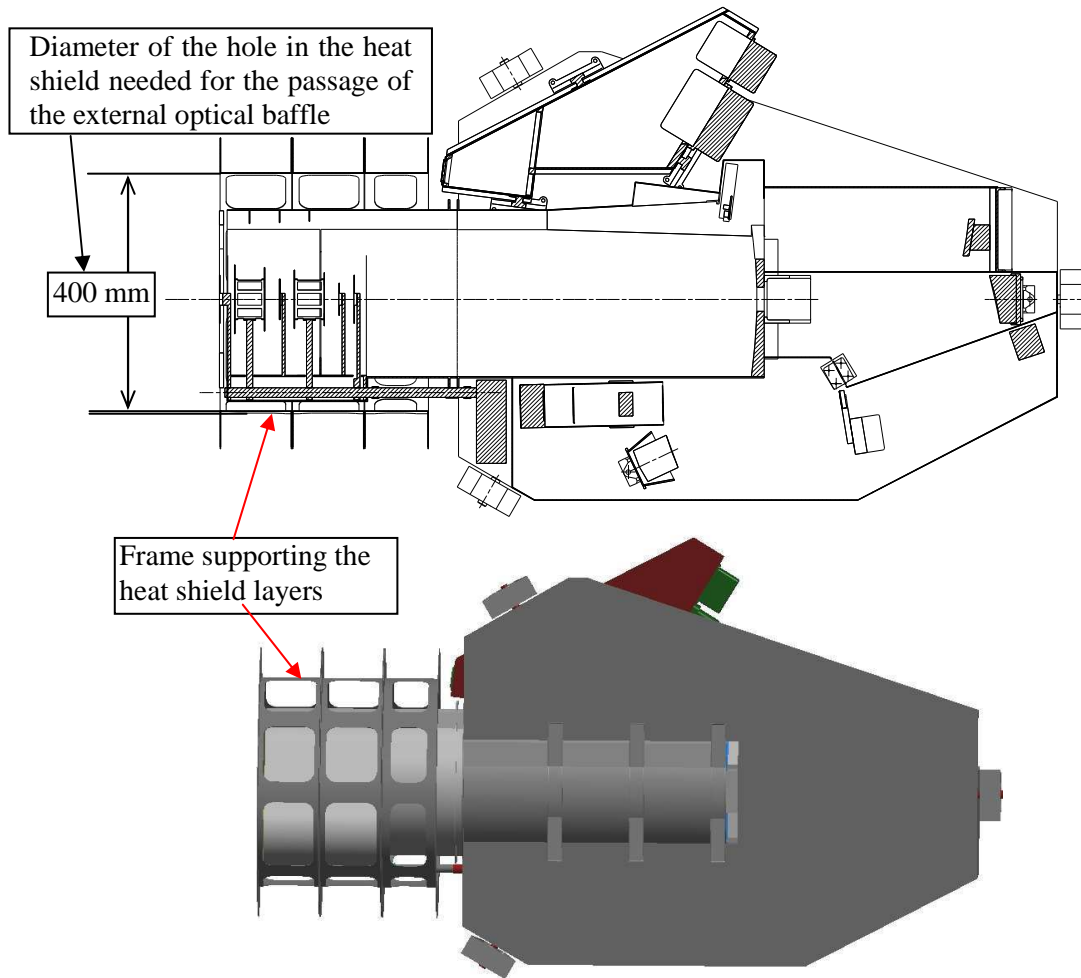
Figure 4.39. Interface between the heat shield and the external optical baffle.

Baffle isolating the sun disk light beam from the sun corona light beam

METIS
EID - PART B

REF: INAF/OATO NR. 94
DATE: 15-JAN-2008
ISSUE 1
page 79 of 108

Baffle isolating the
COR detector area
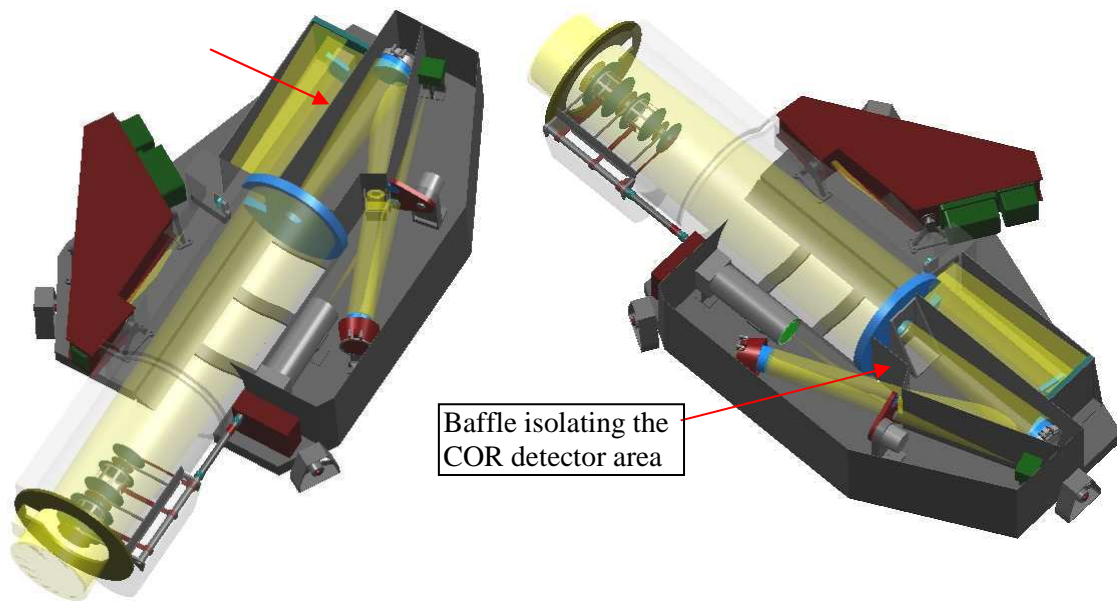
Figure 4.40. Optical baffles installed on the METIS bench.

4.6.5 Doors

An external door shall be provided by the S/C for closing the entrance aperture of METIS when it is not observing. The door shall be located on the top of the front shield, as shown in Figure 4.41. All opening and closing modes and the required number of cycles will be defined in the first phase of the project.
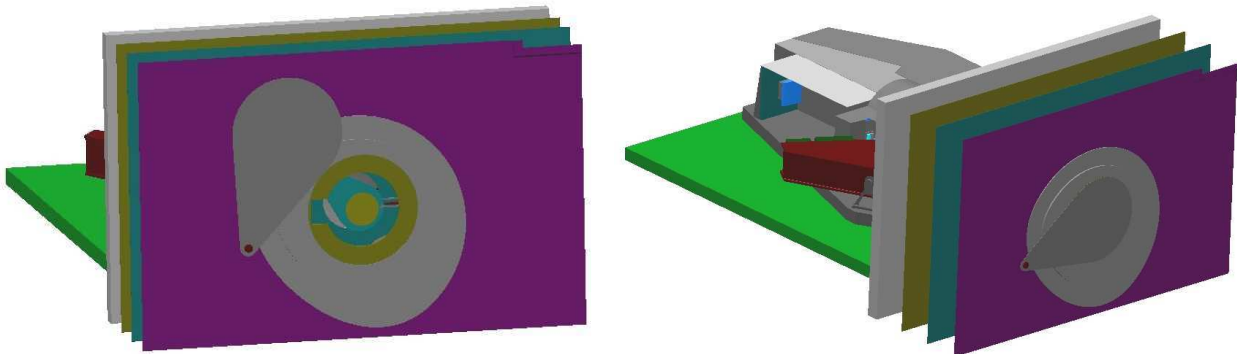
Figure 4.41. Example of accommodation of the external door closing the instrument aperture when not in operation.

4.6.6 Mechanical Environment

The METIS instrument will be designed to withstand the mechanical environment during all phases of AIT/AIV, qualification and acceptance testing (as specified in Section 6.4.5 of RD-1) and that produced at launch.

4.6.7 Structural Design

The METIS structure will be designed to comply with the factors of safety defined in the section 4.6.6.1 of RD-1 and with the design loads specified in the section 4.6.6.2 of RD-1. The structure will be sized so that

METIS
EID - PART B

REF: INAF/OATO NR. 94
DATE: 15-JAN-2008
ISSUE 1
page 80 of 108

all the fundamental resonance frequencies are above 140 Hz. In addition, the structure will guarantee the dimensional stability required for the maintenance of the mutual alignment of the optical elements under the experienced thermal loads, and shall minimize the heat transfer to the optical bench.

The optical bench, on which all the METIS elements are mounted, will provide structural interface for all the instrument items (optics, detectors, filters, mechanisms) and for the attachment to the S/C. The optical bench will also guarantee the required alignment stability of the optics during the mission.

To integrate strength, alignment and thermal stability performance, the optical bench is a 40 mm thick sandwich panel with CFRP skins (1 mm thick) and CFRP honeycomb. Titanium inserts are embedded in the honeycomb in correspondence of the mounts of the optical items installed on its surface. The inserts will be mounted with slight protrusion with respect to the panel surface in order to machine a common interface plane after insert integration. Three special inserts are foreseen at the edge of the panel to provide the attachment interface to the spacecraft, via dedicated "pseudo-kinematics mounts" providing a quasi-isostatic support, designed to carry the launch loads and to minimize at the same time the transfer to the bench of stresses originated by deformations of the spacecraft structure. Each pseudo-kinematics mount is designed to constrain the two degrees of freedom orthogonal to the pivot axis.

In the optical bench a cut-out is foreseen in order to partially accommodate inside the internal optical baffle and the M0 mirror. This allows to reduce the separation between the optical axis and the bench plane, so enabling to realize a more compact and light instrument configuration.

The optical baffle will integrate the optical performance with structural, alignment stability and temperature resistance performance, since it is used to support and maintain in position the external occulter, facing the direct Sun light. This integrated choice has been made for mass saving and reduction of the volume occupied inside the heat shield.

The optical baffle is composed of two parts, one internal and one external to the optical bench. The external part is mounted on the internal one and crosses the spacecraft heat shield. The internal one is attached to the optical bench through two rails and four transversal ribs (which have also the scope to create structural link between the two sides of the bench panel separated by the cut-out).

The splitting of the optical baffle in two segments (external, internal) has been introduced to create a thermal cut between the external and internal segments, so to limit the heat flux towards the instrument. Due to the high temperature environment to which the external optical baffle is subject, is shall be preferably made of Carbon/Carbon composite (CTE = 0.2 µm/m/°C, thermal conductivity = 34 W/m/°C, Elastic Modulus = 66 GPa) which is free from volatile resins. The internal optical baffle can be instead realized in CFRP. Dedicated thermal isolators shall be interposed at the interface between the two parts. The thickness of both the external and internal optical baffle walls is 1 mm.

The disks of the external occulter and their support rods are made of Titanium alloy (CTE = 9.2 µm/m/°C at 250°C, thermal conductivity = 16.4 W/m/°C). The same material is utilized for the shaft connecting the removable external occulter to its rotation stage on the optical bench.

The main structural elements of METIS are indicated in Figure 4.42.

METIS
EID - PART B

REF: INAF/OATO NR. 94
DATE: 15-JAN-2008
ISSUE 1
page 81 of 108

Optical
bench

Ribs

Rail

Optical bench-S/C panel
mounting interface
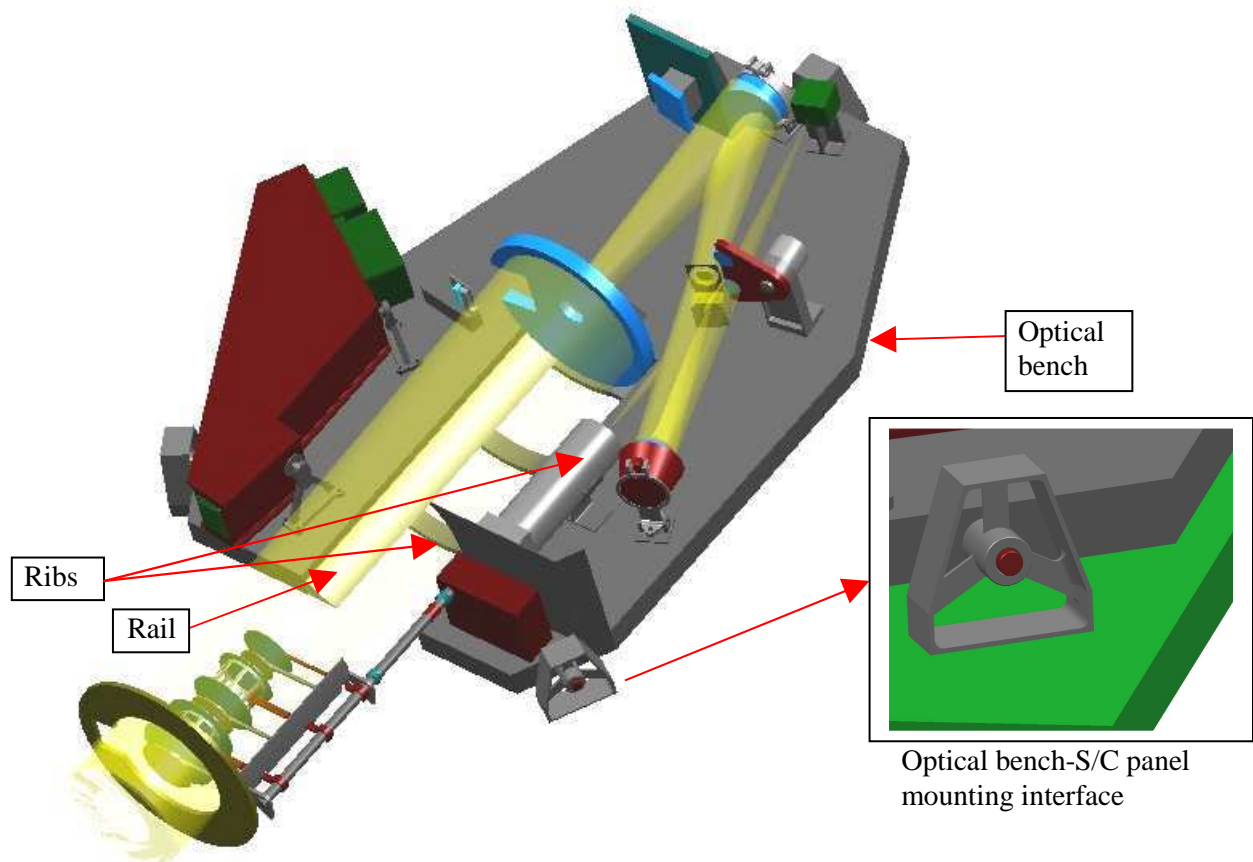
Figure 4.42. Main structural elements of the METIS instrument.

4.6.8 Payload Generated Disturbances

The instrument generated disturbances to the satellite pointing can be produced by the METIS internal mechanisms and in particular by the rotation of the removable external occulter from the storage position to the operational position and viceversa. This mechanism is planned to be operated just before the satellite performs the manoeuvre for off pointing the optical axes of the remote sensing instruments from the sun center, and therefore not during the observation phase.

The other METIS mechanism (EUS primary mirror scan mechanism, SOCS primary mirror translator, slit mask translator, filter wheel rotator, internal occulter positioner) moves small masses and are operated only from time to time (not continuously). An evaluation of the disturbances induced by all these mechanisms will be performed during the first phase of the project and will include the moving mass and the movement frequencies and characteristics.

4.7 Thermal interfaces

4.7.1 Thermal Control Definitions and Responsibilities

The thermal control of the METIS instrument will be performed by the Instrument Team, in compliance with the responsibility and definitions provided in section 4.7.1 of RD-1.

4.7.2 Thermal Environment

The METIS instrument will be compatible with the thermal environment specified section 4.7.2 of RD-1.

METIS
EID - PART B

REF: INAF/OATO NR. 94
DATE: 15-JAN-2008
ISSUE 1
page 82 of 108

4.7.3 Thermal Interfaces – Definitions

The thermal interfaces of the METIS instrument will be mentioned in accord with the definitions given in section 4.7.3 of RD-1.

4.7.4 Thermal Interfaces – Requirements

The thermal interface figures given in section 4.7.4 (tables 8, 9, 10) and subsections of RD-1 will be taken as reference values for the METIS instrument design.

In order to reduce the input power from outside, the disks of the external occulter (EO, fixed or removable) will be mirror-coated on the outer side so to maximize the back reflection of the heat and minimize its absorption. The inner side of the EO disks can be instead preferably black coated (TBC after detailed thermal analysis) to let them radiating the residual absorbed heat and so minimizing their temperature increase. The radiated heat will be absorbed by the walls of the internal optical baffle (i.e. the section of the optical baffle crossing the heat shield), that in turn will dissipate the heat inside the gaps between the layers of the S/C heat shield. Each disk of the fixed EO is connected to a mounting frame (installed on the external optical baffle) by means of thin titanium rods with interposition of thermal washers.

Each disk of the fixed EO is connected to a mounting frame (installed on the external optical baffle) by means of thin titanium rods with interposition of thermal washers.

The outer side of the external occulter mask will be also mirror coated and connected to the external optical baffle with the interposition of thermal washers.

The five disks forming the removable EO are connected by means of three titanium rods (the four outer disks are connected two by two) to a hollow shaft made in titanium and linked to the motor installed on the optical bench. A thermal breaker made of ceramic material is introduced along the shaft to prevent the heat propagation towards the bench.

The external optical baffle is black coated and is connected to the internal optical baffle (that surrounds the sun disk and corona light beam till the sun disk rejection mirror M0) through an interface frame and the interposition of thermal washers at any bolted connection (bolts are in titanium) to cut the heat flux towards the bench.

Preferably, the external optical baffle should not be surrounded by an additional thermal baffle, but just by a frame (spacecraft provided) supporting the various layers of the heat shield, avoiding the direct physical contact between the shield and the baffle, but letting the optical baffle sides free to radiate the heat in the gaps between the layers of the heat shield with a good view factor (see Figure 4.43). On top of the front shield, the frame shall overlap by about 1 cm the external occulter mask (so to cover the gap between the optical baffle and the front shield) but again without a physical contact.

The instrument elements which are subjected to the largest solar radiation flux (excluding the EO) are the COR sun disk rejection mirror M0 and the EUS M1 mirror. The M0 mirror will reflect to space >90% of the incoming flux, while the EUS M1 will transmit by transparency ~83% of the impinging flux to a heat absorber located on the back. In order to maintain their temperature within the operating limits, they shall be made of a high thermal conductivity material (SiC or Cesic for M0, metal for the heat absorber) and shall be connected to a radiator through thermal straps (instrument provided) and heat pipes (S/C provided).

METIS
EID - PART B

REF: INAF/OATO NR. 94
DATE: 15-JAN-2008
ISSUE 1
page 83 of 108

The detectors may be kept at their operational temperature by TECs connected by straps to the cold finger interface provided by the spacecraft.
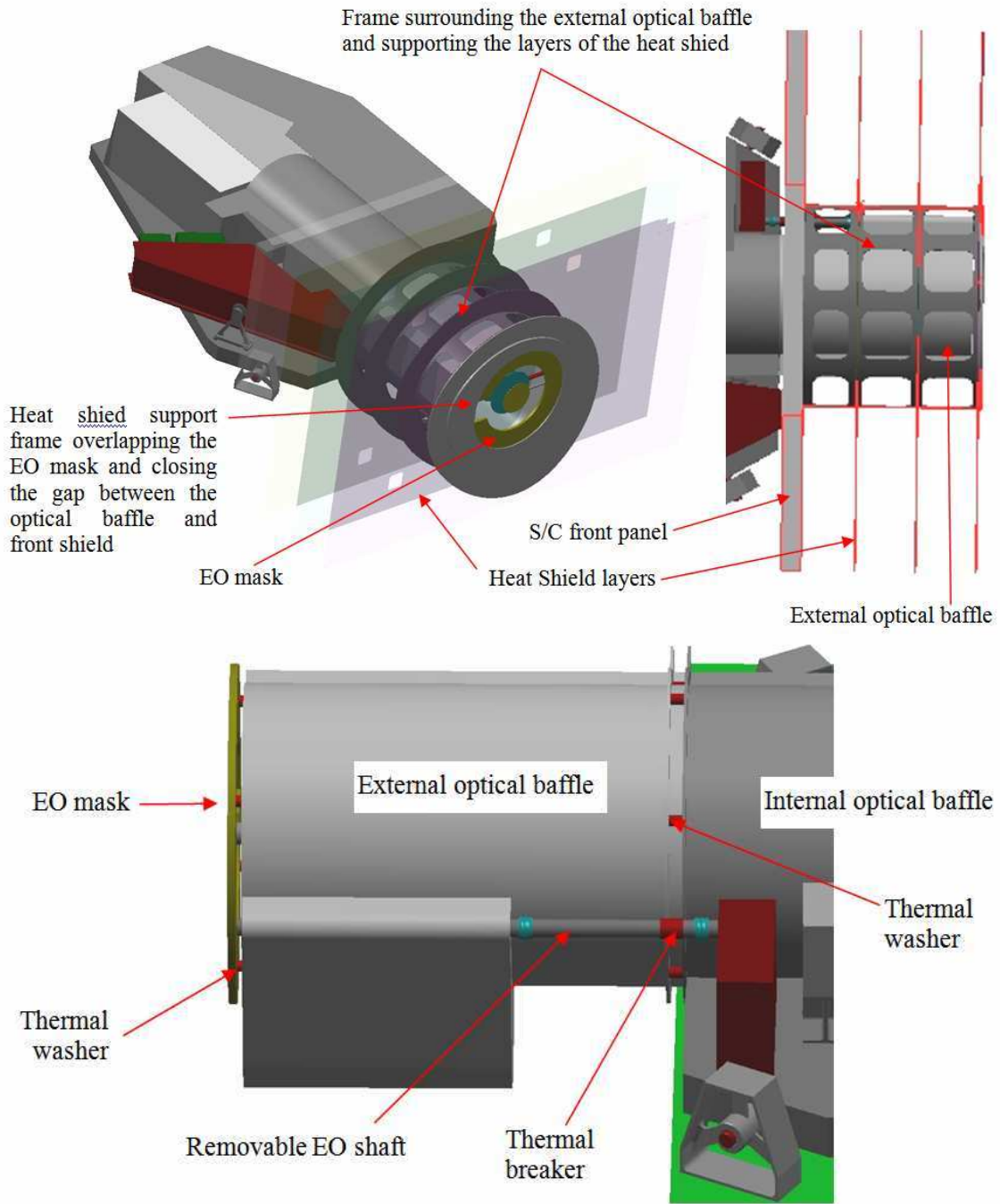
Figure 4.43. Thermal interfaces between the EO, the optical baffle and the heat shield.

4.7.5 Thermal Hardware Interfaces

The METIS instrument thermal hardware will be compatible with the interface requirements specified in section 4.7.5 of RD-1.

METIS
EID - PART B

REF: INAF/OATO NR. 94
DATE: 15-JAN-2008
ISSUE 1
page 84 of 108

4.8   Electrical Interfaces

The MPPU, (METIS Processing & Power Unit) is the unique interface of the instrument with the Spacecraft (Power, Science Data, TM&TC). The high-level architecture of the METIS electronics is provided in Figure 4.44, where the MPPU links with Spacecraft and detectors are shown.
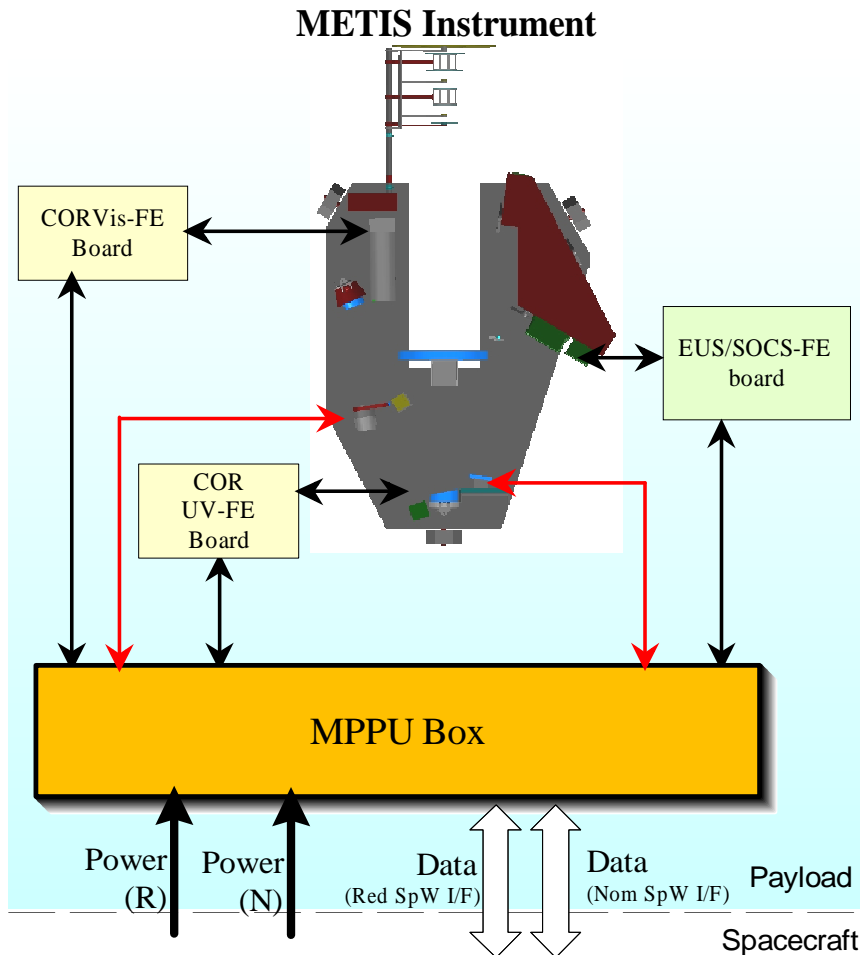
Figure 4.44. METIS High Level Electronic Architecture.

4.8.1 Electrical Power Design and Interface Requirements

The MPPU is in charge of generating regulated supply voltages for all the METIS instrument items from the S/C regulated bus voltage.

From the power point of view, the MPPU interfaces the Spacecraft with two (one Nominal and one Redundant) regulated power lines on separate connectors.

The nominal voltage of the power lines should be 28 V, with 26 V and 29 V as minimum and maximum values.

METIS will safely survive both to any standing or fluctuating voltage in the full range 0 V to 32 V and transient up to 1 ms and 33 V without performance degradation.

In case of failure, both the nominal and the redundant power lines can be applied simultaneously, so MPPU box will include isolation to avoid loss of one power source by a failure in the other power source.

The Nom/Red power lines are placed in OR by means of input diodes.

METIS
EID - PART B

REF: INAF/OATO NR. 94
DATE: 15-JAN-2008
ISSUE 1
page 85 of 108

METIS instrument will survive an intentional or unintentional switch-off in any configuration without degradation of nominal performance. And, when powered up, it will have an initial electrical safe status which is independent of the switch-off configuration.

MPPU DC/DC converters will be equipped with:
- short circuit protection
- in-rush current limiter
- LCL
- reverse polarity protection

The current estimate of the METIS instrument power consumption budget is provided in Table 4.8.1-1. The power figures include a 25% contingency margin.

Table 4.20. METIS instrument current power budget.

Item	Primary Power [W]	Note
FEE boards (including detector)	13.2	
MPPU	37	
Actuators	negligible	The power dissipated in average by the mechanism is considered negligible due their very short duty cycle.
Total Average	**50.2**	

4.8.2 Data Handling Electrical Interface Requirements

From the data lines point of view, the MPPU interfaces the S/C with two (one Nominal and one Redundant) SpaceWire data I/F, on separate connectors, which will be addressed and routed separately to the spacecraft data handling.
METIS will be able to receive SpaceWire time codes according to ECSS-E-50-12.
The SpaceWire remote terminal controller will be the ESA RTC or an equivalent device.

The METIS elements provisional data volume per orbit and the compression factor required are summarized in Table 4.21. The available telemetry rate for COR is 10 kb/s and 17 kb/s for EUS + SOCS. The *required* telemetry rate is computed on the basis of 110 days operational HGA.

Table 4.21. METIS instrument current telemetry budget.

Element	NOM 30 days [bit]	TSOM 10 days [bit]	> 0.5 AU 110 days [bit]	Compression factor	Data volume/orbit [bit]	Telemetry rate [kb/s]
COR	8.4E11	8.8E10	5.1E10	10	9.8E10	10.3
EUS	2.5E11			2	1.6E11	16.5
SOCS	4.8E10	9.4E09	6.9E09			
Total	1.1E12	9.7E10	5.8E10		2.6E11	26.8

4.9 Software Interface and design requirements

4.9.1 Software design requirements

The only METIS unit containing SW is the MPPU.
As a baseline, the on-board S/W will comply with the software standard ECSS-E-40.

METIS
EID - PART B

REF: INAF/OATO NR. 94
DATE: 15-JAN-2008
ISSUE 1
page 86 of 108

In view of the in-flight S/W maintenance, the instrument S/W will assign functionally distinct areas of memory to:
- code
- fixed constants
- variable parameters.

A minimum boot S/W will reside in PROM.

The main resources of the instrument will be accessible in boot mode, including EEPROM updates and hardware check capability.

On-board S/W will be structured, as a baseline, such that modifications can be made to a S/W module without affecting other module positions in the memory.

On-board S/W maintenance activities will not cause a blockage of the instrument and will be able to be cleared by a power cycling of the instrument (TBC).

The payload software design will ensure that erroneous operation cannot cause a safety hazard.

As a goal, the resources utilized by on-board software will be telemetered (e.g., memory usage, central processor unit (CPU) usage and I/O usage).

S/W will be provided with the capability to check that on-board software has been correctly uploaded before enabling it.

Enabling of on-board S/W will use only a single telecommand.

Any communication between the ground and an on-board software function or software task will be effected by means of telecommand and telemetry source packets specifically designed for the purpose.

Whenever a condition that forces a processor reset is detected by software, an event report shall be generated and sent prior to enforcement of the reset.

Whenever a processor overload condition is detected, an event report will be generated.

Whenever an unexpected arithmetic overflow condition is detected, an event report will be generated.

Whenever an illegal program instruction is encountered during execution of a program code, an event report will be generated.

Whenever a data bus error is detected by S/W, an event report will be generated.

Whenever a memory corruption is detected by an error detection and correction mechanism, an event report will be generated.

Whenever a checksum error is detected, an event report will be generated.

Instrument computers shall reset and resume operations from a defined mode in case of power on/off cycling.

4.9.2 Software Interface Requirements

In the METIS communication software, a SpaceWire Link Interface building block will be implemented to interface with the network / packet router. The implementation will be compliant up to the packet & network levels of SpaceWire Standard.

4.10 EMC design

4.10.1 General Concept

The EMC requirements will have to ensure the proper system functions, which are characterized by low electrical sensor signals and extensive use of computer high rate digital equipment.

The spacecraft/payload EMC requirements described in the following sections cover the system imposed aspects:
• Section 4.10.2: Design requirements, which ensure a coherent satellite system design
• Section 3.6.3: Performance requirements, at system and unit levels, which quantify the applicable emission and susceptibility levels to ensure the required safety margin at system level.

METIS
EID - PART B

REF: INAF/OATO NR. 94
DATE: 15-JAN-2008
ISSUE 1
page 87 of 108

4.10.2 Design Requirements

4.10.2.1 Grounding and Isolation

METIS will apply a modified distributed single point ground scheme based on the following principles:

Power:
- The primary DC power will be grounded to structure in one point within the power subsystem only.
- All return lines will be isolated from the structure.
- Each unit will generate his own secondary power isolated from the input power.
- The return of each secondary power will be connected to the structure in one point ONLY by an external removable connection which serves as the signal reference ground, for all the circuits fed by that secondary power.
- The signal reference ground will be connected to structure via a unit-external and removable grounding strap.
- Power Lines Isolation will be in accordance with section 4.8.1.4 of RD-1.

Signal grounding and isolation:
- Between electrical units, signal driver outputs will be referenced to ground and signal receiver inputs will be isolated from ground.
- The connection to ground will be anyway made only on one side of electrical connections between units.
- Isolating receivers will provide common mode rejection capability. Balanced differential signals are preferred.

4.10.2.2 Electrical Bonding and Case shielding

Each unit will be housed in a non-magnetic metallic case which will form an electromagnetic shield.

The case will not contain any apertures other than those essential for sensor viewing or outgassing vents. If outgassing vents are required they should be as small as possible (less than 5 mm in diameter) and should be located in the case surface which is closest to the spacecraft $-X_{OPT}$ face.

Electrical connectors for pyros and RF are to be considered as part of the case; all connectors will include a metallic outer shell such that when the mating cable harness connector is inserted in the box mounted part, the whole connector is completely shielded. The shell of the box mounted part will be bonded to the equipment case as required by this specification.

The case of each unit will be grounded to the spacecraft structure, with a low impedance bonding strap.

The DC resistance across the electrical bond between any two adjacent parts, including connector shells, will not exceed the 2.5 (TBC) mOhm (test at 100 mA and with both directions of polarity using a 4-wire measurement) limit for both test polarities.

Non-metallic conductive structure parts will be electrically bonded to the metallic reference in order to avoid differential charge build-up. This applies also to external thermal blankets and baffles.

4.10.2.3 Cable Shielding and Separation

Power and signal lines will be grouped into the following EMC classes:
- Class 1: Power lines and Heater Lines
- Class 2: Digital lines (TM/TC)
  Non-sensitive analog lines (except RF)
- Class 3: Pyro / Mechanisms
- Class 4: Low level sensitive lines
- Class 5: RF

Lines of different EMC classes will be separated by at least 5 cm.
Lines of different EMC classes will not be routed parallel (as a goal)

METIS
EID - PART B

REF: INAF/OATO NR. 94
DATE: 15-JAN-2008
ISSUE 1
page 88 of 108

Lines of different EMC classes will be routed through separate connectors. Where this is not possible, separation will be implemented by a row of grounded pins.

Redundant lines will be routed through separate connectors.

Lines of Class 2 to Class 5 will be shielded.

All line bundles of classes 1 to 5 will have an overshield grounded to the structure at intervals of no more than 15 cm.

These rules will also be preferably applied within electrical units.

The active wire(s) will be twisted with the return wire. The twisted wires will be routed through a connector on adjacent pins to minimize the wire loop.

Cable shield will not be used as the return path for signal or power.

Harness and connector layout will permit the termination of cable shields at both ends.

For category 3 connectors shields will be terminated on metallic shell all-over 360 deg.

For less sensitive signal lines only (i.e. class 2) the pig-tail connection to connector metallic shell will be allowed.

The pig-tail length will be less than 5 cm.

The ground connection of the shield via a connector pin will be forbidden.

The unshielded length of any single cable will not exceed 2.5 cm.

The resistance between harness shield and unit will be less than 7.5 mOhm.

4.10.3 Performance Requirements

The EMC requirements will be met for any operating mode of the instrument, following the indication given in section 4.10.3 of RD-1.

4.11 Instrument Handling

4.11.1 Definition of Transport Container

The PI will provide an adequate transport container for the METIS units.

4.11.2 Instrument Cleanliness Plan

The PI will provide an adequate cleanliness plan for instrument handling, following the indications that will be given in RD-1.

4.11.3 Physical Handling Requirements

The PI will provide adequate METIS handling requirements, following the indications that will be given in RD-1.

4.11.4 Instrument Purging Requirements

During the system AIV programme, dry nitrogen purging will have to be continuously provided to METIS, owing to its stringent cleanliness requirements.

Individual purge rates for METIS will be specified by the PI and will be controlled by means of pipe throttling.

The exact location of the purging interface will be agreed with the ESA Project Office and the selected Prime, and will be defined in this document.

The PI will specify the purging requirements for METIS during spacecraft integration and testing, transportation and the launch campaign.

4.12 Environment Requirements

METIS will be designed to withstand the environment defined in the RD2, predicted for the worst case extended mission duration.

METIS
EID - PART B

REF: INAF/OATO NR. 94
DATE: 15-JAN-2008
ISSUE 1
page 89 of 108

4.12.1 Cleanliness

The PI will provide the METIS contamination plan.

4.12.1.1 Particulate and molecular cleanliness

METIS is an optical instrument mainly dedicated to observations in the EUV, and to coronagraphic analysis. Both this points need an extremely tight cleanliness and contamination control, both in terms of molecular and particular contamination, during AIT activities. To maintain the foreseen instrumental performance, the PI will provide the definition of the particulate and molecular cleanliness levels with justification.

The instrument will be designed to withstand with the particulate and molecular contamination levels in the clean room environment and thermal vacuum facilities as described in the section 4.12.1.1 of RD-1.

4.12.1.2 Magnetic Cleanliness

The PI will list all magnetic materials in use in METIS with an estimated magnetic dipole moment for the instrument to maintain the magnetic cleanliness environment requirements described in section 4.12.1.3 of RD-1.

4.12.2 Radiation

METIS will be designed to withstand the radiation environment defined RD2, predicted for the worst case extended mission duration, and following the indications given in section 4.12.2 of RD-1.

4.12.3 Micrometeorite Environment

METIS will be designed to withstand the micro-meteorite environment defined in the Mission Environment Specification [RD2], predicted for the worst case extended mission duration.

Specific design protection will be incorporated wherever needed, e.g. all external wiring will have sufficient shielding.

METIS
EID - PART B

REF: INAF/OATO NR. 94
DATE: 15-JAN-2008
ISSUE 1
page 90 of 108

5. Operational Interfaces

5.1 Definition of Instrument Modes

A provisional definition of the METIS operational modes of the instrument for both ground and in flight operations is given in section 3.4. The list of the presently foreseen observational modes is given in Table 3.3.

5.2 Ground Operations

5.2.1 Ground Support Equipment Requirements

The PI will deliver and support equipment to be located at the MOC as required for operations.

5.2.2 Facility Requirements

TBW

5.3 Flight Operations

5.3.1 Ground segment

TBW

5.3.2 Mission operations

TBW

5.3.3 Instrument Deliverables to the Operational Ground Segment

TBW

5.3.4 Instrument Inputs to the Science Ground Segment

TBW

5.3.5 Mission Products

TBW

5.3.6 PI Support to Operations

TBW

METIS
EID - PART B

REF: INAF/OATO NR. 94
DATE: 15-JAN-2008
ISSUE 1
page 91 of 108

6. Instrument Verification Plan

6.1 General

he qualification approach selected for METIS follows the guidelines stated in section 6 of the RD-1.

The instrument verification plan specifies the intended qualification approach and describes the adopted model philosophy, including also prototypes and other non-deliverable models, and the build standard relevant to each model. Critical items are also identified, and the required steps for their development are described.

The verification plan specifies all the activities to be performed at subsystem, unit and experiment levels; moreover, also the experiment most critical items will be verified as appropriate throughout their development (design and hardware production) to guarantee the fulfilment of their specific requirements. The methods of verification are also described.

All design, development and verification activities will be carried on following ECSS standards.

6.1.1 Introduction

The METIS Verification Programme will demonstrate to ESA and its selected Prime that the instrument design is fully compliant
- with the instrument scientific goals;
- with the mission environment;
- with the spacecraft performance;
- with the spacecraft interface requirements;
- with the operational requirements;
- with the provided operational documentation;

hence capable to contribute to the overall scientific goals.

6.1.2 Responsibilities

The PI will verify, in a systematic manner, the instrument design and build against each requirement specified in the EID-A and B [Qualification].

The PI will verify, in a systematic manner, the FM instrument certification for flight against each requirement specified in the EID-A and B [Acceptance].

The PI will include in the Instrument Development Plan (IDP) the tests and analyses that collectively demonstrate that hardware and software complies with the requirements.

6.1.3 Definitions

METIS verification plan will comply with the definition given in section 6.1.3 of RD-1.

6.1.4 Documentation

The PI will provide a documentation compliant with section 6.1.4 of RD-1.

6.2 Verification concept

Instrument verification will be accomplished preferably by testing. But in certain cases, when testing is not possible, one or more of the following verification methods will be applied:
- Analysis (Structural, Thermal), when verification is achieved by performing theoretical or empirical evaluation by accepted techniques
- Functional Tests (FFT, AFT) or Environmental Tests (Vibration, TB/TV, EMC), when requirements have to be verified by measuring product performance and function under various simulated environments

METIS
EID - PART B

REF: INAF/OATO NR. 94
DATE: 15-JAN-2008
ISSUE 1
page 92 of 108

- Inspection: Verification is achieved by visual determination of physical characteristics (such as construction features, hardware conformance to document drawing or workmanship requirements)
- Review-of-design (Similarity Assessment): Verification is achieved by validation of records or by evidence of validated design documents or when approved design reports, technical descriptions, engineering drawings unambiguously show the requirement is met.

6.3 Analysis

Verification by analysis will be carried out extensively for the validation of the structural and thermal design at system and subsystem levels (optical bench, cameras and spectrometers optical heads and detectors, etc).
A radiation sensitivity analysis will be performed to evaluate the radiation impact on electrical components such as FPGAs, A/D converters, array detectors.
During the experiment development, breadboards of specific items and the STOM (Structural, Thermal and Optical Model) will be used to tie the results of analysis based on mathematical models with tests results, based on actual performance measurements under controlled environmental conditions.
In the overall, the numerical models which will be produced to guarantee analytical compliance to a given requirement will cover, whenever necessary, the following topics:

- Radiation sensitivity analysis
- Structural analysis
- Mechanisms analysis
- Thermal analysis
- Electrical performance evaluation
- Part stress analysis

Analysis reports will be generated for each analysis verification, and submitted to the SO Project Office.
.

6.3.1 Structural Mathematical Analysis

METIS mechanical performance will be calculated by means of structural mathematical models (SSMs)
The PI will use models for his own design and will also provide model(s) to the Agency for use during spacecraft design and test results predictions. The PI will update the models according to instrument and system test results.
The instruments SMMs will be delivered according to the dates TBD. They will comply with the detailed requirements for each model / analysis as listed in section 6.3.1 of RD-1.

6.3.2 Thermal Analysis

METIS thermal analysis will be performed to:
- verify that internal parts and materials are below their maximum allowed temperatures under acceptance/qualification testing;
- verify the ability of the thermal design to maintain the internal required temperatures and intended heat flow pattern that ensure performance requirements under the worst flight cases;
- verify the compliance with the spacecraft interface requirements under the worst flight cases.
METIS thermal analysis will comply with the requirements listed in section 6.3.2 of RD-1.

6.4 Testing

6.4.1 General

The verification activities will be divided in
- Qualification Programme
- Acceptance Programme
- Recertification
- Incoming Inspection

METIS
EID - PART B

REF: INAF/OATO NR. 94
DATE: 15-JAN-2008
ISSUE 1
page 93 of 108

The test programme will be arranged in a way to best disclose problems and failures associated with the characteristics of the hardware and the mission objectives.

METIS testing activities will comply with the requirements listed in section 6.4.1 of RD-1.

In the following, an overview is given of the tests that will be performed during the development of METIS to validate the design and qualify the hardware and software for flight. Tests will be performed also on BreadBoards and Prototype models to validate specific technical solutions.

Reference is made with respect to the general tests requirements and program as given in section 6.4 of RD-1.

6.4.2 Functional Testing at Instrument Level

The Full Functional (Performance) Test (FFT) will be a detailed demonstration that the hardware and software meet their performance requirements within allowed tolerances, compliant with the requirements described in section 6.4.2.1 of RD-1.

In case FFT is impracticable, an Abbreviated Functional (Performance) Tests (AFT) could be performed, compliant with the requirements described in section 6.4.2.2 of RD-1.

6.4.3 Functional Testing at System Level

The functional testing at system level will be performed on the basis of the requirement that will be specified in the SO EID-A.

6.4.4 EMC Testing

The EMC testing will be performed following the requirements indicated in section 6.4.4 of RD-1.

6.4.5 Structural Testing

Structural testing will be performed following the requirements indicated in section 6.4.5 of RD-1.

6.4.6 Mechanism Testing

METIS mechanisms testing will be performed following the requirements indicated in section 6.4.6 of RD-1.

6.4.7 Thermal Testing

Thermal tests will be performed following the requirements indicated in section 6.4.7 of RD-1.

6.5 Inspections

6.5.1 Visual Inspection

Visual inspection will be performed at the beginning and end of acceptance and qualification testing, following the indications given in section 6.5.1 of RD-1.

6.5.2 Physical Properties

METIS physical properties will be measured to determine the equipment physical characteristics, i.e. dimensions, mass, centre of gravity and momentum of inertia.

The interface and envelope (including envelope of separate electronics box, filter, etc. if applicable) dimensions, as a minimum, will be verified

6.6 Calibration

The PI will provide a calibration plan adapted to the scientific requirements and the overall development plan of the instrument and of the satellite.

The instrument will be delivered fully calibrated.

It will be defined and scientifically justified if calibration activities at system level will be necessary.

METIS
EID - PART B

REF: INAF/OATO NR. 94
DATE: 15-JAN-2008
ISSUE 1
page 94 of 108

The calibration plan will be part of the Instrument Development Plan.

6.7 Final Acceptance

6.7.1 General Approach

The acceptance process will demonstrate that METIS has been fully verified in terms of:
- scientific performance (including calibration and characterization)
- behavior versus environmental conditions (including EMC)
- all functional interfaces

The acceptance of the Instrument will follow the sequence hereafter:
- completion of acceptance tests, including calibration/characterization at the Instrument supplier premises, in order to verify that the Instrument together with its ground support equipment meet all interface specifications and that the Instrument is ready, for integration onto the satellite
- acceptance review of the tests results and of the completeness of the acceptance data package at instrument manager premises and release of a consent to ship if the acceptability is stated by the review board
- delivery to the satellite AIT site of the Instrument together with the ground support equipment (including test software and documentation) and the acceptance data package
- performance - by the Instrument supplier - of a post shipment inspection and at an incoming test at the AIT site
- after successful completion of the incoming verifications by the Principal Investigator and formal incoming inspection by system level QA, the Instrument will be released for integration onto the satellite
- notwithstanding the mandatory Instrument level tests, the Instrument software will only be accepted after successful S/C level tests.

6.7.2 Acceptance Review

The acceptance review will check and ascertain the following topics:
- visual inspection and completeness of the hardware to be delivered
- compliance of the interfaces measurements (Spacecraft interfaces)
- availability of a complete set of functional performances data (using both the AFT and FFT procedures)
- availability of calibration and characterization data
- ground support equipment relevant characteristics and documentation
- verification of the S/W configuration
- verification of the built standard
- completeness of the Acceptance Data Package

6.8 System Level AIT

6.8.1 Model Philosophy

The instrument model philosophy, defined according to the satellite AIT philosophy and requirements described in section 6 of RD-1 and to the METIS development and qualification program consists of:
- Breadboard Model (BBM), already implemented during the instrument Phase B in support to the development of the METIS equipments (in particular: detectors, FEE, mechanisms, optics, baffles, electronics and software) and of the design of the thermal control and of the mechanical interfaces.
- Structural Thermal Optical Model (STOM), for the qualification by test of the METIS structure (including external occulter, baffles, optics), mechanisms, thermal control, the verification of the structural and thermal mathematical models, the verification of the instrument-S/C mechanical, thermal and optical interfaces. After the tests at instrument level, the STOM will be delivered to the SO Prime Contractor.

METIS
EID - PART B

REF: INAF/OATO NR. 94
DATE: 15-JAN-2008
ISSUE 1
page 95 of 108

- Engineering Model (EM), for the verification of the electrical and software interfaces inside the instrument (between MPPU, FEE, detectors and mechanisms) and between the instrument and the S/C, verification of the operational modes and procedures, qualification of the instrument flight software, verification by test of the electromagnetic compatibility of the electronics, detectors and mechanisms. The MPPU and the FEE are planned to be realized at Engineering Qualification Model (EQM) level and subject to qualification tests before being used in the instrument EM. After the tests at instrument level, the STOM will be delivered to the SO Prime Contractor.
- Flight Model (FM), to be subjected to environmental and functional test campaign at acceptance level before the delivery the SO Prime Contractor.

Flight Spares (FS) for the replacement of failed or damaged equipment at integration and launch site will be also realized. The list of the items for which a FS will be realized will be defined during the instrument Phase A and discussed/agreed with ESA.

All these models will be tested on the basis of the indications given in section 6.8.1 of RD-1.

6.8.2 System Integration and Test Flow

Since the METIS suite is a composite instrument which includes different elements each characterized by its own specific scientific and operational task, plus some common parts, which functions are common to all the channels (MPPU, optical bench), the AIT / AIV activities at system level are of large relevance.

A diagram illustrating the flow of integration activities that shall be performed on METIS is shown in Figure 6.1. It includes all levels of integration from equipment (e.g. optics, detectors, mechanisms), through elements, up to system integration.
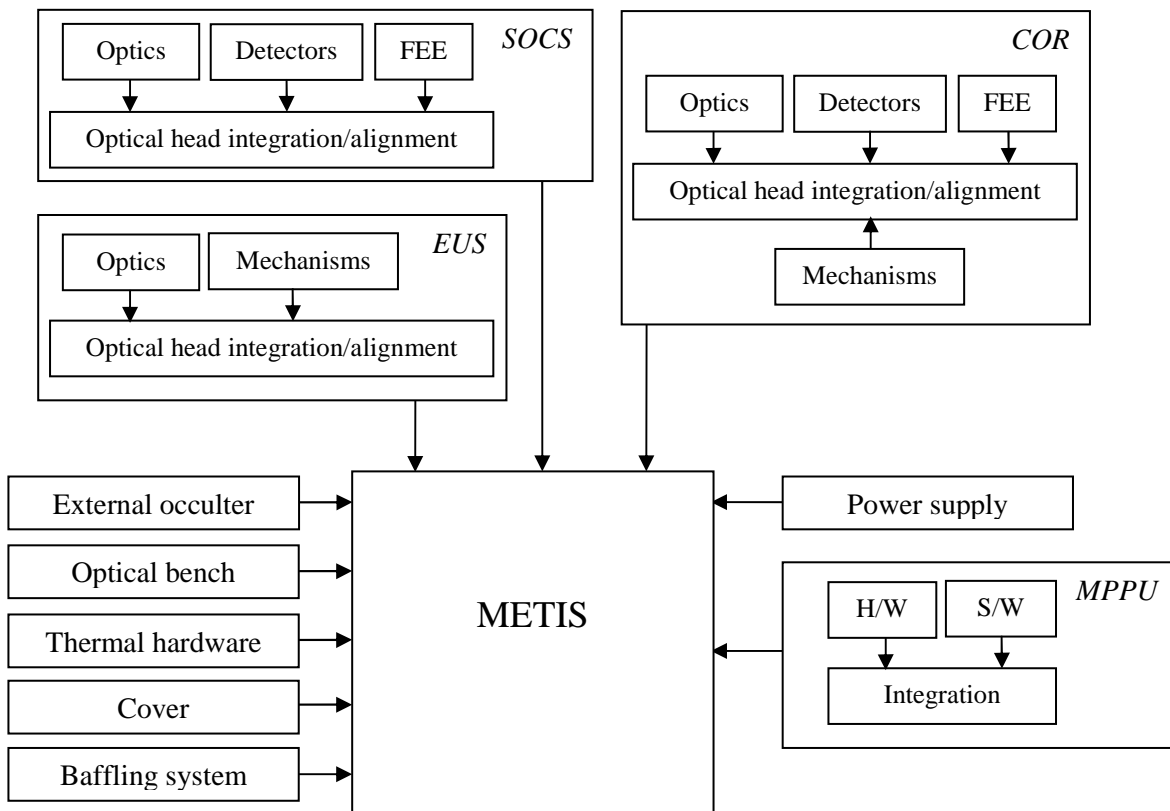
Figure 6.1. Flow diagram of the foreseen METIS integration activities.

METIS
EID - PART B

REF: INAF/OATO NR. 94
DATE: 15-JAN-2008
ISSUE 1
page 96 of 108

To obtain the best scientific return from the chosen instrument suite approach, co-alignment and cross calibration of the different channels, as well as functionalities of the common main electronics, will be the subject of verification at a system level. The system level test flow is shown in Figure 6.2.

For those items that can be fully characterized at a lower level only performance tests shall be performed at a system level.
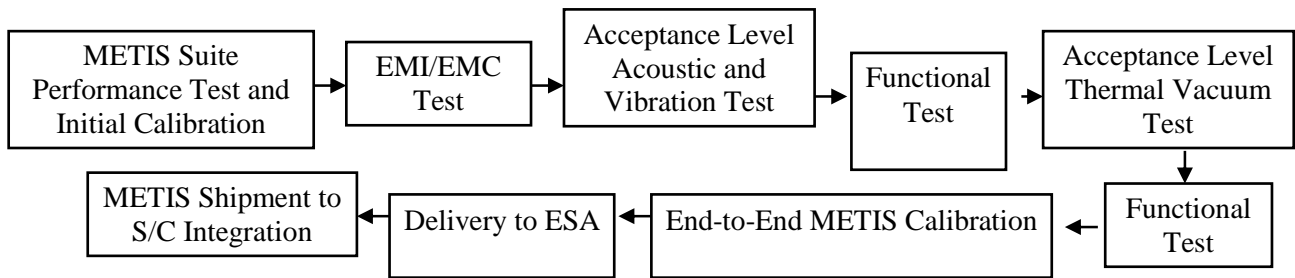
Figure 6.2. Flow diagram of the foreseen METIS system level test activities.

6.8.3 Ground Support Equipment

Ground Support Equipment (GSE) is clarified in section 7.3.10 of RD-1 as: "Optical, mechanical, fluidic, electrical and software support equipment or systems used for calibration, measurements, testing, simulation, transportation, handling... of space segment or of space segment elements."

Together with each instrument model, the PI will deliver the Mechanical Ground Support Equipment (MGSE) necessary to transport, handle and integrate the instrument hardware, accompanied by appropriate documentation and proof load and calibration certificates and the Electrical Ground Support Equipment (EGSE) necessary to stimulate the instrument and to perform quick look analysis of instrument TM during system tests. The PI will remain responsible for the maintenance of this equipment and will provide the necessary manpower and expertise support to integrate the instrument EGSE into the system EGSE.

The PI will define the functional requirements of the instrument and auxiliary equipment (e.g. MGSE, EGSE, etc.) at instrument and spacecraft system level.

METIS
EID - PART B

REF: INAF/OATO NR. 94
DATE: 15-JAN-2008
ISSUE 1
page 97 of 108

7. Product Assurance Plan

The Product Assurance Plan is the Part IV document of the Proposal.

METIS
EID - PART B

REF: INAF/OATO NR. 94
DATE: 15-JAN-2008
ISSUE 1
page 98 of 108

8. Management Plan

The Management Plan is the Part V document of the Proposal.

METIS
EID - PART B

REF: INAF/OATO NR. 94
DATE: 15-JAN-2008
ISSUE 1
page 99 of 108

9. Document References

9.1 Applicable Documents

AD-1

9.2 Reference Documents

RD-1   Experiment Interface Document – Part A Issue 1.0 – ref. SOL-EST-IF-0050 – October 2007
RD-2   Solar Orbiter Environmental Specification – issue 1.3 – ref. TEC-EES-03-034/JS – January 2006

METIS
EID - PART B

REF: INAF/OATO NR. 94
DATE: 15-JAN-2008
ISSUE 1
page 100 of 108

10. Acronyms

ADC	Analog to Digital Converter
AFT	Abbreviated Functional Test
AIT	Assembly, Integration and Test
AOCS	Attitude and Orbit Control System
APS	Active Pixel Sensor
BB	Breadboard
BBM	Bread-Board Model
CCD	Charge Couple Device
CFRP	Carbon Fiber Reinforced Plastic
CME	Coronal Mass Ejections
CNR	Consiglio Nazionale delle Ricerche
CNRS	Centre National de la Recherche Scientifique
CoI	Co-Investigator
CoM	Center of Mass
CoPI	Co-Principal Investigator
COR	METIS Visible and EUV Coronagraphic imager
CTE	Coefficient of Thermal Expansion
DMS	Data Management System
ECSS	European Cooperation for Space Standardization
EEO	Extended External Occulter
EEOM	EEO Mechanism
EM	Electrical Model
EM	Experiment Manager
EO	External occulter
EOM	External occulter Mechanism
EQM	Electrical Qualification Model
ESA	European Space Agency
EUI	EUV Imager
EUS	METIS EUV disk Spectrometer
EUV	Extreme UltraViolet
EUVC	EUV Channel
FEE	Front End Electronics
FEM	Filter Exchange Mechanism
FFT	Full Functional Test
FM	Flight Model
FOV	Field Of View
FS	Flight Spare
FWHM	Full Width at Half Maximum
GSE	Ground Support Equipment
H/W	Hardware
HeF	Aluminum low-pass filter of the coronagraph
HELEX	Heliophysical Explorers
HERSCHEL	Helium Resonance Scattering in the Corona and Heliosphere
HF	Narrow-band multilayer filter of the coronagraph
HGA	High Gain Antenna
HVPS	High Voltage Power Supply
HWRP	Half Wave Retarder Plate
IAC	Instituto de Astrofísica de Canarias

METIS
EID - PART B

REF: INAF/OATO NR. 94
DATE: 15-JAN-2008
ISSUE 1
page 101 of 108

IAPS	Itensified APS
IAS	Institut d'Astrophysique Spatiale
IASF	Istituto di Astrofisica Spaziale e Fisica cosmica
IDP	Instrument Development Plan
IFE	Instrument Front End
IFSI	Istituto di Fisica dello Spazio Interplanetario
ILS	Instrument Line of Sight
INAF	Istituto Nazionale di AstroFisica
INFM	Istituto Nazionale Fisica della Materia
IO	Internal Occulter
IOM	Internal Occulter Mechanism
IR	Infrared
LAM	Laboratoire d'Astrophysique de Marseille
LCL	Latching Current Limiters
LCVR	Liquid Crystal Variable Retarder
M0	Sun-disk rejection mirror of the coronagraph
M1	Primary mirror of the coronagraph
M2	Secondary mirror of the coronagraph
MCP	Micro Channel Plate
METIS	Multi Element Telescope for Imaging and Spectroscopy
MGSE	Mechanical Ground Support Equipment
ML	Multilayer
MOC	Mission Operation Center
MoI	Moment of Inertia
MPPU	METIS Processing & Power Unit
MPS	Max-Planck-Institut fuer Sonnensystemforschung
MSSL	Mullard Space Science Laboratory
N/A	Not Applicable
NASA	National Areonautics and Space Administration
NOM	Nominal Observing Mode
NRL	Naval Research Laboratory
OAA	Osservatorio Astronomico di Arcetri
OACN	Osservatorio Astronomico di Capodimonte Napoli
OACt	Osservatorio Astronomico di Catania
OAPa	Osservatorio Astronomico di Palermo
OAR	Osservatorio Astronomico di Roma
OATo	Osservatorio Astronomico di Torino
OATs	Osservatorio Astronomico di Trieste
OGSE	Optical Ground Support Equipment
OP	Off Pointing
PA	Product Assurance
PI	Principal Investigator
PoliTo	Politecnico di Torino
QE	Quantum Efficiency
RD-n	Reference Document n
S/C	Spacecraft
S/W	Software
SC	Sun Center
SCORE	Sounding-rocket Coronagraphic Experiment
SEP	Solar Energetic Particles
SMM	Structural Mathematical Model
SO	Solar Orbiter

METIS
EID - PART B

REF: INAF/OATO NR. 94
DATE: 15-JAN-2008
ISSUE 1
page 102 of 108

SOCS	METIS Solar Orbiter Coronal Spectrometer
SOHO	Solar and Heliospheric Observatory
STOM	Structural Thermal Optical Model
TBC	To Be Confirmed
TBD	To Be Defined
TBW	To Be Written
TEC	Thermo Electric Coooler
TM	Telemetry
TSOM	Time Share Observing Mode
TVLS	Toroidal Variable Line Space
UFOV	Unobstructed Field Of View
UniAq	Università di Aquila
UniCal	Università della Calabria
UniFi	Università di Firenze
UniPD	Università di Padova
UniPd	Università di Padova
UniPg	Università di Perugia
UniPv	Università di Pavia
UniRm	Università di Roma
UORF	Unit Optical Reference Frame
URF	Unit Reference Frame
UV	Ultraviolet
UVC	UV channel
UVD	Ultraviolet Detector
VD	Visible Detector
VIM	Visible Imager & Magnetograph
VLC	Visible Light Channel
VUV	Vacuum ultraviolet

METIS
EID - PART B
ANNEX 1

REF: INAF/OATO NR. 94
DATE: 15-JAN-2008
ISSUE 1
page 103 of 108

11. Annex 1. Expected count rates

The Sun disk radiances are shown in Table A1. 1. The corresponding count rates are shown in **Errore. L'origine riferimento non è stata trovata.**. The off-limb radiances and count rates are shown in Table A1. 3.

Table A1. 1. Disk radiances.

Wavelength (nm)	Line	log T_{max}	Radiance (mW m^{-2} sr^{-1})								
			CHIANTI	V&R	CHIANTI	V&R	SUMER	Sandlin	CHIANTI	V&R	CHIANTI
			CH	*CH*	*QS*	*QS*	*QS*	*QS*	*AR*	*AR (Avg)*	*C Flare*
Band: A											
1st order											
97.25	H I 97.25	4.0		101.05		168.68	145.12			1452.20	
97.70	C III 97.70	4.8	550.28	797.65	646.03	963.06	789.76		2207.29	3666.46	53991.00
102.57	H I 102.57	4.0		445.52		747.17	792.14			6253.08	
103.19	O VI 103.19	5.5	126.22	188.76	168.44	305.28	269.86		894.91	2459.69	8262.77
103.76	O VI 103.76	5.5	62.90	132.89[1]	83.93	204.3[1]	121.03		445.79	1519.04[1]	4117.49
2nd order											
104.13	Si XII 52.07	6.2	0.02		24.02	25.44			1030.85	543.45	7129.60
156.66	He I 52.22	4.5		13.47		27.49				234.81	
107.41	He I 53.70	4.5		34.01		70.73				618.00	
Band: B											
1st order											
117.55	C III 117.55	4.8	124.51	248.28	223.88	314.80	233.45		1152.48	1747.59	30455.96
120.65	Si III 120.65	4.7	663.56	527.18	921.28	694.59	470.94		4666.97	3561.52	83194.90
121.57	H I 121.57	4.0		40557.24		64567.93	78146.72	58961.22		220267.64	
123.88	N V 123.88	5.3	15.69	36.44	21.03	61.37	92.51		63.51	549.35	1211.49
124.28	N V 124.28	5.3	7.83	19.17[2]	10.50	36.46[2]	41.82		31.71	310.54[2]	605.13

METIS
EID - PART B
ANNEX 1

REF: INAF/OATO NR. 94
DATE: 15-JAN-2008
ISSUE 1
page 104 of 108

ISTITUTO NAZIONALE DI ASTROFISICA
NATIONAL INSTITUTE FOR ASTROPHYSICS

Wavelength (nm)	Line	log T_{max}	Radiance (mW m^{-2} sr^{-1})								
			CHIANTI	V&R	CHIANTI	V&R	SUMER	Sandlin	CHIANTI	V&R	CHIANTI
			CH	*CH*	*QS*	*QS*	*QS*	*QS*	*AR*	*AR (Avg)*	*C Flare*
2nd order											
116.87	He I 58.43	4.4		250.12		544.98	507.65			5470.68	
118.45	Fe XIX 59.22	6.8			0.00				10.69		1147.47
118.52	Fe XII 59.26	6.1	0.05		2.44				35.58		36.88
124.99	Mg X 62.49	6.1	2.25	2.62	53.91	51.43	65.59		999.20	397.64	4304.71
125.95	O V 62.97	5.4	327.70	285.77	392.33	334.97	783.69		987.01	1018.65	17345.79
Band: C											
1st order											
152.67	Si II 152.67	4.0					191.37	79.94			
153.34	Si II 153.34	4.0					182.26	99.92			
154.82	C IV 154.82	5.0	107.89		152.30		557.90	207.93	388.23		11242.73
155.08	C IV 155.08	5.0	53.83		75.98		263.22	97.82	193.75		5609.65
2nd order											
151.74	O V 75.87	5.4	5.40	6.05	6.57	7.68	4.46		19.43	41.29	721.61
151.89	O V 75.94	5.4	4.15		5.05		3.56		15.04		571.54
152.05	O V 76.02	5.4	3.10	14.58	3.77	17.71	2.89		11.23	85.44	426.84
152.09	O V 76.04	5.4	16.04		19.51		13.23		57.74		2144.05
152.23	O V 76.11	5.4	0.31		0.45				3.87		425.44
152.40	O V 76.20	5.4	5.11		6.22		4.44		18.55		704.78
152.67	N III 76.33	4.9	2.89	53.92	3.82	46.64	2.88		11.58	109.91	300.56
152.87	N III 76.44	4.9	5.58		7.36		4.87		22.32		579.08
153.03	N IV 76.52	5.1	57.56		77.80		66.05		144.29		3273.52
154.07	Ne VIII 77.03	5.8	25.65	20.45	71.57	53.75	32.47		708.46	600.18	3147.93
155.98	O IV 77.99	5.2	2.30	10.70	3.04	25.93			7.14	306.37	218.69
156.05	Ne VIII 78.03	5.8	12.89		35.88		16.79		354.28		1574.28
157.29	S V 78.65	5.2	16.81	39.70	22.79	44.39	30.09		50.56	102.38	1443.18

METIS
EID - PART B
ANNEX 1

REF: INAF/OATO NR. 94
DATE: 15-JAN-2008
ISSUE 1
page 105 of 108

Wavelength (nm)	Line	log T_{max}	Radiance (mW m^{-2} sr^{-1})								
			CHIANTI	V&R	CHIANTI	V&R	SUMER	Sandlin	CHIANTI	V&R	CHIANTI
			CH	*CH*	*QS*	*QS*	*QS*	*QS*	*AR*	*AR (Avg)*	*C Flare*
157.54	O IV 78.77	5.2	54.45		73.04		57.29		162.60		4404.87
158.03	O IV 79.02	5.2	108.88	74.25	146.00	83.15	115.84		323.37	184.03	8692.27
3rd order											
152.22	O III 50.74	5.0	4.17		5.72				15.16		432.69
152.30	O III 50.77	5.0	12.52	28.12	17.19	24.62			45.55	58.20	1299.55
152.45	O III 50.82	5.0	20.87		28.66				75.94		2166.76
154.69	He I 51.56	4.5		6.01		15.02				146.54	
156.20	Si XII 52.07	6.2	0.02		24.02	25.44			1030.85	543.45	7129.60
156.66	He I 52.22	4.5		13.47		27.49				234.81	

Table A1. 2. Count rates.

Wavelength (nm)	Line	log T_{max}	Coating	Counts rate (counts s^{-1})								
				CHIANTI	V&R	CHIANTI	V&R	SUMER	Sandlin	CHIANTI	V&R	CHIANTI
				CH	*CH*	*QS*	*QS*	*QS*	*QS*	*AR*	*AR (Avg)*	*C Flare*
Band: A												
1st order												
97.25	H I 97.25	4.0	KBr		52.04		86.87	74.74			747.88	
97.70	C III 97.70	4.8	KBr	290.39	420.93	340.92	508.22	416.76		1164.81	1934.84	28491.70
102.57	H I 102.57	4.0	KBr		285.65		479.05	507.88			4009.18	
103.19	O VI 103.19	5.5	KBr	86.24	128.97	115.09	208.58	184.38		611.45	1680.59	5645.57
103.76	O VI 103.76	5.5	KBr	45.63	96.35[1]	60.88	148.13[1]	87.80		323.38	1101.38[1]	2986.89

METIS
EID - PART B
ANNEX 1

REF: INAF/OATO NR. 94
DATE: 15-JAN-2008
ISSUE 1
page 106 of 108

Wavelength (nm)	Line	log T_{max}	Coating	CHIANTI CH	V&R CH	CHIANTI QS	V&R QS	SUMER QS	Sandlin QS	CHIANTI AR	V&R AR (Avg)	CHIANTI C Flare
2nd order												
104.13	Si XII 52.07	6.2	KBr	0.00		0.39	0.41			16.75	8.83	115.84
104.44	He I 52.22	4.5	KBr		0.24		0.50				4.25	
107.41	He I 53.70	4.5	KBr		1.31		2.72				23.74	
Band: B												
1st order												
117.55	C III 117.55	4.8	KBr	100.49	200.38	180.69	254.06	188.41		930.12	1410.41	24579.81
120.65	Si III 120.65	4.7	Bare	29.77	23.65	41.33	31.16	21.13		209.38	159.79	3732.56
121.57	H I 121.57	4.0	Bare+Att.		164.26		261.50	316.49	238.79		892.08	
123.88	N V 123.88	5.3	KBr	9.26	21.51	12.41	36.23	54.61		37.49	324.28	715.13
124.28	N V 124.28	5.3	KBr	4.51	11.03[2]	6.05	20.98[2]	24.08		18.26	178.72[2]	348.43
2nd order												
116.87	He I 58.43	4.4	Bare		14.09		30.70	28.60			308.16	
118.45	Fe XIX 59.22	6.8	Bare			0.00				0.72		77.00
118.52	Fe XII 59.26	6.1	Bare	0.00		0.16				2.41		2.49
124.99	Mg X 62.49	6.1	Bare	0.24	0.28	5.83	5.57	7.10		108.14	43.03	465.87
125.95	O V 62.97	5.4	Bare	37.58	32.77	45.00	38.42	89.89		113.20	116.83	1989.34
Band: C												
1st order												
152.67	Si II 152.67	4.0	KBr					5.89	2.46			
153.34	Si II 153.34	4.0	KBr					4.86	2.66			
154.82	C IV 154.82	5.0	KBr	2.09		2.96		10.83	4.04	7.54		218.22
155.08	C IV 155.08	5.0	KBr	0.99		1.39		4.83	1.80	3.56		102.97
2nd order												
151.74	O V 75.87	5.4	Bare	0.98	1.10	1.19	1.39	0.81		3.52	7.48	130.74
151.89	O V 75.94	5.4	Bare	0.75		0.91		0.64		2.72		103.51
152.05	O V 76.02	5.4	Bare	0.56	2.64	0.68	3.21	0.52		2.03	15.47	77.28

METIS
EID - PART B
ANNEX 1

REF: INAF/OATO NR. 94
DATE: 15-JAN-2008
ISSUE 1
page 107 of 108

ISTITUTO NAZIONALE DI ASTROFISICA
NATIONAL INSTITUTE FOR ASTROPHYSICS

Wavelength (nm)	Line	log T_{max}	Coating	Counts rate (counts s^{-1})								
				CHIANTI	V&R	CHIANTI	V&R	SUMER	Sandlin	CHIANTI	V&R	CHIANTI
				CH	CH	QS	QS	QS	QS	AR	AR (Avg)	C Flare
152.09	O V 76.04	5.4	Bare	2.90		3.53		2.39		10.45		388.12
152.23	O V 76.11	5.4	Bare	0.06		0.08				0.70		76.99
152.40	O V 76.20	5.4	Bare	0.92		1.13		0.80		3.35		127.47
152.67	N III 76.33	4.9	KBr	0.79		1.04		0.79		3.16		82.00
152.87	N III 76.44	4.9	KBr	1.53	14.80	2.02	12.80	1.34		6.13	30.17	158.99
153.03	N IV 76.52	5.1	KBr	15.88		21.46		18.22		39.81		903.11
154.07	Ne VIII 77.03	5.8	Bare	4.61	3.67	12.85	9.65	5.83		127.22	107.78	565.27
155.98	O IV 77.99	5.2	Bare	0.41	1.90	0.54	4.60			1.27	54.34	38.77
156.05	Ne VIII 78.03	5.8	Bare	2.28		6.36		2.97		62.78		278.95
157.29	S V 78.65	5.2	Bare	2.95	6.95	4.00	7.77	5.27		8.86	17.99	252.99
157.54	O IV 78.77	5.2	Bare	9.52		12.77		10.02		28.44		770.35
158.03	O IV 79.02	5.2	Bare	18.95	12.92	25.41	14.47	20.16		56.27	32.03	1512.69
3rd order												
152.22	O III 50.74	5.0	Bare	0.17	1.16	0.23	1.01			0.62	2.39	17.70
152.30	O III 50.77	5.0	Bare	0.51		0.71				1.87		53.38
152.45	O III 50.82	5.0	Bare	0.86		1.19				3.14		89.61
154.69	He I 51.56	4.5	KBr		0.78		1.95				19.01	
156.20	Si XII 52.07	6.2	Bare	0.00		1.16	1.23			49.91	26.31	345.22
156.66	He I 52.22	4.5	KBr		1.85		3.78				32.25	

Notes

(1)=blended with C II doublet
(2)=blended with Fe XII line

References

METIS
EID - PART B
ANNEX 1

REF: INAF/OATO NR. 94
DATE: 15-JAN-2008
ISSUE 1
page 108 of 108

V&R: Vernazza & Reeves (1978), ApJS, **37**, 485
Sandlin: Sandlin et al. (1986), ApJS, **61**, 801
SUMER: Teriaca (2007, internal communication)
CHIANTI: Andretta (2007, internal communication)

Table A1. 3. Off-limb radiances from coronal structures and relative count rates for the OVI 103.2 nm line.

Instrument	Coronal structure	Radiance $(mW\,m^{-2}\,sr^{-1})$	Count rate $(counts\,s^{-1})$
SUMER+UVCS	Coronal hole @ 1.1 R0	10	6.83
SUMER+UVCS	Coronal hole @ 1.2 R0	0.3	0.20
SUMER+UVCS	Coronal hole @ 1.4 R0	0.15	0.10
UVCS	Mid-Latitude streamer (1997) @ 1.4 R0	0.58	0.39
UVCS	Mid-Latitude streamer (2000) @ 1.4 R0	1.93	1.32

References
SUMER+UVCS: SUMER+UVCS plume/interplume data (L. Teriaca internal communication)
UVCS: Ventura et al. (2005) A&A, **430**, 701